Ohmic contacts for organic optoelectronic devices

Zur Erlangung des akademischen Grades eines

DOKTOR-INGENIEURS (Dr.-Ing.)

von der KIT-Fakultät für

Elektrotechnik und Informationstechnik
des Karlsruher Instituts für Technologie (KIT)

genehmigte

DISSERTATION

Von

Naresh Kotadiya

geb. In: Gujarat, Indien

Tag der mündlichen Prüfung: 31.01.2020
Hauptreferent: Prof. Dr. Uli Lemmer
Korreferent: Prof. Dr. Paul W. M. Blom

Hauptreferent:	Prof. Dr. Uli Lemmer LTI, KIT, Karlsruhe, Germany
Korreferent:	Prof. Dr. Paul W. M. Blom Max Planck Institut für Polymerforschung und Johannes Gutenberg Universität, Mainz

Vorsitzender:	Prof. Dr.-Ing. Sebastian Randel IPQ, KIT, Karlsruhe, Germany
Weiterer Prüfer:	Prof. Dr. rer. nat. Olaf Dössel IBT, KIT, Karlsruhe, Germany
Weitere Prüferin:	Prof. Dr. Tabea Arndt ITEP, KIT, Karlsruhe, Germany

.

To,

Bhagwan Swaminarayan and my Gurus

for inspiring my dreams and blessing me.

In the joy of others, lies our own

by H.D.H. Pramukh Swami Maharaj.

Abstract

In last three decades, great progress has been made in the field of organic electronics. Researchers have put tremendous efforts to make new materials and device architectures, which has resulted in a great commercial success of organic light emitting diodes in mobile phone and television display screens. Despite that, still today it is challenging to make organic electronic devices that are efficient in performance, stable in operation and are economical in production at the same time. The objective of this thesis is to understand fundamental charge transport properties of small molecules based organic semiconductors and to develop novel organic electronic device architectures.

One of the prime requirements for efficient organic optoelectronic devices is to have ohmic charge injection contacts. Therefore, first a charge injection strategy for making ohmic hole contacts is developed. Using this strategy, ohmic hole contacts are achieved on organic semiconductors with an ionization energy up to 6 eV. As a result, the hole transport in a wide range of organic small molecules with ionization energy between 5 to 6 eV could be investigated. Despite the difference in their chemical structures, similar bulk hole mobilities in the range of 1×10^{-4} $\mathrm{cm^2V^{-1}s^{-1}}$ were observed for all molecules. The hole transport was also investigated using molecular multiscale simulations, an excellent agreement was obtained with the experimental results. Despite fullerene derivatives being known as electron conductors, It was found that the fullerene derivative ICBA has a very good hole mobility of 1.4×10^{-3} $\mathrm{cm^2V^{-1}s^{-1}}$ which is the same as bulk electron mobility, demonstrating the intrinsic bipolar charge-trasnport character of organic semiconductors. It is found that charge trapping is causing the frequently observed unipolarity in organic semiconductors, causing preferential conduction of either holes or electrons. This limits the efficiencies and stabilities of the organic optoelectronic devices. By investigating charge trapping in a wide range of organic semiconductors, we have identified that when the electron affinity is lower than 3.6 eV, electron transport becomes trap limited and when ionization energy is higher than 6 eV hole transport becomes trap limited. As a result, within this energy window of about 2.4 eV trap-free charge transport is observed. Combining this energy window for trap-free transport with our developed charge injection strategy, an efficient and stable single layer OLED based on a neat thermally activated delayed fluorescence emitter is demonstrated. The OLED has a maximum external quantum efficiency of 19% at a luminance of 500 $\mathrm{cdm^{-2}}$and a lifetime to 50% of initial luminance of 1000 $\mathrm{cdm^{-2}}$ of 1,880 h. It has an exceptionally low operating voltage of 2.9 V at a luminance of $10,000$ $\mathrm{cdm^{-2}}$, which resulted in a maximum power efficiency of 87 $\mathrm{lmW^{-1}}$.

Kurzfassung

In den letzten drei Jahrzehnten wurden auf dem Gebiet der organischen Elektronik große Fortschritte erzielt. Die Forscher haben enorme Anstrengungen unternommen, um neue Materialien und Bauelementarchitekturen zu entwickeln, was zu einem großen kommerziellen Erfolg von organischen Leuchtdioden in Mobiltelefonen und Fernsehbildschirmen geführt hat. Trotzdem ist es bis heute eine Herausforderung, organische elektronische Geräte herzustellen, welche effizient arbeiten, stabil im Betrieb und gleichzeitig wirtschaftlich in der Produktion sind. Ziel dieser Arbeit ist es, grundlegende Ladungstransporteigenschaften von organischen Halbleitern auf der Basis kleiner Moleküle zu verstehen und neuartige Architekturen für organische elektronische Bauelemente zu entwickeln.

Eine der Hauptanforderungen für effiziente organische optoelektronische Bauelemente besteht darin, ohmsche Ladungsinjektionskontakte zu haben. Daher wird zunächst eine Ladungsinjektionsstrategie zur Herstellung ohmscher Lochkontakte entwickelt. Mit dieser Strategie werden ohmsche Lochkontakte auf organischen Halbleitern mit einer Ionisierungsenergie von bis zu 6 eV erzielt. Infolgedessen konnte der Lochtransport in einem breiten Spektrum von organischen kleinen Molekülen mit einer Ionisierungsenergie zwischen 5 und 6 eV untersucht werden. Trotz der unterschiedlichen chemischen Strukturen wurden für alle Moleküle ähnliche Bulk-Loch-Beweglichkeiten im Bereich von 1×10^{-4} $\mathrm{cm^2V^{-1}s^{-1}}$ beobachtet. Der Lochtransport wurde ebenfalls mittels molekularer Multiskalensimulationen untersucht, wobei eine hervorragende Übereinstimmung mit den experimentellen Ergebnissen erzielt wurde. Obwohl Fullerenderivate als Elektronenleiter bekannt sind, wurde festgestellt, dass das Fullerenderivat ICBA eine sehr gute Lochbeweglichkeit von $1,4 \times 10^{-3}$ $\mathrm{cm^2V^{-1}s^{-1}}$ aufweist, was der Beweglichkeit von Bulk-Elektronen entspricht und damit den intrinsischen bipolaren Ladungtransportcharakter organischer Halbleiter aufweist. Es wurde festgestellt, dass das Einfangen von Ladungsträgern die häufig beobachtete Unipolarität in organischen Halbleitern verursacht, die eine bevorzugte Leitung von Löchern oder Elektronen bewirkt. Dies begrenzt die Wirkungsgrade und Stabilitäten der organischen optoelektronischen Bauelemente. Durch die Untersuchung des Ladungsträgerdefekte in einer Vielzahl organischer Halbleiter haben wir festgestellt, dass bei einer Elektronenaffinität von weniger als 3,6 eV der Elektronentransport begrenzt wird und bei einer Ionisierungsenergie von mehr als 6 eV der Lochtransport begrenzt wird. Infolgedessen wird innerhalb dieses Energiefensters ein Ladungstransport von etwa 2,4 eV beobachtet. In Kombination dieses Energiefensters für den defektfreien Transport mit unserer entwickelten Ladungsinjektionsstrategie wird eine effiziente und stabile einschichtige OLED auf der Basis eines Emitters mit thermisch aktivierter verzögerter Fluoreszenz (TADF) demonstriert. Die OLED besitzt einen maximalen externen Wirkungsgrad von 19% bei einer Leuchtdichte von 500 $\mathrm{cdm^{-2}}$ und weist eine Lebensdauer von 1.880 h unter Reduktion zu 50% der anfänglichen Leuchtdichte von 1000 $\mathrm{cdm^{-2}}$ auf. Sie weist eine außergewöhnlich niedrige Betriebs-

spannung von 2,9 V bei einer Leuchtdichte von 10.000 cdm^{-2} auf, was zu einer maximalen Energieeffizienz von 87 lmW^{-1} führt.

Contents

1. Introduction

Organic electronic devices such as organic light emitting diodes (OLEDs), organic solar cells or photovoltaic cells (OPVs) and organics field-effect transistors (OTFTs) are based on organic semiconductors (small molecules or polymers). They offer complementary functionalities compared to conventional inorganic semiconductor based devices. Organic semiconductor based devices are light in weight, consume less energy, and in addition they can be made transparent, flexible and disposable, ideally suited for use in wearable electronics, bio electronics and augmented reality based applications [1, 2, 3, 4, 5].

Since the first demonstration of efficient electroluminescence at low voltages by Tang and VanSlyke in 1987 [6], OLEDs have evolved significantly. Today, OLEDs are widely commercialized in displays for mobile phones and televisions. In OLED displays, individual pixels can be turned ON or OFF which offers high color purity and contrast, in addition they can have a 180° wide viewing angle [7, 8, 9, 10]. OLEDs also has a great potential for lighting applications, however their commercial success is hindered by the cost, efficiency and lifetime compared to conventional lighting sources [11, 12, 13]. OPVs can be fabricated on transparent substrates, such as polyethylene terephthalate, which can be fixed on the windows or walls of a high rise building as energy harvesting curtains. Efforts are being made for their commercialization, however their present efficiency and stability are much lower than their inorganic counterparts [14, 15, 16, 17, 18]. For the commercial applications of OTFTs, much work is needed to improve the charge carrier mobilities and operational stability [19, 20].

Commercial OLED displays and OPVs are based on vacuum-deposited small molecule semiconductors and uses complex multilayer device architectures. Still today, it is a big challenge to make devices that are efficient, have a long lifetime and are economical at the same time. Researchers have made great efforts to solve this issue by developing new materials such as phosphorescent [21, 22] and thermally assisted delayed fluorescence (TADF) emitters [23, 24], new device architectures such as p-i-n type based on doped charge injection and transport layers [12, 25], and new fabrication methods. However, relatively much less work is done to understand charge transport in small molecule based organic electronic devices. Understanding the charge transport mechanisms in the organic semiconductors can play a vital role in identifying the factors that limits the device performance and stability. Once identified, such factors can be eliminated to make improved materials and subsequently better devices.

In this thesis, a thorough study of the charge transport in a wide range of organic small molecules is performed. These molecules are commonly used for hole transport, electron transport, and light emission. Devices were fabricated using both high vacuum-based thermal evaporation methods, as well as low cost solution processing techniques. Novel

device architectures were developed for single carrier devices and OLEDs, the device performance is investigated using rigorous experimental work and theoretical models.

Theoretical concepts of the charge transport in organic semiconductors are presented in chapter 2. Initially, the basic properties of organic semiconductors are described, followed by the theoretical description of charge transport and charge trapping models for organic semiconductors. Subsequently, the device architectures and current-voltage characteristics of single carrier devices and OLEDs are discussed. In chapter 3, a novel hole injection method for making ohmic contacts in organic semiconductor devices is presented. In chapter 4, detailed experimental and theoretical studies of routinely used hole transport materials is presented. In chapter 5, hole and electron transport properties of the fullerene derivative indene-C_{60} bisadduct (ICBA) are presented. In chapter 6, charge trapping in a wide range of organic semiconducting materials is investigated. Traps were identified both theoretically and experimentally and key considerations to make trap free materials are also discussed. In chapter 7, a highly efficient and stable single layer OLED developed in this thesis is presented, marking the end of the thesis.

2. Theoretical Background

2.1. Organic semiconductors

Organic semiconductors are carbon based conjugated materials, which are classified into two types, small molecules and polymers. They are significantly different compared to inorganic semiconductors. In solid form, they are bonded by weaker van der Waals forces. This leads to a de-localization of the electron wave functions between adjacent molecules or polymer chains, such that the electronic structure of organic semiconductors preserves that of a single molecule or a polymer chain. In contrast, in inorganic semiconductors, atoms are covalently bonded, which leads to de-localization of electron wave functions over the entire lattice. So, electrons can move easily resulting in better conductivity compared to organic semiconductors [26, 27, 28].

2.1.1. sp^2 hybridization and conjugation

Both molecular and polymeric organic semiconductors mainly consist of carbon and hydrogen. In addition, some low atomic weight elements such as nitrogen, oxygen and sulfur are often present in them. Their semiconducting property originates from carbon atoms connected by alternating single and double bonds, which is known as conjugation. The carbon atom has six electrons and its ground state electronic configuration is C: $1s^2$, $2s^2$, $2p_x^1$, $2p_y^1$, $2p_z^0$. Since 2s and 2p orbitals lies energetically very close to each other, one electron from the 2s orbital can be easily promoted to the empty $2p_z$ orbital. It gives an excited state electronic configuration of the carbon atom as C*: $1s^2$, $2s^1$, $2p_x^1$, $2p_y^1$, $2p_z^1$ as shown in Figure 2.1.

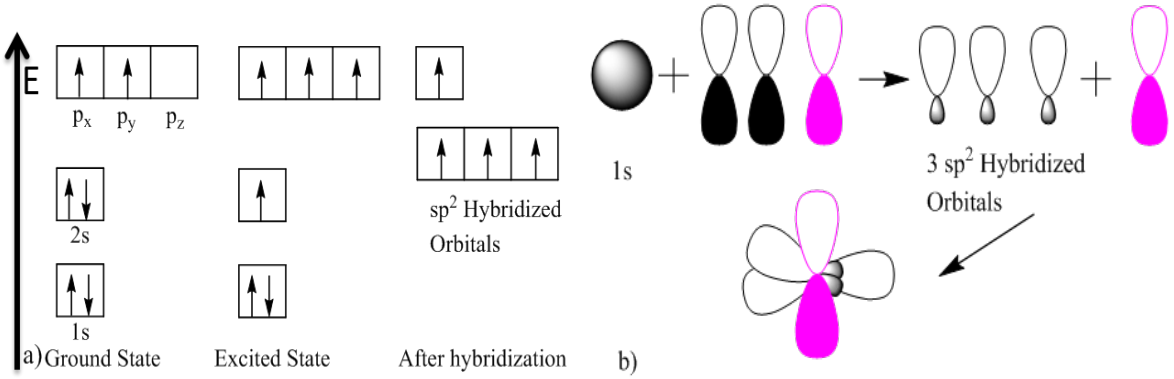

Figure 2.1.: sp^2 Hybridization process. (a) Ground state and excited state electronic configuration and (b) formation of sp^2 hybridized orbitals in carbon atom.

The sp^2 hybridization process results from an intermixing of 2s, p_x and p_y orbitals of

the excited carbon atom, producing three sp^2 hybrid orbitals of equal energy. These three sp^2 hybrid orbitals organize themselves in triangular planar geometry around the carbon atom, at an angle of 120° with respect to each other. The remaining un-hybridized p_z orbital lies perpendicular to the triangular plane of the hybrid orbitals as shown in Figure 2.1. As an example, let us consider the simple structure of the ethene (C_2H_4) molecule.

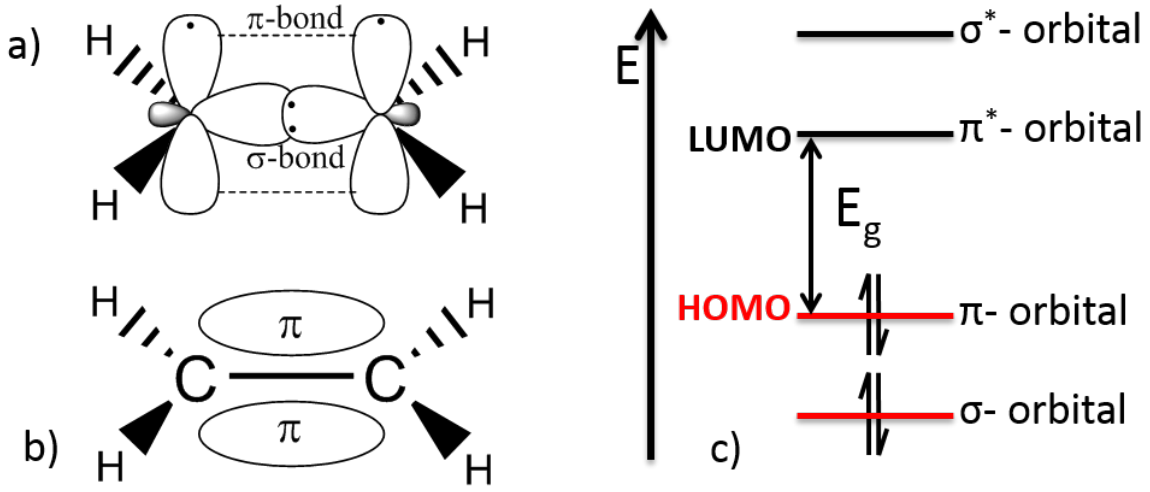

Figure 2.2.: Formation of energy levels in ethene molecule. (a) Formation of σ and π bonds and (b) delocalization of π electron cloud over it. (c) Energy levels corresponding to bonding and antibonding molecular orbitals [26].

Three sp^2 hybrid orbitals from each carbon atom interact to form five σ-bonds. One C-C bond between carbon atoms (by an interaction of two sp^2 hybrid orbitals: one from each carbon atom) and four C-H bonds between carbon and hydrogen atoms (by an interaction of the sp^2 hybrid orbital of a carbon atom with the s orbital of the hydrogen atom). The unhybridized p_z orbitals of both carbon atoms overlap sideways to form another C-C bond called π-bond. Due to a strong interaction and overlapping of the sp^2 hybrid orbitals in the molecular plane, σ-bonds are very strong and forms the backbone of the molecule. On the other hand, the p_z orbitals form considerably weaker π-bonds due to a much lower overlap between them.

According to the molecular orbital theory, both σ-bonds and π-bonds can form bonding and anti-bonding molecular orbitals. Bonding orbitals will stabilize the molecule and have lower energy than the participating single orbitals, while anti-bonding orbitals will destabilize the molecule and have a higher energy than the participating single orbitals [29, 26]. Figure 2.2 shows the energy levels of the molecular orbitals in ethene, where electrons are placed in the orbitals with increasing energy using Pauli's exclusion principle. In the ground state, all bonding orbitals in ethene are filled and all anti-bonding orbitals are empty. As π-orbitals have a higher energy than σ-orbitals, they form the Highest Occupied Molecular Orbitals (HOMO). Due to the weak bonding of π-orbitals, the lowest electronic excitation possible is from the bonding π-orbital to the

anti-bonding π^*-orbital. Thus, the π^*-orbital represents the Lowest Unoccupied Molecular Orbital (LUMO). The HOMO can be roughly compared to the valence band and the LUMO to the conduction band of inorganic semiconductors. The energy difference between HOMO and LUMO corresponds to the band gap (denoted as E_g) of inorganic semiconductors.

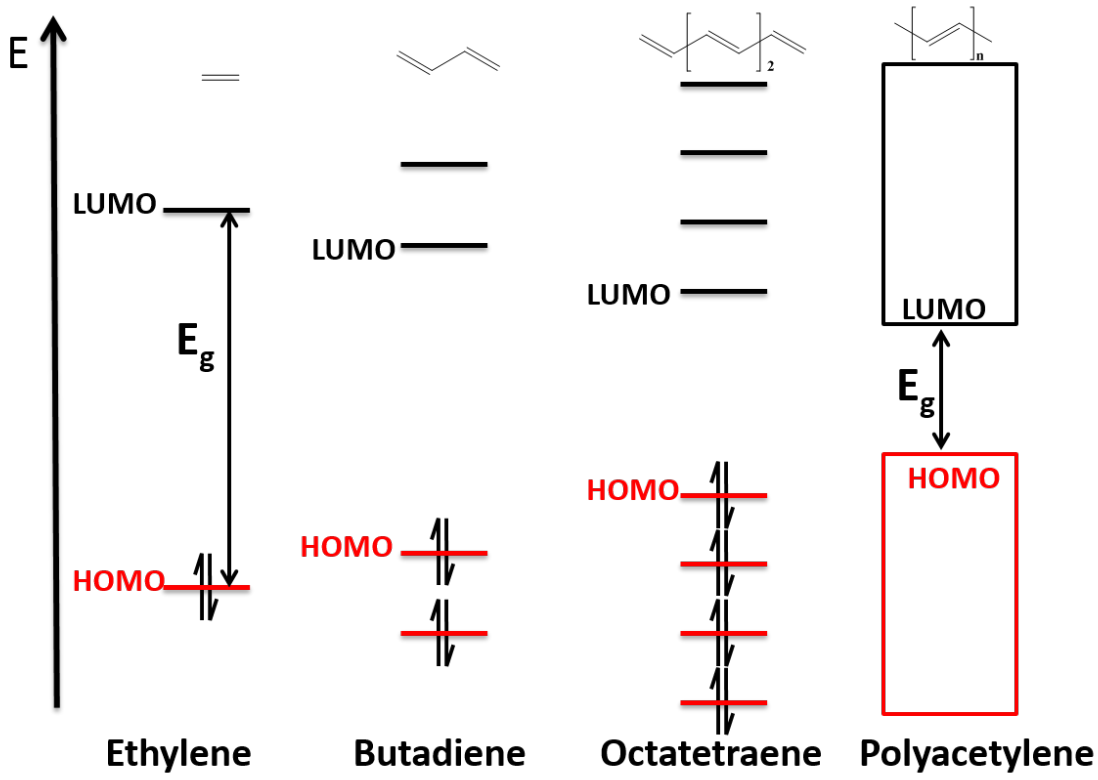

Figure 2.3.: Control of the band gap in organic semiconductors. As the degree of conjugation increases from ethylene to polyacetylene, the HOMO energy value increases (gets shallower) and the LUMO energy value decreases (gets deeper). So eventually the band gap decreases as conjugation increases [30].

The band gap of organic semiconductors (either small molecules or polymers) can be easily tuned by changing the degree of conjugation. As shown in Figure 2.3, as we move from ethylene to polyacetylene the amount of available π and π^* orbitals increases and also the degree of conjugation increases. Correspondingly, this leads to the increase of HOMO value in energy (gets shallower) and decrease of LUMO values in energy (gets deeper). As a result, the band gap decreases from ethylene to polyacetylene. In this way, the band gap can be easily controlled between 1.5 to 3 eV, allowing the light emission from such semiconductors in the entire visible region.

In solid films, each molecule or polymer chain will have slightly different orientation or surroundings, this leads to local variations in the polarization energies [26, 29, 31]. As a

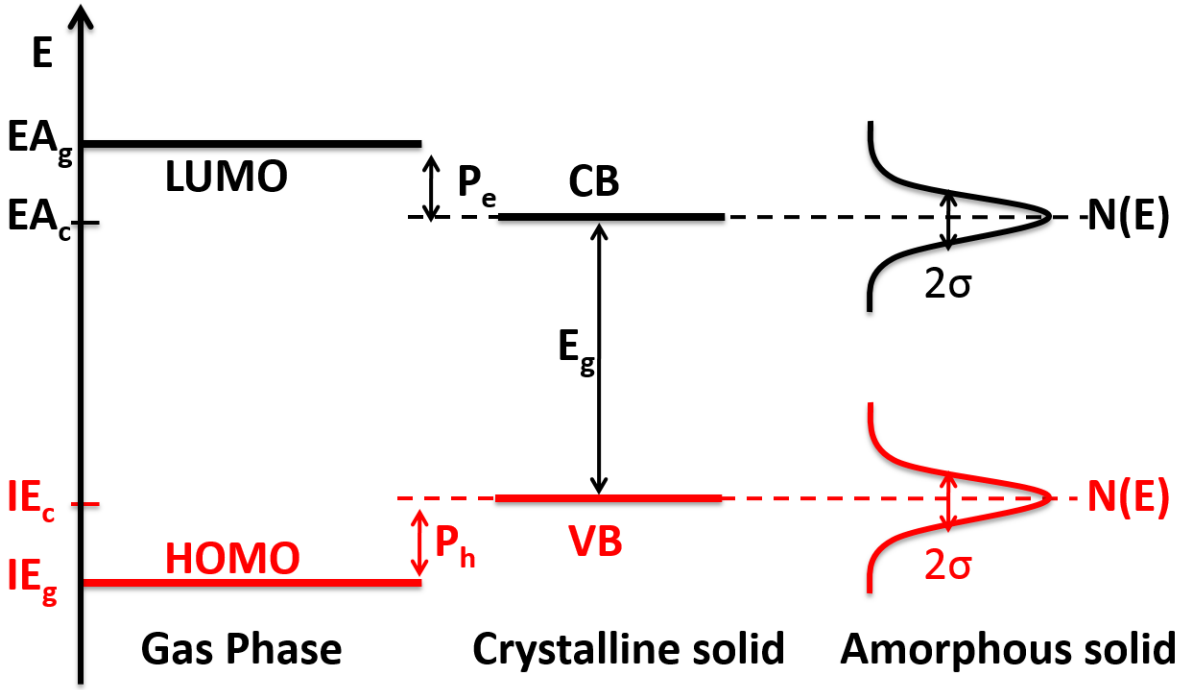

Figure 2.4.: Density of states of the molecules in the gas phase, molecular solids in a crystalline and amorphous state. IE_g is the ionization energy and EA_g is the electron affinity in gas phase, IE_c and EA_c represents quantities in the crystalline state. Due to the polarization energies P_h (positive polaron or hole) and P_e (negative polaron or electron) charged states are stabilized in the crystal. E_g is the energy band gap [26].

result, the energy distribution of localized states in organic semiconductors is described by a Gaussian distribution, the details will be discussed in the next section. Figure 2.4 shows the density of states in crystalline and amorphous molecular semiconductors.

2.2. Charge Transport Models

2.2.1. Gaussian Disorder Model (GDM)

Knowledge of the charge transport mechanisms in organic semiconductors can help to relate microscopic parameters such as disorder and charge transport to physically determinable quantities such as the charge carrier mobility [32, 28]. A charge transport model was proposed by Bässler et al, which is known as the Gaussian Disorder Model (GDM) [33]. It assumes that hopping sites are localized and the energies of the adjacent sites are uncorrelated (independent of each other). The charge transporting sites are randomly distributed in energy and the energetic distribution is given by Gaussian distribution

$$g(\epsilon) = \frac{N}{\sigma\sqrt{2\pi}} \exp\left[-\frac{1}{2}\left(\frac{\epsilon}{\sigma}\right)^2\right] \tag{2.1}$$

where N represents total density of charge transport sites, σ_{DOS} the width of the Gaussian distribution and ϵ represents the energy relative to the center of the DOS.

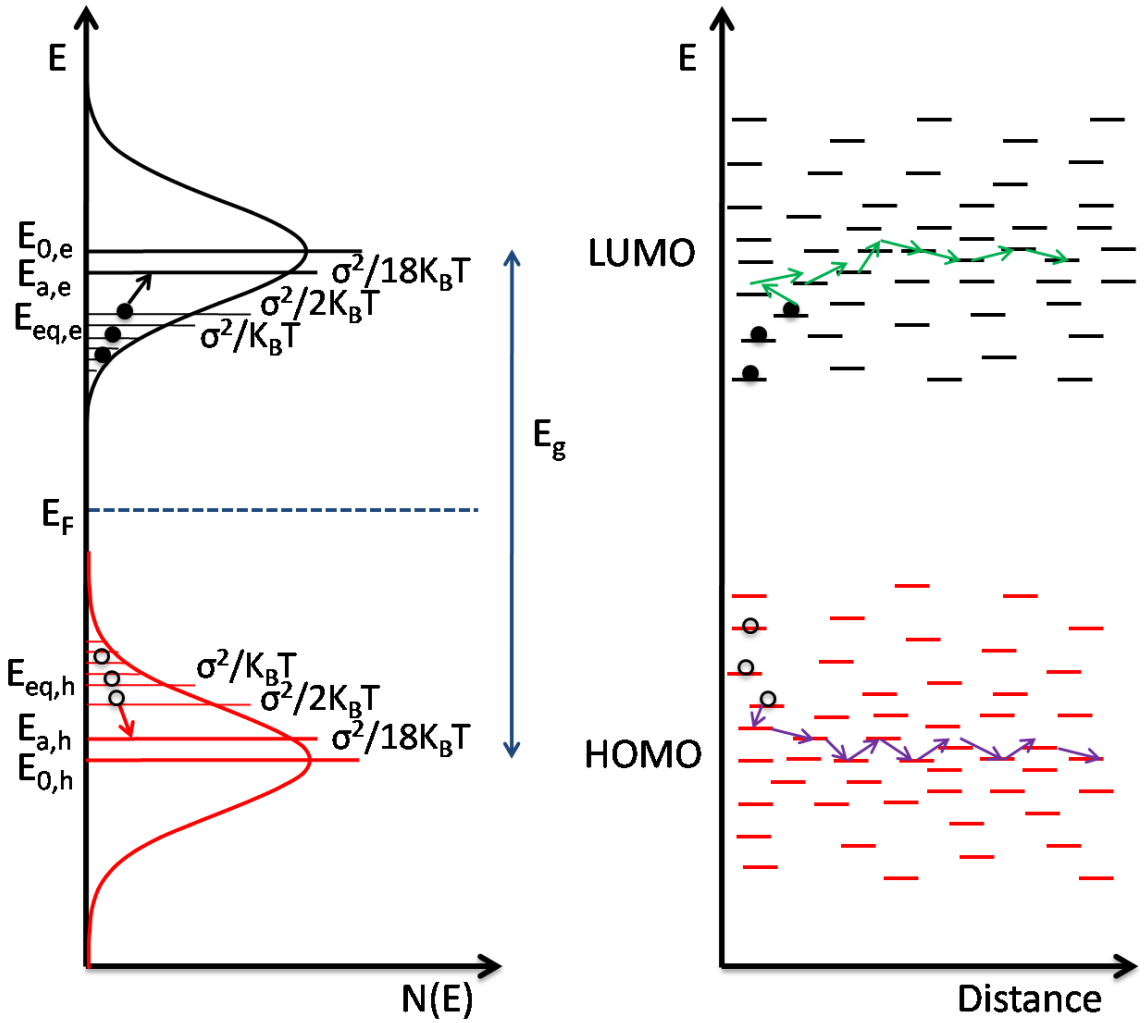

Figure 2.5.: The Gaussian disorder model. Left: shows the Gaussian distribution of LUMO and HOMO energy levels. $E_{0,e}$ and $E_{0,h}$ are the center of DOS for electron and holes respectively. $E_{eq,e}$ and $E_{eq,h}$ are the equilibrium energy levels for electron and holes respectively. E_a, e and E_a, h are the transport energy levels for electron and holes respectively. The energy values of these levels with respect to the center of DOS are also indicated. Right: Distribution of charge transport sites in LUMO and HOMO and the hopping motion of charge carriers from one site to another.

When charges hop (move) from one site to the other, the energy difference between two sites is compensated by the absorption or emission of a phonon. In this phonon assisted hopping (or tunneling) process, the probability for a charge carrier located at the site i, to move to the unoccupied j site is given by the Miller and Abrahams hopping

rates ν_{ij}

$$\nu_{ij} = \nu_0 \exp\left[-2\gamma a \frac{r_{ij}}{a}\right] \times \exp\left[-\left(\frac{\epsilon_j - \epsilon_i}{k_B T}\right)\right] \qquad for\ \epsilon_j \geq \epsilon_i \tag{2.2}$$

$$\nu_{ij} = \nu_0 \exp\left[-2\gamma a \frac{r_{ij}}{a}\right] \times 1 \qquad for\ \epsilon_j < \epsilon_i \tag{2.3}$$

where, the prefactor ν_0 is the phonon vibration frequency, represent the attempts to escape (or hop) rate, γ is the inverse localization radius which depends on the electronic coupling between adjacent sites, a is the average lattice distance (for the assumed cubic cell), r_{ij} represents the relative distance between sites i and j, and ϵ_i, ϵ_j represents the energy of the sites i and j respectively [34].

The mobility μ of the charge carriers depends on how fast they hop between the Gaussianly distributed transport sites from one site to other. Which in turn depends on the energetic difference and spatial distance between hopping sites.

Figure 2.5 schematically describes the Gaussian disorder model, important energy levels for electrons and holes are marked by suffix e and h, respectively. Bässler et al developed the GDM using Monte Carlo (MC) simulation methods and found that under thermal equilibrium, charges present in the material relax to the so-called equilibrium energy level $\mathrm{E}_{eq,e}$, situated at $\frac{\sigma^2}{\kappa_B T}$ below the center of the DOS $\mathrm{E}_{0,e}$. At $\mathrm{E}_{eq,e}$, very few transport sites are present, so that charges need to be excited to the so-called transport energy level $\mathrm{E}_{a,e}$. At $\mathrm{E}_{a,e}$ charges have a sufficient amount of transport sites to hop form one site to the other. Theoretical calculations predicted that $\mathrm{E}_{a,e}$ is located close to the center of the DOS at $\frac{\sigma^2}{18\kappa_B T}$, and an activation energy of $\frac{4\sigma^2}{9\kappa_B T}$ is required for charges to hop to the transport level. This means that charge carriers located around $\frac{\sigma^2}{2\kappa_B T}$ jump to the transport energy level and mainly contribute to the charge transport [33, 35]. The temperature-dependent activation energy gives rise to the temperature dependence of μ.

When an external electric field is applied the site energies get modified by the electrostatic energy term. As a result, the energetic gap between sites decreases under an applied electric field. So, for electrons, the probability to jump upward to a site higher in energy increases while the downward jump to the lower energy site remains unaffected [36, 37, 38]. Hence, the μ also depends on the applied electric field. In short, μ depends on temperatures (T) and the applied electric field (E) due to the energetic disorder of transport sites. The results from MC simulations can be summarized into following empirical relations constituting the GDM, which directly connects the physically measurable quantity mobility μ to the microscopic disorder parameter σ.

$$\mu_{GDM} = \mu_\infty \exp\left[-\left(\frac{2\sigma}{3k_B T}\right)^2\right] \times \exp\left[C\left(\left(\frac{\sigma}{k_B T}\right)^2 - \Sigma^2\right)\sqrt{E}\right] \quad for\ \Sigma \geq 1.5 \tag{2.4}$$

$$\mu_{GDM} = \mu_\infty \exp\left[-\left(\frac{2\sigma}{3k_B T}\right)^2\right] \times \exp\left[C\left(\left(\frac{\sigma}{k_B T}\right)^2 - 2.25\right)\sqrt{E}\right] \quad for\ \Sigma < 1.5 \tag{2.5}$$

where, μ_∞ is a mobility prefactor in the limit of $T \to \infty$, $C = 3 \times 10^{-4}$ $\mathrm{cm}^{\frac{1}{2}}\mathrm{V}^{-\frac{1}{2}}$ is a site spacing dependent constant and Σ represents the degree of positional disorder of hopping sites.

The GDM model for the calculation of μ takes into account the temperature (T) and the electric field (E) dependence of μ. However, it was found that μ also depends on the charge carrier concentration (n for electrons or p for holes). Tanase et al observed that the mobility of $\mathrm{OC_1C_{10}}-$PPV measured in a transistor configuration is around 3 orders of magnitudes higher than measured in a diode configuration [39]. Such a huge difference in mobility was explained by the strong dependence of the mobility μ on the charge carrier concentration n for electrons (or p for holes). In a field-effect transistor, the charge concentration is much higher than in a diode. This is a result of the gate-induced charge-carriers in the channel of a field-effect transistor. Because of the higher charge-carrier density and the density dependence of the mobility, a higher mobility is observed in a field-effect transistor.

2.2.2. Extended Gaussian Disorder Model (EGDM)

By taking into account the charge carrier density (p) dependence of the mobility into the original Gaussian disorder model, Pasveer et al, developed a new charge transport model. This model is often termed as the extended Gaussian disorder model (EGDM). In the EGDM it was found that at room temperature p dependence dominates the mobility, while at lower temperature and high applied electric fields the E dependence plays a major role [40]. The results of the EGDM can be summarized in the following parameterized equations for the mobility μ.

$$\mu(T, p, E) = \mu_p(T, p) \times f(T, E) \tag{2.6}$$

The first term in the above expression describes the carrier concentration (p) and temperature (T) dependence, which is given by

$$\mu_p(T, p) = \mu_0 C_1 \exp\left[-C_2 \left(\frac{\sigma}{k_B T}\right)^2 + \frac{1}{2}\left(\left(\frac{\sigma}{k_B T}\right)^2 - \left(\frac{\sigma}{k_B T}\right)\right)\left(2pa^3\right)^\delta\right] \tag{2.7}$$

where the δ is given by

$$\delta = 2\frac{\ln\left(\left(\frac{\sigma}{k_B T}\right)^2 - \left(\frac{\sigma}{k_B T}\right)\right) - \ln(\ln 4)}{\left(\frac{\sigma}{k_B T}\right)^2} \tag{2.8}$$

The second term in equation 2.6 describes the electric field (E) dependence, which is given by

$$f(T,E) = \exp\left[0.44\left(\left(\frac{\sigma}{k_BT}\right)^{\frac{3}{2}} - 2.2\right) \times \sqrt{1 + 0.8\left(\frac{Eea}{\sigma}\right)^2} - 1\right] \tag{2.9}$$

In the limit of zero charge carrier concentration and zero field ($p \to o$ and $E \to o$) the equation 2.6 gives a simplified temperature dependence of the mobility.

$$\mu_0(T) = \mu_0 C_1 \exp\left(-C_2\left(\frac{\sigma}{k_BT}\right)^2\right) \qquad where \quad \mu_0 = \frac{a^2 \upsilon_0 e}{\sigma} \tag{2.10}$$

In the above equations, μ_0 is a mobility prefactor, υ_0 is the attempt to hop frequency from the MA model, e is electronic charge, σ the width of the Gaussian disorder. $C_1 = 1.8 \times 10^{-9}$ and $C_2 = 0.42$ are constants. k_B is Boltzmann's constant, T is the temperature and a is the lattice constant.

The EGDM has been widely used to investigate charge transport properties of solution processed polymer based organic semiconductors and excellent agreement has been obtained with experimental results [41, 42, 39, 43, 44]. However, not much is known about the applicability of the EGDM to organic small molecules, within this thesis we have investigated the EGDM for thermally evaporated and solution processed organic small molecules. As shown in chapter 4 and chapter 5, the EGDM is equally applicable to organic small molecules.

2.3. Physics of trap limited currents

The EGDM model explained in last section, is suitable to describe the charge transport in materials where trapping of charge carriers is absent. However, the majority of organic semiconductors shows trapping behavior for one of the charge carriers, either electrons or holes. To understand trap limited charge transport, additional knowledge about trap limited currents is required, which will be discussed in this section.

An early description of trap limited currents, in organic semiconductors was derived by Mark and Helfrich [45]. They considered trapping sites that were exponentially distributed below the conduction band edge, given by

$$N_t(E) = \left(\frac{N_t}{k_BT_t}\right)\exp\left[\frac{E - E_c}{k_BT_t}\right] \tag{2.11}$$

Here, $N_t(E)$ is the density of traps (trapping sites) at energy E, N_t is the total number of traps and E_C the energy of the conduction band edge. T_t is a characteristic temperature, which defines the characteristics energy of the trap distribution $E_t = k_BT_t$.

Charge carriers that are trapped do not contribute to the current. As a result, the drift current in such a device will remain much lower than the current in a trap-free

insulator, until all traps are filled. The current in this regime is called trapped-charge limited current or trap-limited current (TCLC or TLC). Mark and Helfrich derived an expression for the trap limited current-voltage characteristics given by

$$J_{TCLC} = N_C e\mu \left(\frac{\varepsilon}{eN_t}\right)^r \left[\left(\frac{2r+1}{r+1}\right)^{r+1} \left(\frac{r}{(r+1)}\right)^r\right] \frac{V^{r+1}}{L^{2r+1}} \tag{2.12}$$

where N_c is the total density of states in the conduction band having values in the range of $10^{19} - 10^{21}$ cm^{-3}. e is the elementary charge and μ the charge carrier mobility. $\varepsilon = \varepsilon_0\varepsilon_r$ is the dielectric constant of the semiconductors and L is the thickness of the organic layer. $r = T_t/T$ is a constant that depends on the trap distribution and can be directly determined from the $\log(J)$ vs $\log(V)$ and thickness dependence of the trap limited currents.

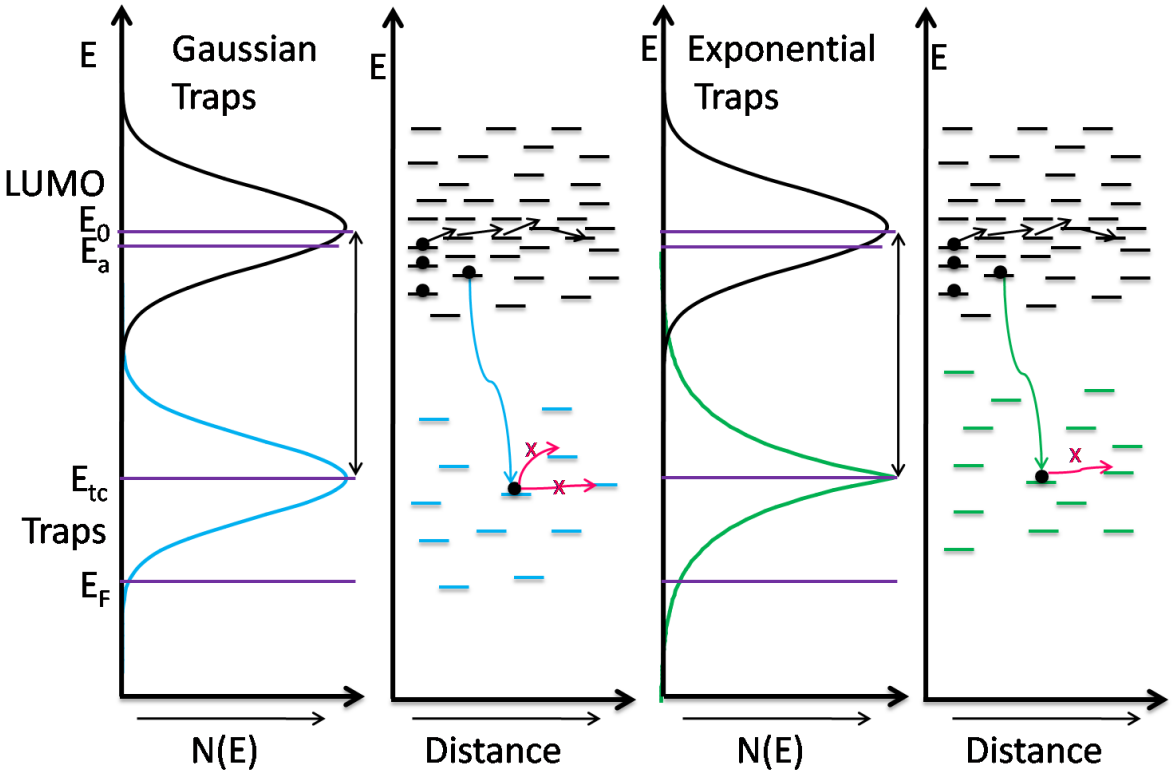

Figure 2.6.: Electron traps in organic semiconductors. Left: shows the Gaussian distributed LUMO, and the Gaussian distributed traps. E_0 and E_{tc} are the center of LUMO and traps respectively. E_a is a transport energy level and E_F is Fermi energy level. Right: shows the LUMO and exponentially distributed traps.

Equation 2.12, was able to describe trap-limited currents in PPV based organic polymers at room temperature. However, it predicts much stronger temperature dependence

than experimentally observed [46]. The reason for that is the organic semiconductors frequently have a Gaussian distribution of states in the LUMO (or HOMO) as opposed to the sharp conduction band edge in inorganic semiconductors, as shown in Figure 2.6. The charge transport occurs via hopping in those Gaussianly distributed states. The energetic distribution of hopping sites results in an effective conduction band edge located at an energy E_a below the center (E_o) of the Gaussian DOS. The result is that the trap depth is no longer measured with respect to the center of the distribution of LUMO states, but is reduced by a term E_a. Therefore, equation 2.12 needs to be modified as following

$$J_{TCLC} = N_C e \mu_e \left(\frac{\varepsilon}{e N_t \exp\left[\frac{(E_{tc}-E_a)}{k_B T_t}\right]} \right)^r \left[\left(\frac{2r+1}{r+1} \right)^{r+1} \left(\frac{r}{(r+1)} \right)^r \right] \frac{V^{r+1}}{L^{2r+1}} \tag{2.13}$$

where E_{tc} is the trap depth w.r.t (below) the center E_0 of the Gaussian distributed LUMO. $E_a = \sigma^2/2k_BT$ serves as the energy of the effective conduction band edge, and is dependent on the energetic disorder and the temperature. It lies below center E_0 of the LUMO, can be regarded as a conduction band edge, as shown in Figure 2.6.

An effective density of trap states $N_{t(eff)}$ can be defined as

$$N_{t(eff)} = N_t \exp\left[\frac{(E_{tc}-E_a)}{k_B T_t}\right] \tag{2.14}$$

which depends on the trap depth E_{tc}. Since E_a depends on temperature, also the effective trap density becomes temperature dependent. In the equation 2.14, the total density of trapping sites N_t has constant value, however in order to determine it, one needs to find out the trap depth E_{tc} and vice versa. Incorporating this additional temperature dependence term, the modified Mark-Helfrich equation 2.13, now successfully describes the (experimentally observed), weaker temperature dependence in PPV based organic semiconductors.

For materials with trap limited currents, one of the important quantities to determine the effect or severity of traps is the ratio of number of trapped n_t and number of free n charge carriers, which is given by

$$\frac{n}{N_0} = \left(\frac{n_t}{N_{t(eff)}} \right)^r \qquad ; r = \frac{T_t}{T} \tag{2.15}$$

Where N_0 is total density of the hopping or charge transport sites and N_t is total density of trapping sites.

The value $r = T_t/T$ is a constant which depends on the trap distribution. From equation 2.13, the current density has a power-law dependence on voltage and layer thickness according to $J \propto (V^{r+1}/L^{2r+1})$. So, by plotting $\log(J)$ vs $\log(V)$ for different thicknesses we can directly determine the value of r. For $r = 1$, $J \propto V^2$, this will give a slope of 2 (same as Mott-Gurney law), which corresponds to trap free transport. For $r > 1$, $J \propto V^m$; where $m > 2$ this will give a slope higher than 2 and corresponds to trap limited charge transport. Once r is known, using equation 2.15 the ratio of trapped and free charge carriers can be easily determined.

Generally the density of trapping sites is several orders of magnitude lower than the density of charge transport sites. As mentioned in last section, for efficient transport, the charge transport sites should be located closely in energy and distance. For an electron hopping or moving in the LUMO, it is energetically favorable to go to trap sites as they are located at lower energy. Once a charge reaches a trap site, it can not move to neighboring trapping sites as they are energetically and spatially far apart as shown in Figure 2.6. So, charges that are trapped do not contribute to the current. As a result the currents in materials with traps are often few orders of magnitudes lower than in materials without traps [47].

The assumption in the previous equations was that the traps are exponentially distributed in energy. This is not necessarily the case in organic semiconductors. For instance, trapping sites could also have a Gaussian distribution in energy, just like the HOMO and LUMO states [48, 49]. In such a case distribution of trapping sites is given by

$$N_{t(gauss)}(E) = \left(\frac{N_t}{\sigma_t\sqrt{2\pi}}\right) \exp\left[-\frac{[E-(E_a-E_{tc})]^2}{2\sigma_t^2}\right] \tag{2.16}$$

where $N_{t(gauss)}(E)$ is the density of traps (trapping sites) at energy E, N_t the total trap density, σ_t is the width of the trap distribution, E_{tc} is the trap depth w.r.t (below) the center E_0 of the Gaussianly distributed LUMO. And $E_a - E_{tc}$ is the effective trap depth, which becomes temperature dependent in the case of disordered semiconductors.

While the trap-limited current for Gaussianly distributed traps cannot be described easily with analytical equations, an approximation can be obtained by modifying the Mark-Helfrich equation 2.13. Here the trap exponent r is modified by $r^{'}$ as following

$$r^{'} = \sqrt{1 + 2\pi\left(\frac{\sigma_t}{4k_BT}\right)^2} \tag{2.17}$$

and the effective density of trap is modified by

$$N^{'}_{t(eff)} = \frac{N_t}{2} \exp\left[\frac{E_t}{r^{'}k_BT}\right] \tag{2.18}$$

Figure 2.6, shows the cases of Gaussian and exponential traps and the process of trapping of charge carriers. Nicolai et al investigated a numerical Gaussian trap model for the electron traps in PPV based organic semiconductors. They found that traps can be described equally well by the Gausssian trap model and the exponential trap model [48]. Later, the Gaussian trap model was applied to a wide range of organic semiconducting polymers, which resulted in the identification of a common trap depth around 3.6 eV for electron transport in conjugated polymers [50].

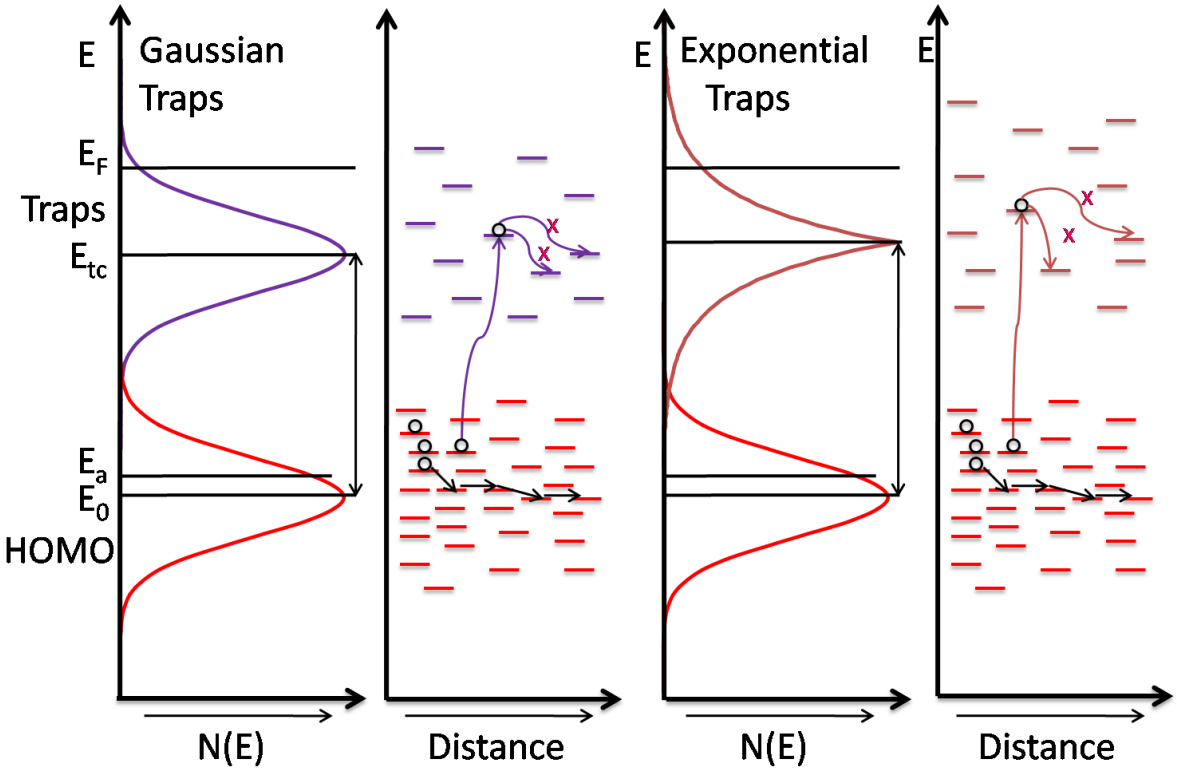

Figure 2.7.: Hole traps in organic semiconductors. Left: shows the Gaussian distributed HOMO, and the Gaussian distributed traps. E_0 and E_{tc} are the center of HOMO and traps respectively. E_a is a transport energy level and E_F is Fermi energy level. Right: shows the HOMO and exponentially distributed traps.

In the present thesis, we investigate the electron and hole traps in a large number of organic small molecules. Similar to organic polymers, a common trap depth for electron transport at 3.6 eV was observed for thermally deposited small molecules. In addition, a common trap depth for hole transport was found at around 6.0 eV. This leads to a small energy window of about 2.4 eV for trap free charge transport in organic semiconductors. Figure 2.7, shows the HOMO, Gaussian and exponential distributed traps. Unlike electrons, for holes it is easy to go higher in energy, so hole traps are located above the HOMO. Similar to electron trapping explained earlier, holes that move to a trap site

can not move to neighboring trap sites or the HOMO as shown in Figure 2.7, reducing hole currents by several orders of magnitude. A detailed discussion about origin of hole traps is presented in chapter 6.

2.4. Charge carrier injection

Since organic semiconductors have a low amount of free charge carriers, in organic optoelectronic devices such as OLEDs, OPVs or OTFTs they need to be injected from the contacts. This process of charge injection thus plays a critical role in the performance of optoelectronic devices. When metal and organic semiconductors are brought into contact, at their interface a barrier for charge injection from the metal into the organic semiconductor is generated. Figure 2.8(a) shows the energy band diagram at the metal/organic semiconductor interface. Φ_b denotes the original charge injection barrier, which is formed due to the energetic difference between the Fermi energy E_F of the metal and the LUMO of the organic semiconductor. When an electron is injected from the metal into the organic semiconductor, it induces an equal positive charge called image charge on the metal surface. For an electron with charge q at distance x from the metal surface, the image potential is given by $\Phi_i = -q/(16\pi\varepsilon x)$. When an external field F is applied to the device, the barrier at the interface will be lowered by $\Delta\Phi = \sqrt{(qF)/(4\pi\varepsilon)}$ due to the combined effect of the applied field and the image potential. This phenomenon is known as Image-force barrier lowering [51, 52].

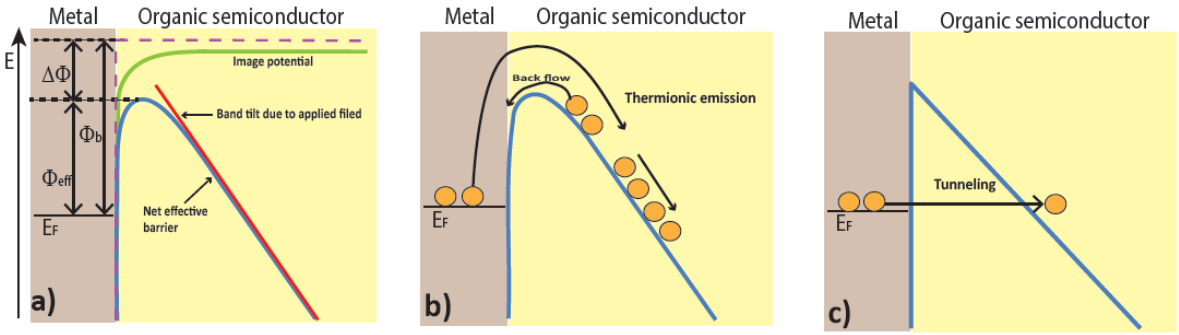

Figure 2.8.: Energy band diagram at the metal/organic semiconductor interface. (a) The band tilt due to the applied field is shown by the straight line (red). Due to the image potential (green curve), the barrier height at the interface will be lowered, the blue curve shows the net band bending near the interface. The maximum barrier is lowered by $\Delta\Phi$ at the interface. (b) Charge injection via thermionic emission. In low mobility organic semiconductors, charge carriers will be accumulated at the interface, and can flow back into the metal contact. (c) At high fields, charge injection via Fowler–Nordheim tunneling at a triangular barrier is shown [51].

The charge injection at the metal/semiconductor interface can occur via thermionic emission or tunneling. The thermionic injection process is based on the mechanism that,

if electrons in the metal get enough thermal energy, they can jump over the injection barrier and move into the semiconductor as shown in Figure 2.8(b) [53]. The injected current is described by the Richardson-Schottky equation

$$J = A^* T^2 \exp\left(-\frac{q\Phi_{eff}}{kT}\right) \tag{2.19}$$

where $A^* = (4\pi q m^* k^2)/(h^3)$ is the Richardson constant (which depends on the effective mass m^* of charge carriers), T is the temperature, q is the elementary charge, and Φ_{eff} is the effective barrier height which is given by

$$\Phi_{eff} = \Phi_b - \Delta\Phi = \Phi_b - \sqrt{\frac{qF(0)}{4\pi\varepsilon}} \tag{2.20}$$

Here, $F(0)$ is the electric field at the contact, ε is the dielectric constant of the organic semiconductor, Φ_b is the original injection barrier at the interface, $\Delta\Phi$ is the reduction in barrier height due to the image potential and applied field. As can be see from above equations, the effective barrier height plays a critical role for the thermionic emission of charge carriers.

The above explanation is suitable for inorganic semiconductors, which have high charge mobilities. In organic semiconductors, charge carrier mobilities are a few order of magnitude lower than the inorganic semiconductors, so a large number of injected charge carriers will be accumulated at the interface and they may flow back to the metal contact as shown in Figure 2.8(b) [52, 54, 55]. In this case, diffusion effects are important and the thermionic emission equation needs to be modified to

$$J = qN_c\mu F(0) \exp\left(-\frac{q\Phi_{eff}}{kT}\right) \tag{2.21}$$

where N_c is effective density of states in the LUMO. and μ_0 is the charge carrier mobility in the semiconductor.

At low temperatures, charge carriers will not have enough thermal energy to surmount the injection barrier as descried by thermionic emission. In such a case, if applied voltage is very high (or semiconductor layer is very thin) charge carriers can tunnel through the injection barrier [56, 57]. This process is known as Fowler-Nordheim tunneling, the injected current mainly depends on the applied electric field and is given by

$$J = \left(\frac{q^3}{8\pi h\Phi_b}\right) F^2 exp\left(-\frac{K}{F}\right) \tag{2.22}$$

where K is a parameter that depends on the shape of the barrier. For a triangular barrier, K is given by

$$K = \left(\frac{8\pi\sqrt{2m^*}(q\Phi_b)^{3/2}}{3qh}\right) \tag{2.23}$$

Here, m^* is the effective mass of charge carriers. Figure 2.8(c) shows charge carrier tunneling across a triangular barrier. Also in this case, the injection barrier Φ_b plays a critical role. Experimentally, the injection barrier can be determined by plotting $ln(\frac{J}{F^2})$ Vs F^{-1} plot known as F-N plot.

2.4.1. Ohmic charge injection contacts

At metal/organic semiconductor contacts, when the metal is able to supply more charges than the organic semiconductor can transport the contact is said to be ohmic. Analytically, if the current in a single carrier device is space-charge limited then the contact is ohmic. For organic semiconductor based devices, if contacts are not ohmic, the current in the device can be significantly lower upto an order of magnitude as shown in chapter 3. So, ohmic contacts are significantly important in organic semiconductor based optoelectronic devices.

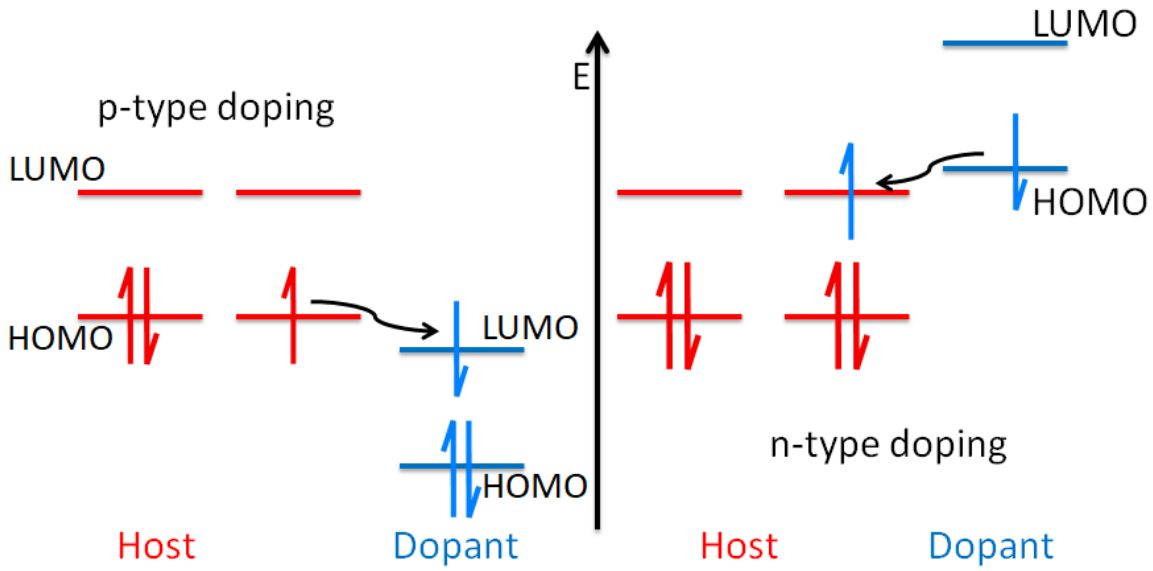

Figure 2.9.: Left: p-type doping in organic semiconductors, an organic dopant with a LUMO deeper than the HOMO of the host can accept an electron from the host. This creates a hole in the host, resulting in p-type doping. Right: n-type doping in organic semiconductors, an organic dopant with a HOMO lower than the LUMO of the host can donate an electron to the host. This creates an extra electron in host, resulting in n-type doping [58].

At present, electrical doping of the organic semiconductor is predominantly used to obtain ohmic contacts. In this method, a p-doped layer of organic semiconductor is deposited on metal contacts for hole injection (or n-doped layer for electron injection). The doping is achieved by adding an electron acceptor that captures an electron from

the HOMO, leaving a hole behind, resulting in p-type doping. For n-type doping, an electron donor with a high HOMO is used to donate an electron to the LUMO, as shown in Figure 2.9. This results in a shift of the Fermi level towards the HOMO (or LUMO). Such shift of energy levels creates a strong band bending at the metal doped layer interface forming a depletion region, resulting in effective lowering of the charge injection barriers as shown in Figure 2.10 [59, 60].

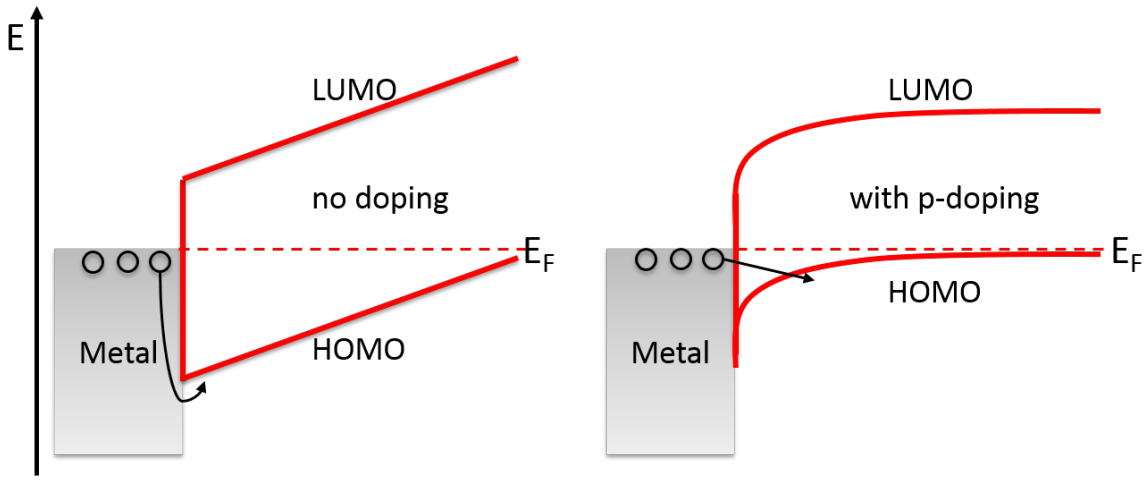

Figure 2.10.: Left: Metal/un-doped organic semiconductor contact, there is a high barrier for hole injection. Right: Metal/p-doped organic semiconductor contact, by doping the organic layer, a strong band bending is created, resulting in the significant reduction of the injection barrier [58]

Apart form lowering the injection barriers, doping also increases the conductivity of organic semiconductors, allowing the flexibility to use thicker injection layers, which can improve the device yield while maintaining low operating voltages [61]. However, doping can only be effective when the LUMO of the dopant (or acceptor) is deeper than the HOMO of the host material for p-type doping or the HOMO of the dopant (or donor) is lower than the LUMO of the host material for n-type doping. Currently, it is challenging to achieve p-type doping in host with a HOMO deeper than -5.5 eV. To inject charges in organic semiconductors having a HOMO of, for instance -6.0 eV, one needs a very strong dopant with a LUMO lower than -6.0 eV. From a synthesis point of view, creating materials with a LUMO deeper than -6.0 eV is extremely challenging. Hence, p-doping is not suitable for charge injection into materials with a deep HOMO. In addition, a single dopant can not be used for all host materials.

In order to overcome this challenge, we have developed a novel charge injection method as shown in chapter 3. Our method can be used for materials with HOMO deeper than -6.0 eV, as described in chapter 3.

2.5. Single carrier devices

2.5.1. Single carrier device architecture

Experimentally, the charge carrier mobilities of organic semiconductors can be obtained by fabricating single carrier hole only (HO) or electron only (EO) devices and subsequently measuring their current-voltage characteristics. For HO (or EO) devices the organic semiconductor is sandwiched between two high (or low) work function electrodes as shown in Figure 2.11. This creates a high barrier for electron (or hole) injection, under the applied voltage only holes (or electrons) will be injected. As a result, the current in the device is only due to holes (or electrons) [62]. If one of the contacts is ohmic, the current in the device will reach the space charge limit from which mobility can be extracted using the Mott-Gurney equation or by numerical modeling.

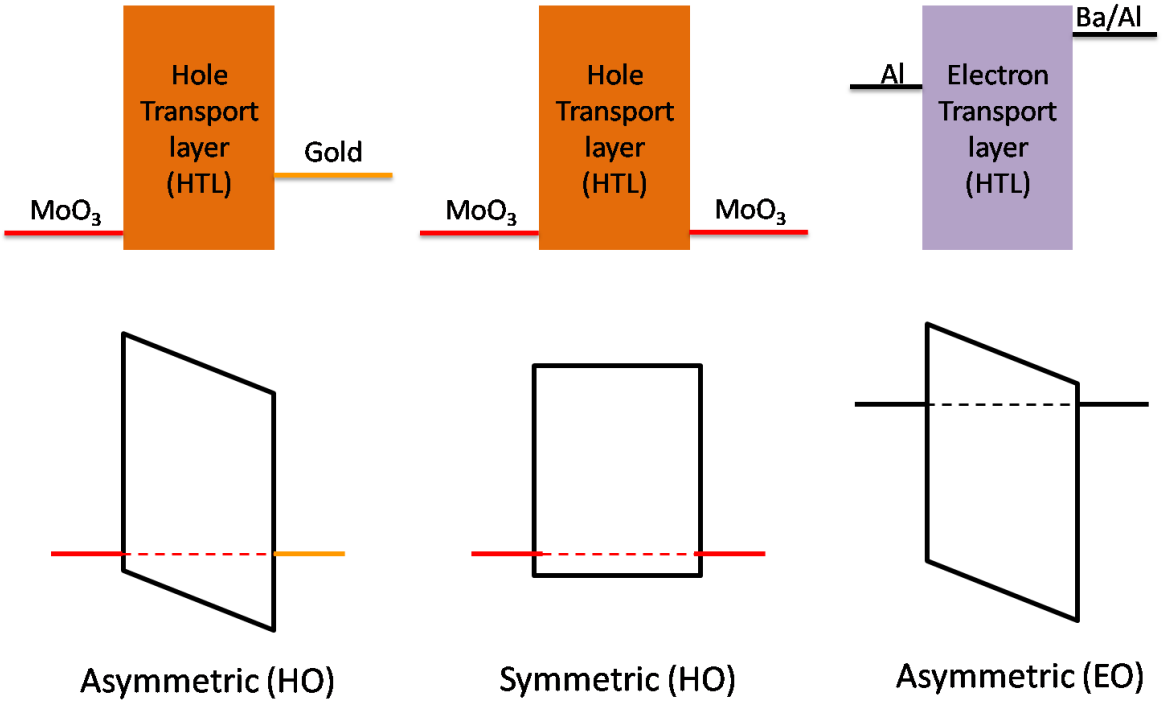

Figure 2.11.: Single carrier device architecture. The top row shows the device structure of symmetric and asymmetric single carrier hole only and electron only devices. The corresponding band diagrams attained after reaching thermal equilibrium are shown in the bottom row.

When the device is fabricated, in order to attain the thermal equilibrium, the fermi level of the electrodes of both sides align with each other. As a result, a built in voltage (V_{bi}) will be established in an asymmetric device (which has electrodes of different work function). For analysis, the voltage scale needs to be corrected by subtracting the built in voltage from the applied voltage. A built in voltage will be absent in the symmetric

device (which has same work function of electrodes), hence no voltage correction will be required in that case.

2.5.2. Single carrier device current-voltage characteristics

The current-voltage characteristic of a symmetric hole only device of Spiro-TAD (a material mainly used as a hole transport layer or host in OLEDs) is shown in the Figure 2.12. It can be divided into two regimes, at low voltages the current is mainly due to charge carriers diffused from the contacts or present intrinsically due to unintentional doping [63, 64]. This charge concentration is independent of the applied voltage, resulting in a current that increases linearly with the applied voltage and is described by Ohm's law as following

$$J = nq\mu\frac{V}{L} \tag{2.24}$$

where n is the diffused charge carrier density, μ the mobility, q is the elementary charge and L is the thickness of the organic layer (or the distance between two electrodes). This regime is called as ohmic regime, as marked by red line with slope of 1 in Figure 2.12.

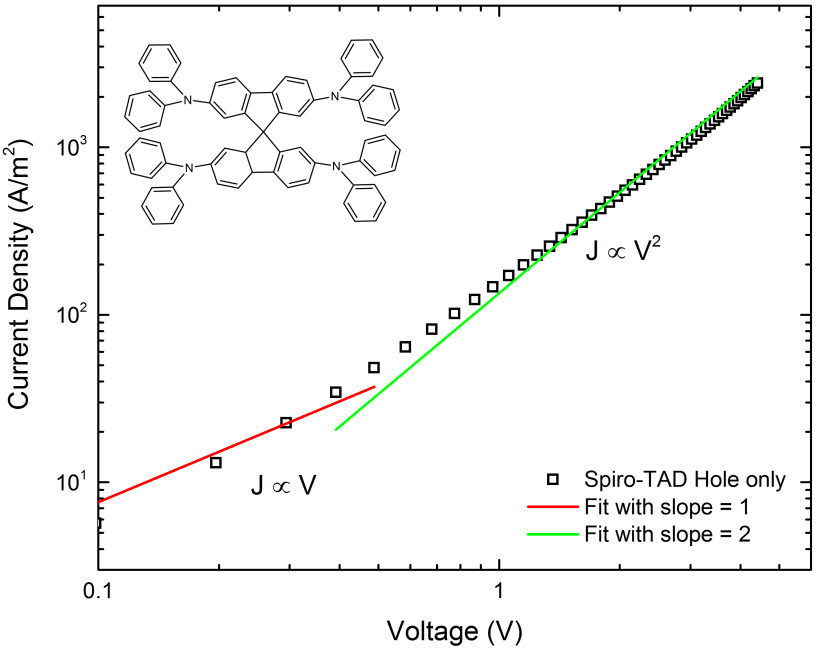

Figure 2.12.: Hole only device characteristics. The current density vs voltage characteristics of a symmetric hole only device of Spiro-TAD are shown here. The red line is a fit with the slope of 1, which corresponds to the ohmic regime, while the green line is a fit with slope of 2 and corresponds to the space charge limited regime.

As the applied voltage increases further, charge carriers are injected from the contact and the current starts to grow rapidly. For an asymmetric device this occurs at the

built-in voltage. The current eventually reaches a slope of 2, which corresponds to the space charge limited current and is described by the Mott-Gurney law [65] as following

$$J_{SCLC} = \frac{9}{8}\varepsilon\mu\frac{(V - V_{bi})^2}{L^3} \tag{2.25}$$

where, ε is the dielectric constant of the organic semiconductor. This current is mainly due to the drift of injected charge carriers under the influence of the applied voltage (electric field), and is known as drift current. This space charge limited current regime is marked by the green line with a slope of 2 in Figure 2.12.

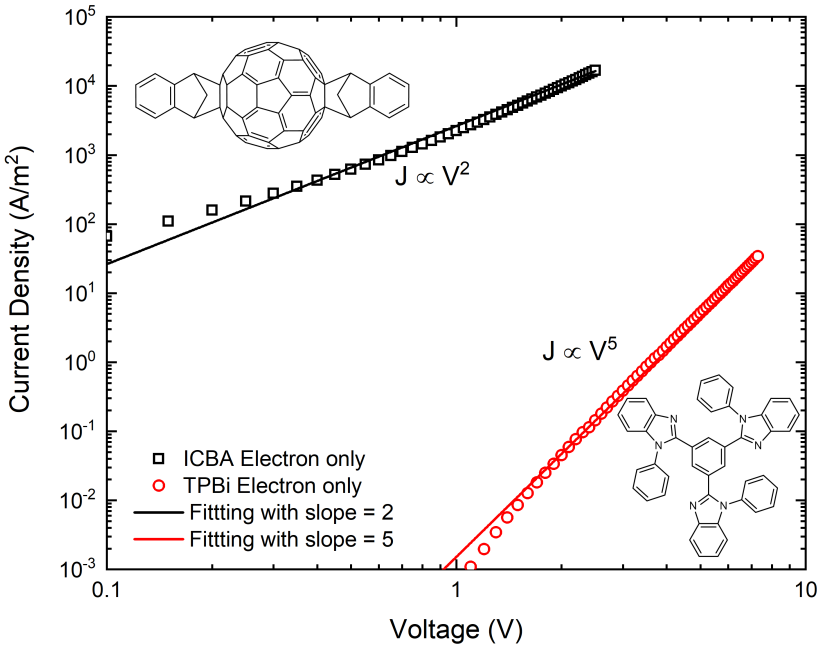

Figure 2.13.: Electron only device characteristics. Current density–voltage characteristics of symmetric electron only device of ICBA and asymmetric electron only device of TPBi are shown here. The ICBA current has a quadratic dependence on voltage, typical behavior for trap free transport. While TPBi current has a stronger voltage dependence, meaning it has trap limited electron transport.

Figure 2.13 shows the electron transport of ICBA and TPBi which are typically used as electron acceptor in organic solar cells and electron transport layer in OLEDs, respectively. For ICBA a space-charge-limited current is measured and shows quadratic dependence on the voltage, a typical signature of trap free transport. The behavior is marked by a fit using a black line with slope of 2 corresponding to the Mott-Gurney law. However, at the same applied voltages, the TPBi current is 5 to 6 orders of magnitude lower than the ICBA current. The TPBi current has stronger voltage dependence as marked by the fit using the red line with slope of 5. This is a signature of trap limited electron transport in TPBi as described by the Mark Helfrich equation explained earlier.

When materials with traps are used as active layers or charge transport layers in organic electronic devices, higher driving voltages will be required and device stability will be reduced. Obtaining trap free and balanced transport in a single material is still a huge challenge. In chapter 6 charge transport in a large number of organic semiconductors is investigated and trap originating factors based on water complexes are discussed in details.

2.6. Excitons

In the performance of organic semiconductor devices, bound electron-hole pairs known as excitons play crucial role. They are formed when charges are injected (e.g. in OLED) or when photons are absorbed (e.g. in solar cells and photo-detectors). In organic semiconductors, excitons are mainly of the Frenkel type, in which the electrons and holes are located on the same molecule as shown in Figure 2.14(a). Frenkel excitons have a strong binding energy of around 0.5 eV, have a small radius of ∼1 nm and well defined spin states such as singlet or triplet. As excitons are charge neutral, they move via diffusion and their motion can be described by Dexter or Forster energy transfer models [29].

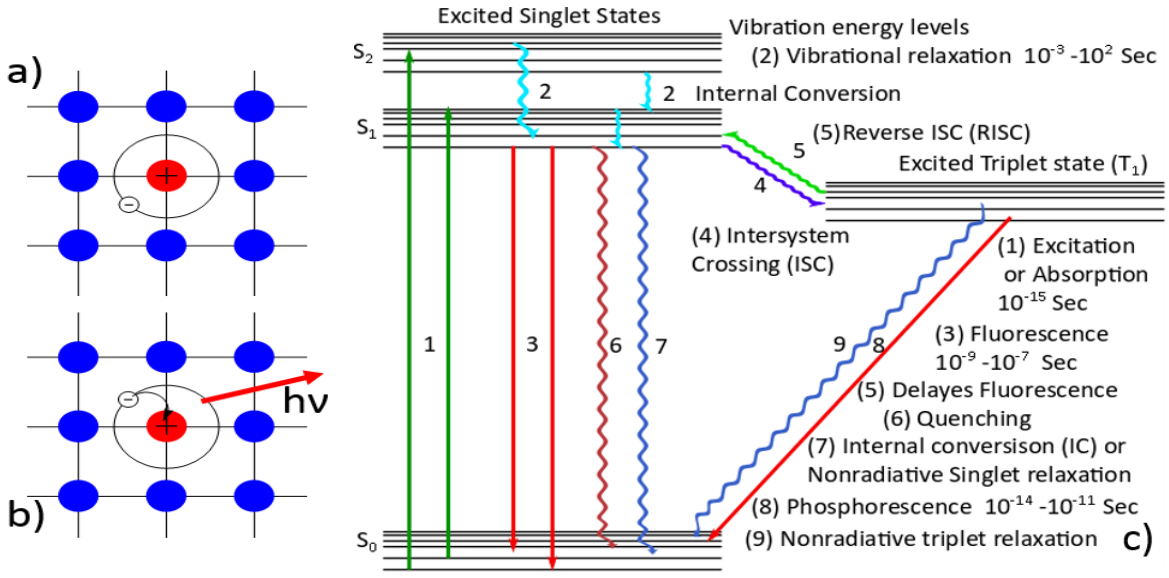

Figure 2.14.: Exciton and excitonic processes. (a) Frenkel exciton localised on a molecule. (b) Radiative decay of Frenkel exciton. (c) Jablonski diagram showing energy levels of singlet and triplet states and different processes [66, 67].

Since both the electron and hole have spins, when they form an exciton four different spin combinations are possible. According to quantum mechanical spin coupling rules,

the total spin of the exciton can either be S = 0 or S = 1. There is one possible spin state with S = 0, which is why this state is called singlet exciton. In contrast, there are three different spin states with S = 1, namely S_3 = 1, S_3 = 0 and S_3 = -1. Therefore, excitons with total spin of S = 1 are called triplet excitons. Accordingly, the statistical probability for forming singlet excitons is 25% and for triplet excitons is 75% [68, 69].

Singlet excitons have a lifetime in the nanoseconds (ns) range, as they can radiatively decay via dipole transitions. In contrast, a decay via dipole transitions is forbidden for triplet excitons by quantum mechanical selection rules. Thus they usually decay non-radiatively, generate heat and have a lifetime in the range of microseconds μs. This limits the internal quantum efficiency (IQE) of polymeric or small molecule OLEDs based on fluorescent (singlet) emitters to 25%. Figure 2.14(c) shows triplet and singlet energy levels along with fluorescence and phosphorescence processes.

Efforts have been made to improve the IQE up to a maximum of 100%. In the first approach, Forrest and co-workers introduced heavy transition metal atoms (e.g. Pt or Ir) into organic molecules, This increases spin-orbit coupling and dipole transitions from the triplet to the ground state become possible [21, 22]. Then, triplet excitons can decay radiatively, via a process called phosphorescence. OLEDs based on phosphorescence are known as PhOLEDs, as both singlet and triplet excitons decay radiatively they can reach IQEs upto 100%. Although PhOLEDs have been widely commercialized, the use of rare heavy metals makes them toxic, expensive, and limits their stability in particular for the blue PhOLEDs.

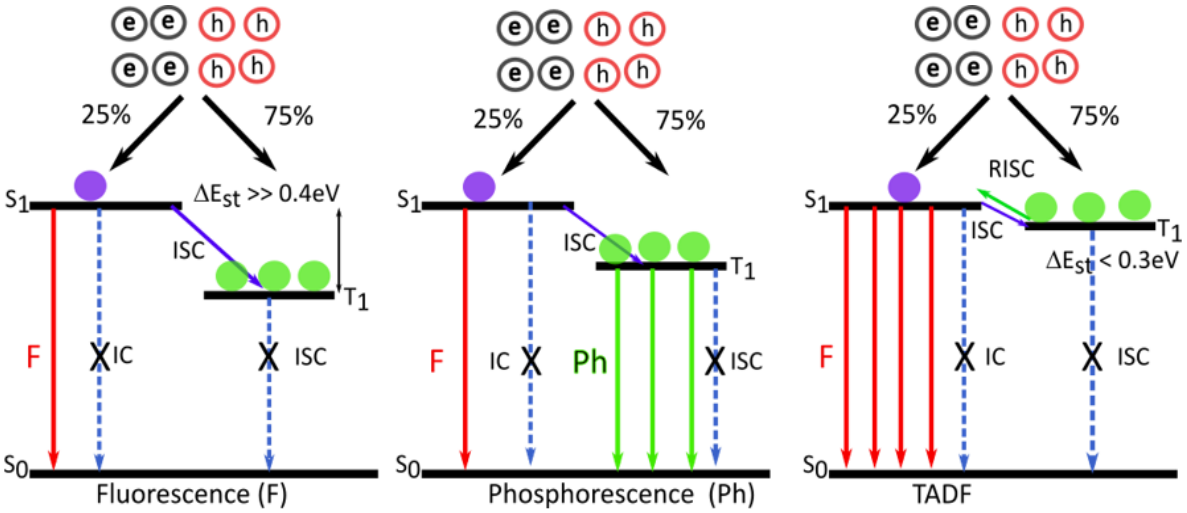

Figure 2.15.: Exciton based classification of organic semiconductors. Energy diagram showing energy levels and excitonic process in fluoroscence, phosphorescence and TADF OLEDs [70].

In conventional fluorescent materials, the energy gap between singlet and triplet en-

ergy levels ΔE_{st} is around 0.5−1.0 eV. So, reverse intersystem crossing (transition of triplet exciton to singlet) RISC is not possible at room temperature. For effective RISC, ΔE_{st} needs to be lower than 100 meV. In the second approach to obtain a higher IQE in OLEDs Adachi and co workers used molecular design methods to lower the ΔE_{st} by spatial separation of the HOMO and LUMO distributions within the molecule [23, 24]. Separation of HOMO and LUMO decreases the transition dipole moment μ for the radiative decay from singlet states $S_1 \rightarrow S_0$. However, a sufficient HOMO and LUMO overlap is possible in the region away from the electrons in the HOMO or LUMO. So, the simultaneous requirement of a low ΔE_{st} for RISC and a high dipole moment μ for the radiative singlet emission is possible. With such a design of low ΔE_{st}, at room temperature triplet excitons can be converted into singlet excitons, which decay radiatively achieving IQEs upto 100% as shown in Figure 2.15. Such materials are commonly known as TADF (thermally assisted delayed fluorescent) materials. Since TADF materials are free of toxic and unstable metal complexes, presently they are investigated intensively for the use in commercial display and lightning panels [70, 71]. Figure 2.15 shows a comparison between excitonic processes in fluoroscence, phosphorescence and TADF materials.

2.7. Organic light emitting diodes (OLEDs)

2.7.1. Single layer OLED

The simplest OLED structure is obtained by sandwiching a semiconducting electroluminescent small molecule or polymer (emitter) between two metal electrodes. One electrode needs to have a high workfunction (Φ) which serves as anode and the other electrode needs to have a low workfunction which serves as cathode. When the electrodes are contacted to the emitter, their Fermi energy (E_F) levels align. Due to the difference in work function of the anode and cathode a built-in potential $\Phi_{bi} = \Phi_A - \Phi_C$ is established across the OLED. In order to inject charge carriers a voltage greater than $V_{bi} = (\Phi_A - \Phi_C)/e$ must be applied [72]. Figure 2.16 shows the band diagram of OLED at different applied voltages (V_{ext}).

The operation of an OLED depends on some important energy levels. Work function (Φ) of the metal, which is given by the energy distance of the Fermi energy (E_F) level from the vacuum level, ionization energy (IE), which is given by the energy distance of HOMO from the vacuum level, and electron affinity (EA), which is given by the energy distance of the LUMO level from the vacuum level.

Due to the energetic difference between the anode workfunction and the ionization energy of the emitter, an injection barrier for holes (Φ_h) exists at the anode/emitter interface and can be approximated by $\Phi_h = \Phi_A - I$. Similarly, due to the difference between the cathode workfunction and the electron affinity of the emitter, an injection barrier for electrons (Φ_e) exists at the cathode/emitter interface and can be approxi-

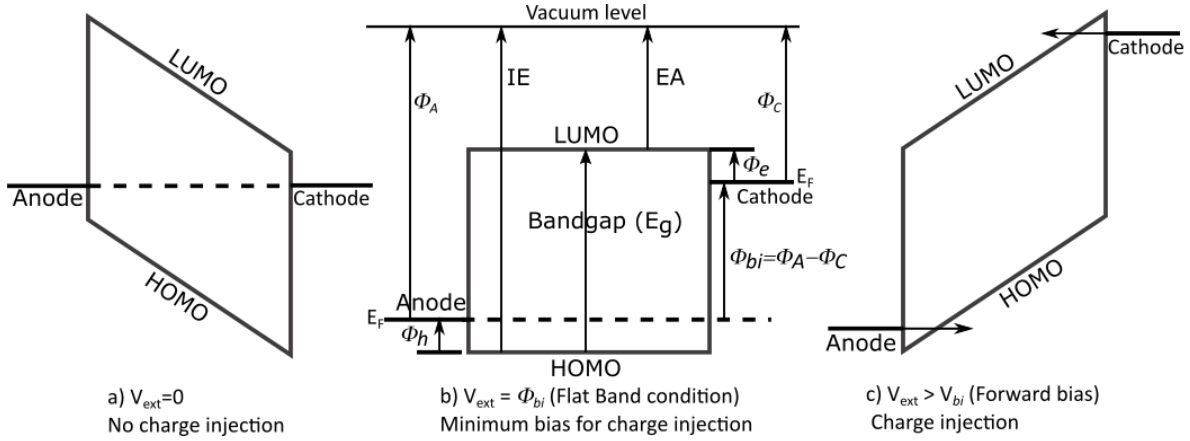

Figure 2.16.: Energy band diagram of OLED at different biased voltages. Ionization energy (IE), electron affinity (EA), work functions of anode (Φ_A) and cathode (Φ_C), Injection barriers for hole (Φ_h) and electron (Φ_e) are also shown.

mated by $\Phi_e = \Phi_C - A$.

In OLEDs, one of the electrodes needs to be transparent, such that the generated light can leave the OLED. Indium tin oxide (ITO) coated on glass is commonly used as transparent anode. The light emitting small molecule or polymer layer, usually with a thickness of around 70-100 nm, is either thermally deposited (for small molecule emitters) or coated from solution (for polymer emitters) on ITO. Following that, a metal cathode is deposited on the emitter by thermal evaporation. The resulting structure consists of ITO(anode)/Emitter/Metal(cathode) as shown in Figure 2.17(a). When an external voltage (V) is applied across such an OLED, charge carriers are injected after surmounting the barriers. Electrons are injected from the cathode into the LUMO of the emitter and holes are injected from the anode into the HOMO. Under the influence of the applied electric field, electrons and holes move in opposite directions via a hopping processes. If they encounter each-other, they recombine to form an exciton and transfer the released binding energy to the lattice. Being charge neutral, excitons are not influenced or drifted by the electric field and thus diffuse in a random direction. When excitons decay (i.e. electron and hole recombine) photons are emitted at a wavelength corresponding to the bandgap of the light emitting small molecule or polymer. Figure 2.17 (b) shows the formation of a singlet exciton and the subsequent photon emission when the exciton decays.

2.7.2. Limitations and ways to improve the performance of OLEDs

For an efficient device operation, one needs to have low injection barriers and a good balance of charge carriers in the emitting material. If the transport of one of the charge carriers dominates in a single layer OLED, excitons will be formed close to one of the electrode interfaces, as shown in Figure 2.18. In such a case, the formed excitons will

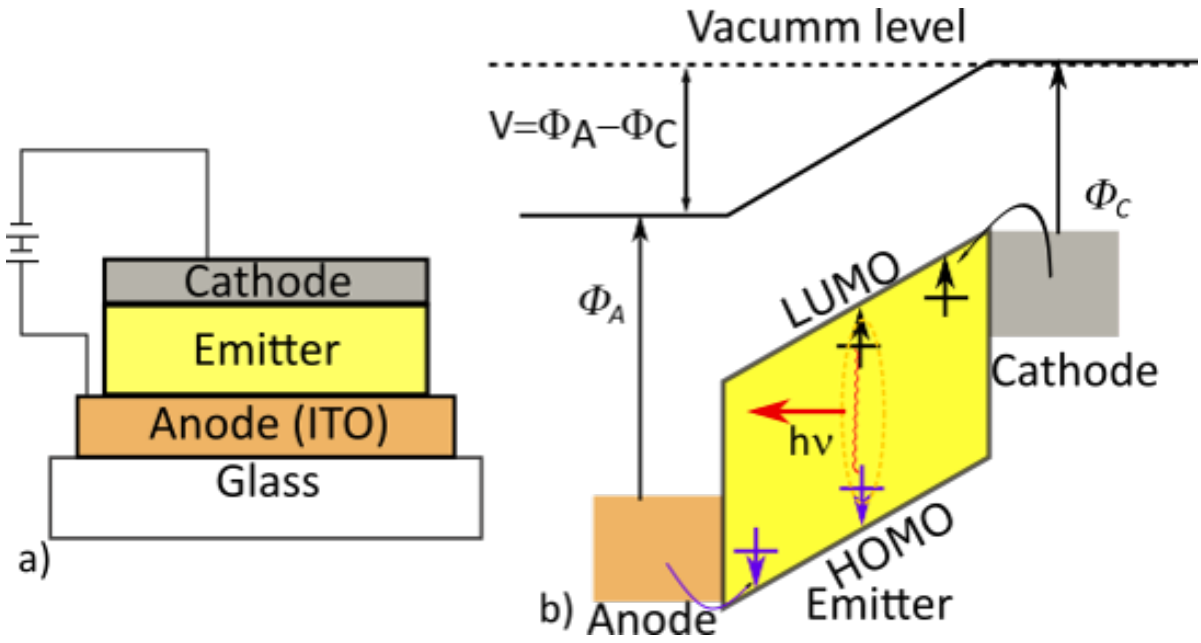

Figure 2.17.: Single layer OLED (a) Simple OLED device structure consisting of ITO(anode)/Emitter/Cathode. (b) Band diagram of an OLED in forward biased condition with applied voltage V. Anode and cathode workfunctions are represented by Φ_A and Φ_C, respectively. Charge injection, singlet exciton formation and photon emission is also shown [73]

.

transfer their energy non radiatively to the electrode. This process is called exciton quenching, which severely reduces the device efficiency [74, 75, 76]. In case of single layer devices, one would like to have the recombination zone in the center of the emitting layer.

Most light emitting organic semiconductors (small molecules or polymers) have superior hole transport compared to electron transport, as they commonly exhibit severe electron trapping. In such emitters, hole transport dominates over electron transport and the recombination zone lies close to the emitter/cathode interface. This leads to quenching of excitons at the metal cathode [47, 50, 77]. In addition, charge injection barriers are often present at the electrode. To resolve this issue, multilayer device architectures have been developed.

A typical multilayer OLED device architecture consist of an emitter, charge injection (EIL and HIL) layers, charge transport layers (ETL and HTL) and charge blocking layers (EBL and HBL) as shown in Figure 2.19. In order to avoid quenching of excitons due to emitter molecules being to close to each other, the emitter is diluted by doping it into a host matrix, constituting the emissive layer. Each layers has a distinct role, the EIL and HIL lower the charge injection barriers for efficient injection of electrons and holes from the metal contacts. The ETL and HTL transport injected electrons and holes

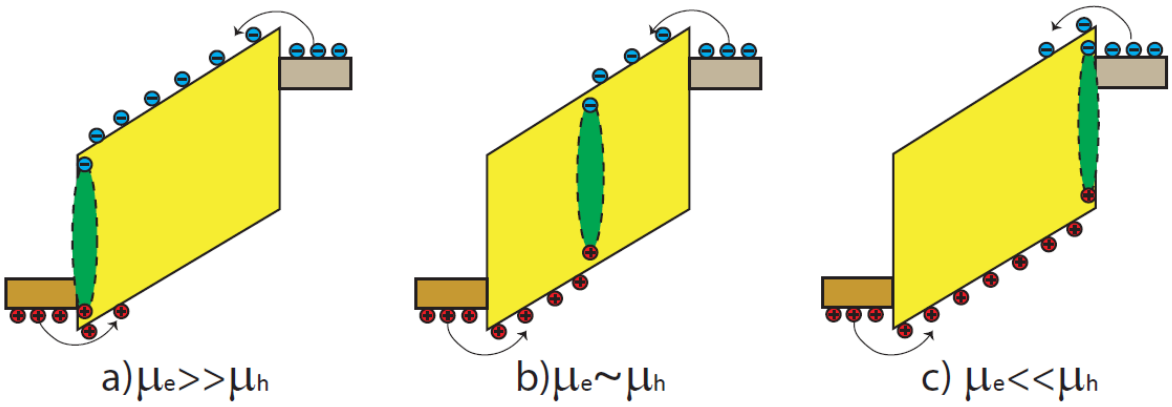

Figure 2.18.: Exciton quenching at electrodes due to unbalanced conduction of electron and holes in the emitter is shown. An efficient OLED requires similar mobilities for electrons and holes.

to the emissive layer. The EBL has LUMO higher than the emitter and the HBL has HOMO deeper than the emitter so they confine the electron and holes in the emissive layer as shown in Figure 2.19. When an external bias is applied, all the excitons will be exclusively formed in the emissive layer and far away from the electrodes, resulting in a very high efficiency [78, 79, 80]. It is often possible to combine charge transport and charge blocking functionalities in one layer (for eg. HTL and EBL), in such case the number of layers can be reduced to five to six compared to seven as shown in Figure 2.19.

Multilayer device architectures exhibit far superior efficiency and stability compared to single layer device architectures, which resulted in their wide commercialization in present days. However, they are expensive as often seven to nine different organic materials are required. In addition, several manufacturing steps are needed to deposit the consecutive layers, which also involves co deposition of two or three materials [12]. In addition, to achieve the best performance, every device layer has to be optimized. Moreover, due to the complexity of the multilayer architecture, it is extremely difficult to identify the factors limiting the operational stability.

An ideal OLED would be efficient, stable and can be produced economically. We have resolved this issue in chapter 7, where by using our charge injection method described in chapter 3 and the knowledge about charge trapping from chapter 6, a novel undoped single layer OLED is designed and fabricated. The device shows good efficiency, improved stability and in addition has a much simpler device structure compared to the commercial multilayer architectures.

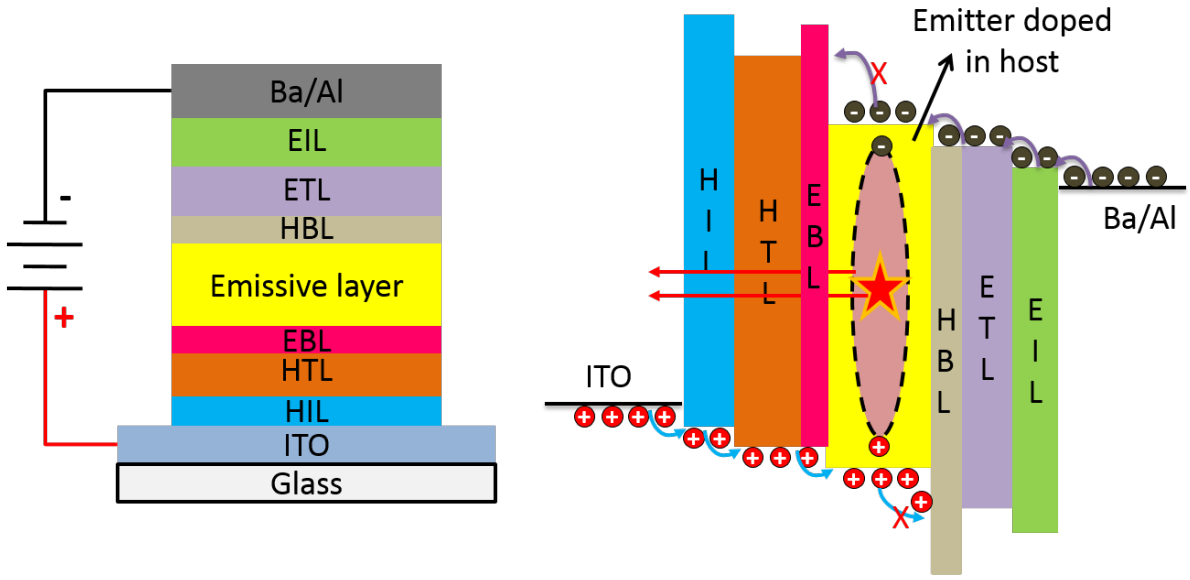

Figure 2.19.: Left: Device architecture of a multilayer OLED, HIL and EIL are hole and electron injection layers respectively, HTL and ETL are hole and electron transport layers respectively, HBL and EBL are hole and electron blocking layers respectively. Right: Energy level diagram of a multilayer OLED, the direction of the motion of electrons, holes and the formation of excitons in the device are shown. Light exits the device through the transparent electrode, for which typically ITO is used. (For simplicity a flat band diagram is shown.)

2.8. Current-Voltage Characteristics of OLEDs

Figure 2.20 shows the current density-voltage characteristics of three different single layer OLEDs represented by red, green and blue curves. The curve shown in red represents an OLED with trap free transport for electron and holes, while those shown in green and blue have trap limited charge transport. The different current regimes are marked by points **1-2 and 3**, which will be explained subsequently in the following sections.

At low voltages until point **1** in Figure 2.20 the current in the device is very low and is called the leakage current. The current in this regime increases linearly with the applied voltage. In the case of a device that has a microscopic shorts, the magnitude of the leakage current will be much higher than shown in the Figure 2.20 [81].

Although, the intrinsic charge carrier concentration in the device is low, some charge carriers diffuse from the metal contact into the active layer of the device (in the single layer OLED structure) [64]. As the applied voltage increases beyond point **1** in the Figure 2.20, the contribution of these diffused charge carriers starts to appear. The current in this regime is mainly due to diffusion of charge carriers (motion due to concentration gradient) under the influence of the applied voltage. This regime is called diffusion regime, and occurs until the applied voltage is less than the built in voltage ($V < V_{bi}$),

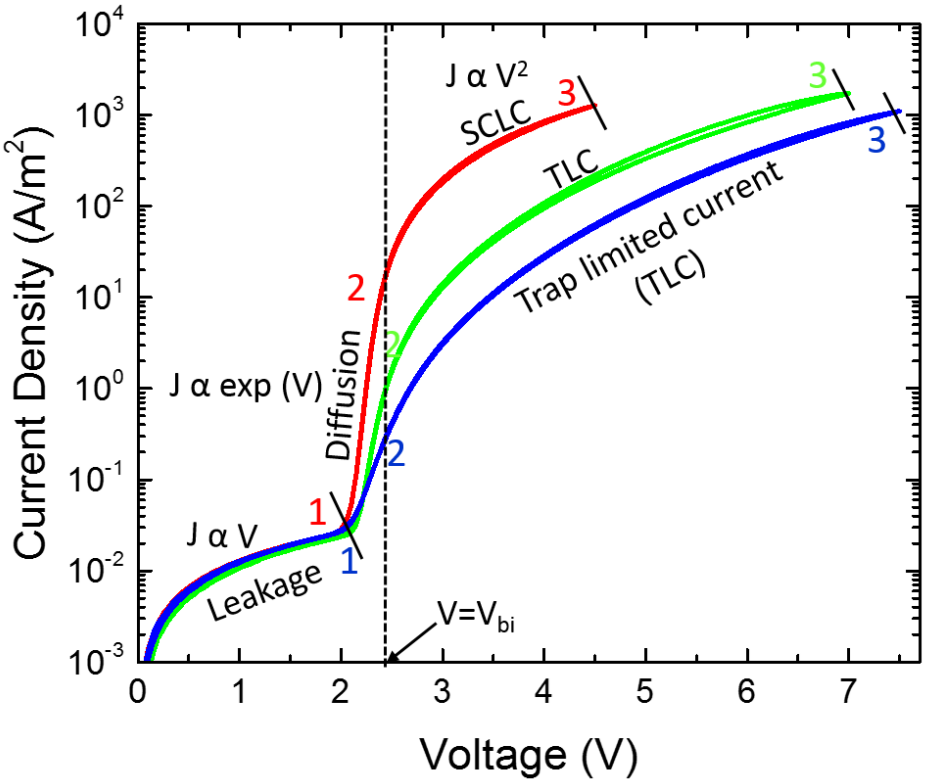

Figure 2.20.: Current density-voltage characteristics of single layer OLEDs. The curve in red is from an OLED having trap free transport of electrons and holes. The green and blue curves are from OLEDs having both electron and hole traps. The OLED in blue curve has a comparatively higher number of traps than the OLED represented by the green curve. The different charge transport regimes are marked by the numbers in the figure. Until point 1, the current increases linearly with the applied voltage and is called leakage current, from point 1 to 2 it increases exponentially and is called diffusion regime. Point 2 markes the built-in voltage, at which a transition from the diffusion-dominated to the drift-dominated current occurs. From point 2 to 3 the current is in the drift regime and is characterized by a space-charge-limited current (SCLC) for the free case (red curve). For an OLED with traps (green and blue curves), at low voltages the current is much lower in magnitude compared to the the trap free case (red). As the voltage increases, traps are filled by charge carriers and the current starts to increase rapidly, so the current in this case is known as the trap limited current (TLC) which has stronger dependence on the applied voltage.

marked by point **2** in the Figure 2.20. In this regime, the current flows against the direction of the built-in electric field, and is therefore dominated by diffusion [82]. The current increases exponentially in this regime with the applied voltage and is described by Shockley equation

$$J = J_0 \left[\exp\left(\frac{eV}{\eta k_B T} \right) - 1 \right] \tag{2.26}$$

where, J_0 is the saturation current density, can be determined by extrapolating to zero voltage, η is ideality factor, whose value ranges between 1 to 2, k_B is Boltzmann constant and T is the temperature.

The ideality factor η in the above equation can be used as a measure of the OLED quality. In the case of an ideal trap free OLED, electron and holes mainly recombine radiatively and η has a value 1. While in the case of OLEDs in which either electron or hole traps are present, the trap assisted recombination process will be dominant, and η has a value 2 [83].

As the applied voltage increases above the built in voltage ($V > V_{bi}$), the current flows in the direction of the electric field inside the device. Now, the current in the device is dominated by the charge carriers injected from the contacts. The current, is mainly due to drift of the charge carriers under the influence of the applied voltage (or electric field). So, this is called as drift-regime occurring between points **2** and **3** in the Figure 2.20. The current in this regime increases quadratically with the applied voltage and is limited by the buildup of space charge. Therefore, the current is referred to as a space-charge-limited current (SCLC).

The above description is valid for an ideal OLED in which there is no significant trapping of charge carriers, as show by red curve in Figure 2.20. However, in reality majority of OLED materials show trapping of charge carriers, while electron trapping is more common, trapping of both electron and holes are often observed. The green and red curves shown in Figure 2.20 are from OLED having both electron and hole traps, the OLED shown in the blue has a higher number of traps compared to the one shown in green. In such case, we have to include the contribution from trapping, which can be determined for the single carrier electron or hole only devices, as described earlier.

At low voltages, the currents in the trap limited OLEDs can be a few order of magnitudes lower than trap free OLEDs as shown by the green and blue curves in the Figure 2.20. As the applied voltage increases, the traps are filled by charge carriers and the current increases rapidly. The current is known as a trap limited current (TLC), which has stronger voltage dependence compared to the trap free case. If only small a number of traps is present, at higher voltages they will be filled by charge carriers and current will eventually reach the space charge limit. However, if a significantly large number of traps is present, even at higher voltages the traps may still not be filled as shown by the blue curve in the Figure 2.20. The charge trapping severely reduces the efficiency of an OLED and still today is a major scientific challenge to be solved.

3. Ohmic Hole Injection in Organic Semiconductors

In this chapter, we discuss the hole injection strategy developed for organic semiconductor based optoelectronic devices. Barrier-free (Ohmic) contacts are a key requirement for efficient organic optoelectronic devices, such as organic light-emitting diodes, solar cells, and field-effect transistors. Here, we propose a simple and robust way of forming an Ohmic hole contact on organic semiconductors with a high ionization energy (IE). The injected hole current from high-work-function metal-oxide electrodes is improved by more than an order of magnitude by using an interlayer for which the sole requirement is that it has a higher IE than the organic semiconductor. Insertion of the interlayer results in electrostatic decoupling of the electrode from the semiconductor and realignment of the Fermi level with the IE of the organic semiconductor. The Ohmic-contact formation is illustrated for a number of material combinations and solves the problem of hole injection into organic semiconductors with a high IE of up to 6 eV. [1]

3.1. Introduction and Background

One of the most important requirements for efficient organic-semiconductor devices is the establishment of Ohmic contacts for holes and electrons. To create an Ohmic contact for holes, the electrode work function should match the ionization energy (IE) of the organic semiconductor. In organic light-emitting diodes (OLEDs), materials with an IE as high as 6 eV are commonly used as hosts and emitters [84, 85]. However, typical electrodes used in organic devices, such as indium-tin oxide (ITO) and poly(3,4-ethylenedioxythiophene)-poly(styrenesulfonate) (PEDOT:PSS) have work functions close to 5.0 eV [86, 87], which give rise to large injection barriers. Since the injected current depends exponentially on the injection barrier [53], it is vital to find hole-injecting electrodes with a considerably higher work function. For example, chlorinated ITO can reach work functions of up to 6.1 eV [87]. However, a sizable contact barrier of about 0.5 eV was still observed when the electrode was put in contact with the popular $4,4'$-bis(N-carbazolyl)-$1,1'$-biphenyl (CBP) organic host material, which has an IE of 6.0 eV [87].

An alternative method to obtain Ohmic contacts is the use of a p-type doped hole-injection layer. The resulting strong band bending in the doped layer then allows for injection via tunnelling. However, a typical p-type dopant such as F6TCNNQ has an

[1] This chapter is published as *Universal strategy for Ohmic hole injection into organic semiconductors with high ionization energies.* Naresh B. Kotadiya, Hao Lu, Anirban Mondal, Yutaka Ie, Denis Andrienko, Paul W.M. Blom, and Gert-Jan A.H. Wetzelaer. Nature materials, 17(4):329, 2018.

electron affinity of ∼5.6 eV [88], such that doping will not be effective for semiconductors with an IE larger than 5.6 eV. Very recently, a strategy was reported to achieve doped organic-semiconductor films with work functions up to 5.8 eV [89]. Using a doped polymer film as a hole-injection layer, it was shown that hole injection into a conjugated polymer with an IE of 5.8 eV was almost as efficient as the injection from a thermally evaporated MoO_3 reference.

MoO_3 is widely used as a hole contact in organic solar cells and OLEDs, owing to its extremely high work function of 6.9 eV [90]. MoO_3 is an n-type semiconductor, with an electron affinity of 6.7 eV and an ionization energy of 9.7 eV [90]. Because of its high electron affinity, MoO_3 can be used as a p-type dopant in CBP [91]. Since transition-metal oxides like MoO_3, V_2O_5 and WO_3 possess the combined quality of optical transparency and a very high work function of 6.7−7.0 eV, they seem to be ideal hole contacts, and are frequently applied in organic-semiconductor devices [92].

Here, we demonstrate that despite their high work function, transition-metal oxides give rise to a considerable injection barrier when put into contact with organic semiconductors. We present a strategy to completely eliminate this injection barrier by electrostatically decoupling the electrode from the organic semiconductor, enabling the formation of an Ohmic contact with organic semiconductors with an IE as high as 6 eV.

3.2. Results and Discussion

A direct way to investigate the hole-injection capability of an electrode into an organic semiconductor is to fabricate so-called hole-only devices. In such a device, an organic-semiconductor layer is sandwiched between two high-work-function electrodes, to prevent the injection of electrons. When applying a voltage across the device, the measured current is carried exclusively by holes, and the magnitude of the current is a measure of the hole-injection capabilities of one of the two electrodes, depending on the sign of the applied voltage. Since the current depends exponentially on the injection barrier [53], the measured current is very sensitive to changes in the barrier height. When the barrier height approaches zero, the contact can be regarded as Ohmic, and a transition from an injection-limited current into a space-charge-limited current will occur, which is governed by the charge-carrier mobility of the organic semiconductor [47, 93].

In Figure 3.1a, the current through a hole-only device of the organic semiconductor $2,2^{'},7,7^{'}$-tetrakis(N,N-diphenylamino)-9,9 -spirobifluorene (Spiro-TAD) is displayed. Here, Spiro-TAD is sandwiched between a PEDOT:PSS bottom electrode and a MoO_3(10 nm)/Al top electrode. Since Spiro-TAD has a moderate IE of 5.3 eV [94], hole injection from MoO_3 with a high work function of 6.9 eV is expected to be efficient. Surprisingly, as can be seen in Figure 3.1, the current injected from MoO_3 (forward bias) is even lower than the current injected from PEDOT:PSS (reverse bias). Apparently, a hole-injection

barrier at the Spiro-TAD/MoO_3 interface is present that lowers the injected current. As also can be observed in Figure 3.1a, the hole injection is improved considerably by inserting a 5 nm layer of tris(4-carbazoyl-9-ylphenyl)amine (TCTA) between Spiro-TAD and MoO_3. By using the TCTA interlayer, the current injected from MoO_3 increases by over an order of magnitude, up to a factor of 30. This is a counterintuitive result, since TCTA has a higher IE (5.7 eV [95]) than Spiro-TAD, which usually aggravates hole-injection problems.

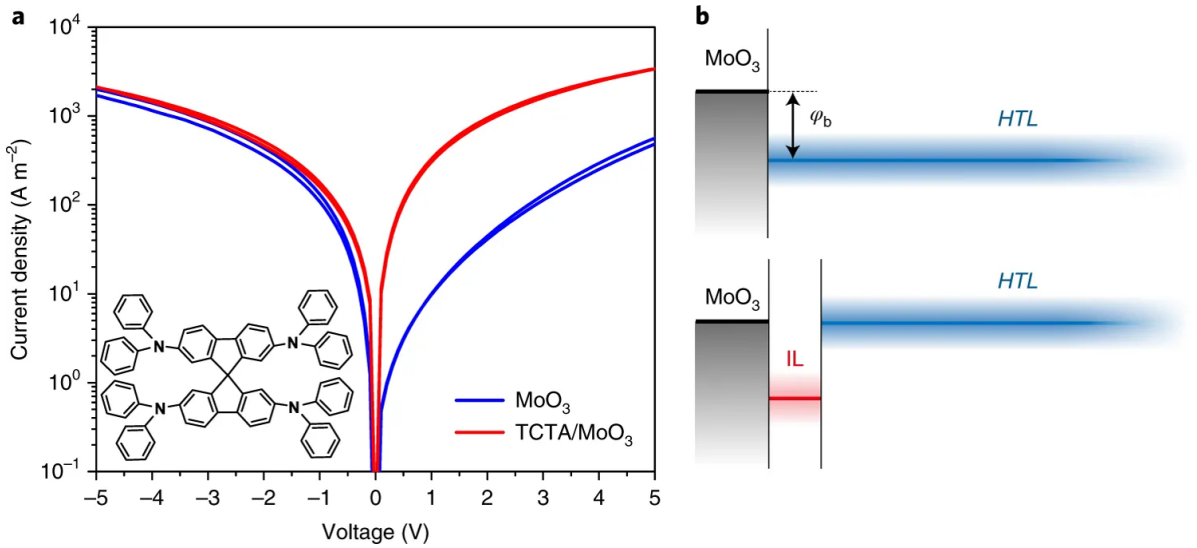

Figure 3.1.: Hole-injection enhancement in Spiro-TAD. **a**, Current density-voltage characteristics of a PEDOT:PSS/Spiro-TAD/MoO_3 hole-only device with and without a TCTA (5 nm) interlayer between the Spiro-TAD (163 nm) transport layer and MoO_3. Negative bias corresponds to hole injection from the PEDOT:PSS, positive bias to hole injection from MoO_3. The inset shows the molecular structure of Spiro-TAD. **b**, Schematic energy-band diagram showing the effective injection barrier (φ_b) between MoO3 and the hole-transport layer (HTL). Introducing an interlayer (IL) with a higher IE realigns the Fermi level with the IE of the HTL.

To demonstrate that the injection barrier at the organic/MoO_3 interface is not an exclusive property of Spiro-TAD, Figure 3.2. shows that a similar hole-injection barrier exists between MoO3 and the organic small molecules TCTA and CBP, which have IE values of 5.7 eV and 6.0 eV, respectively [95]. For both materials, the current injected from MoO_3 is improved by more than an order of magnitude by inserting a 5 nm interlayer of an organic semiconductor with a higher IE. In fact, independent of the material used for the interlayer, the current is universally improved to the same magnitude and voltage dependence, even for a material with a high IE, such as CBP.

Identical improvements were obtained for the high-work-function metal oxides V_2O_5 and WO_3, as shown in the Figure B.1a. It is also demonstrated in the Figure B.1,B.2 that equally high currents are obtained when applying the interlayer strategy to the

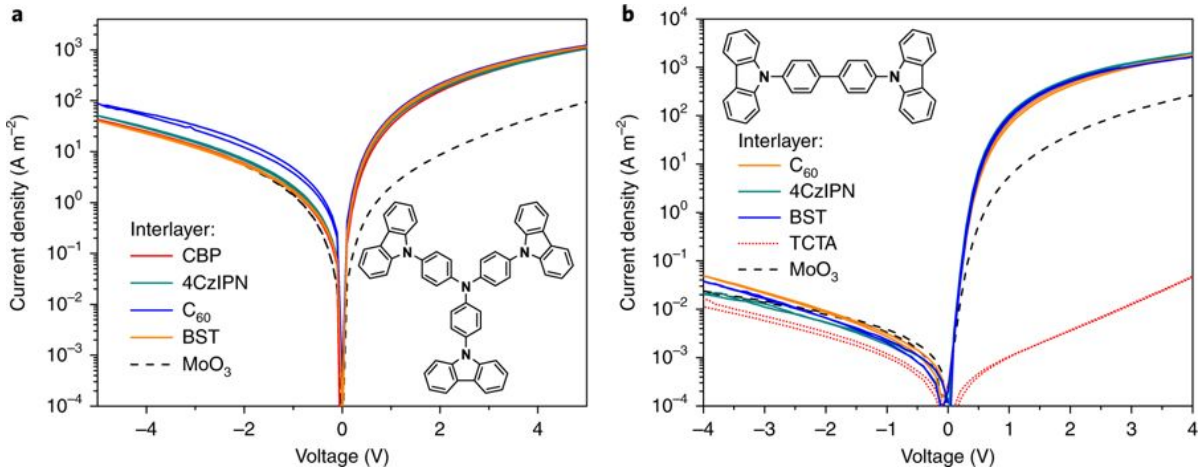

Figure 3.2.: Hole-injection enhancement with different interlayers. **a,b** Current density–voltage characteristics of TCTA (**a;** 239 nm) and CBP (**b;** 215 nm) hole-only devices with different interlayers. The hole current injected from MoO_3 (positive bias) improves to the same level whenever the IE of the interlayer is larger than the IE of the transport layer. For the case of CBP with a TCTA interlayer (**b;** red dotted line), the offset in IE is negative, resulting in a large reduction of the injected current. The insets in **a** and **b** show the molecular structures of TCTA and CBP, respectively.

bottom electrode. MoO_3 can diffuse into the organic layers when it is deposited on top of organic semiconductors, while a non-intermixed interface is obtained when organic layers are deposited on top of MoO_3 [95]. Despite deposition-order inversion, improvements in hole injection are identical, ruling out diffusion of MoO_3 as the mechanism for the observed hole-injection enhancement.

Figure 3.2b also shows how problematic hole injection into CBP is with conventional hole-injection layers such as PEDOT:PSS (reverse bias). The current in reverse bias is around five orders of magnitude lower than the current injected in forward bias, which is the result of the hole-injection barrier arising from the mismatch between the work function of PEDOT:PSS (5.0−5.2 eV) and the IE of CBP.

From the results on Spiro-TAD, TCTA and CBP (shown in B), it is inferred that hole injection is improved universally when the offset between the IE of the interlayer and transport material is larger than $0.2 - 0.3$ eV. Conversely, when the IE of the interlayer is lower than the IE of the transport material, resulting in an energetic staircase, the injected current drops by several orders of magnitude. This is demonstrated in Figure 3.2b for the case of a TCTA interlayer on CBP, for which the IE offset has a negative value of -0.3 eV. It appears that there is no maximum to the value of the offset: the improvement in injection is observed for offsets of more than 1 eV.

The fact that the current for all investigated organic semiconductors reaches a maximum magnitude independent of the interlayer used strongly suggests that the current

is no longer injection limited. This would imply that the use of an interlayer results in the formation of an Ohmic contact. To validate this hypothesis, it should be verified that the injected currents are space-charge limited. A space-charge-limited current is the maximum electrostatically allowed current that can pass through the organic-semiconductor layer. A trap-free space-charge-limited current is characterized by the Mott-Gurney square law [65]

$$J = \frac{9}{8}\varepsilon\mu\frac{(V - V_{bi})^2}{L^3} \tag{3.1}$$

where J is the current density, ε is the permittivity, μ is the charge-carrier mobility, V is the voltage, V_{bi} is the built-in voltage due to asymmetric work functions of the electrodes, and L is the layer thickness.

To test if the injected hole currents are indeed space-charge limited, the current needs to fulfill two important criteria: the current depends quadratically on voltage; and the current scales inversely with layer thickness to the third power. The layer-thickness dependence can be directly confirmed by plotting JL^3 against voltage. In case of a space-charge-limited current, the measured current for a range of layer thicknesses will collapse onto a single curve. This is indeed the case, as shown in Figure 3.3. For all tested organic semiconductors, the L^{-3} layer-thickness dependence is fulfilled. In addition, the experimental current depends on the square of voltage, proving that the injected current is indeed space-charge limited. The establishment of a space-charge-limited current after insertion of the interlayer confirms the formation of an Ohmic hole contact. These results therefore demonstrate the formation of a truly Ohmic contact on organic semiconductors with an IE of up to 6 eV.

A space-charge-limited current can also be used to determine the charge-carrier mobility of organic semiconductors, as is evident from equation 3.1. The mobilities determined for 2-TNATA, Spiro-TAD, TCTA and CBP are in excellent agreement with the low-field values measured by the time-of-flight technique as shown in Table 3.1. It is known that the time-of-flight technique can overestimate the mobility, especially when charge trapping is present [96]. However, the fact the mobilities from space-charge-limited currents are close to the time-of-flight values shows that hole injection is indeed maximized (Ohmic contact) by using an interlayer and also that the current is not decreased by trapping effects. Interestingly, as a result of the high injection efficiency of the interlayer-enhanced contact, the space-charge conductivity of an 88 nm undoped CBP layer amounts to 2.5×10^{-6} Scm^{-1}, which even surpasses the conductivity of highly p-doped CBP with 22.1 mol% of MoO_3 1×10^{-6} Scm^{-1} [91].

Knowing the hole mobilities from the measured space-charge-limited currents, we can now determine the injection barriers from the injection-limited currents observed for transition-metal oxide electrodes (MoO_3,V_2O_5 and WO_3) without an interlayer. For all investigated organic semiconductors and metal oxides, an injection barrier of 0.39 ± 0.03

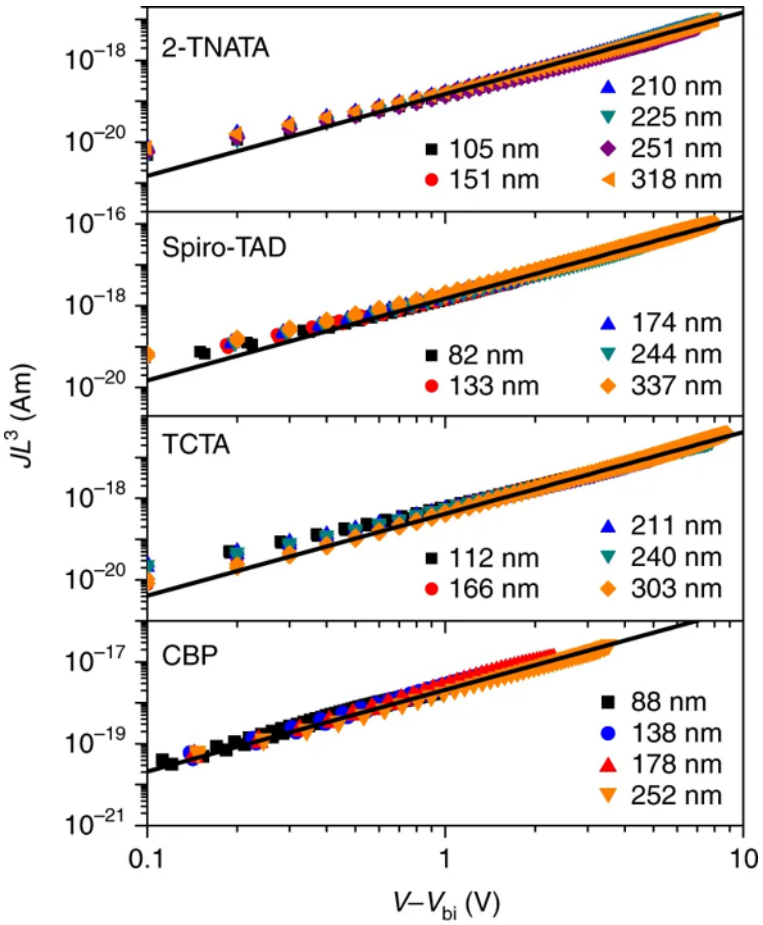

Figure 3.3.: Space-charge-limited hole currents in four different materials. TCTA was used as an interlayer for 4,4′,4″-tris[2-naphthyl(phenyl)amino]triphenylamine (2-TNATA) and Spiro-TAD transport layers, whereas CBP and BST interlayers were used for TCTA and CBP transport layers, respectively. For all materials, JL^3 is plotted for a range of layer thicknesses against voltage, corrected for the built-in voltage and the electrode series resistance. The lines represent fits with equation 3.1, from which the hole mobility is extracted.

eV was determined as shown in Figure B.4, independent of the IE of the organic semiconductor. Interestingly, a universal energy-alignment behaviour between metal oxides and organic semiconductors has been reported, where a general 0.3 eV offset was observed between the work function of the oxide and the IE of the organic semiconductor [97]. These ultraviolet photoelectron spectroscopy (UPS) measurements suggest that the energy offset is manifested as an injection barrier.

To unravel the mechanism of the Ohmic-contact formation, the energy-level alignment in the presence of an interlayer was investigated. For this purpose, UPS measurements were performed layer-by-layer on a representative MoO_3/TCTA/2-TNATA structure, which has an IE offset of 0.7 eV between the TCTA interlayer and 2-TNATA. Figure

Material	**IE (eV)**	**SCLC mobility ($m^2V^{-1}s^{-1}$)**	**TOF mobility ($m^2V^{-1}s^{-1}$)**
2-TNATA	5.0 [97]	5×10^{-9}	3×10^{-9} [98]
Spiro-TAD	5.3 [94]	5×10^{-8}	3×10^{-8} [99]
TCTA	5.7 [95]	1.4×10^{-8}	2×10^{-8} [100]
CBP	6.0 [95, 97]	7×10^{-8}	5×10^{-8} [101]
4CzIPN	6.1 [102]	-	-
C_{60}	6.4 [95]	-	-
BST	7.0(this work)	-	-

Table 3.1.: Ionization energies and hole mobilities of materials used in this work; IEs are obtained with ultraviolet photoelectron spectroscopy. Mobilities are obtained from space-charge-limited currents (Figure 3.3), which are compared to time-of-flight measurements from the literature.

3.4a shows the measured IE as a function of layer thickness. At a TCTA coverage of 1 nm, the Fermi level of MoO_3 is pinned at 0.38 eV below the IE of TCTA, in line with the universal offset in the pinning regime [97]. With increasing TCTA thickness, the IE separates further from the Fermi level to 0.6 eV at 5 nm, which abruptly reduces to 0.16 eV upon 2-TNATA coverage, because of the IE offset between TCTA (5.7 eV) and 2-TNATA (5.0 eV). This shows that, near the interface, the IE of 2-TNATA aligns with the Fermi level, which is the required condition for the formation of an Ohmic contact. The energy offset of 0.16 eV is substantially smaller than the universal offset of 0.3 eV in the monolayer regime as previously observed [97], explaining the improved injection with the help of the interlayer.

To understand the band alignment as well as the (universal) barrier reduction, the IE profile was calculated by solving Poisson's equation, as described in detail in supporting information [103]. The Poisson equation relates charge density to electrostatic potential, both of which depend on the relative alignment of the oxide Fermi level with respect to the density of states (DOS) of the organic semiconductor [104, 105, 106]. As shown in Figure 3.4a, within the first nanometre, a strong band bending is observed as a result of charge transfer between MoO_3 and TCTA to establish thermodynamic equilibrium across the interface. In the monolayer regime, the Fermi level is (universally [95, 97]) pinned at $0.3 - 0.4$ eV below the IE of TCTA, which could be reproduced by considering a broadened DOS near the metal oxide, as suggested in previous publications [105, 107, 108]. Effectively, the Fermi level is pinned to the deeper states in the broadened interface DOS, from which charges have to escape to the narrower bulk DOS, leading to an injection barrier. The band bending for increasing layer thickness is described well by including a Coulomb image potential due to differences in dielectric constants between MoO_3 and the organic semiconductor as described in detail in supporting information [103]. We suggest DOS broadening at the interface and the attractive image potential to be the

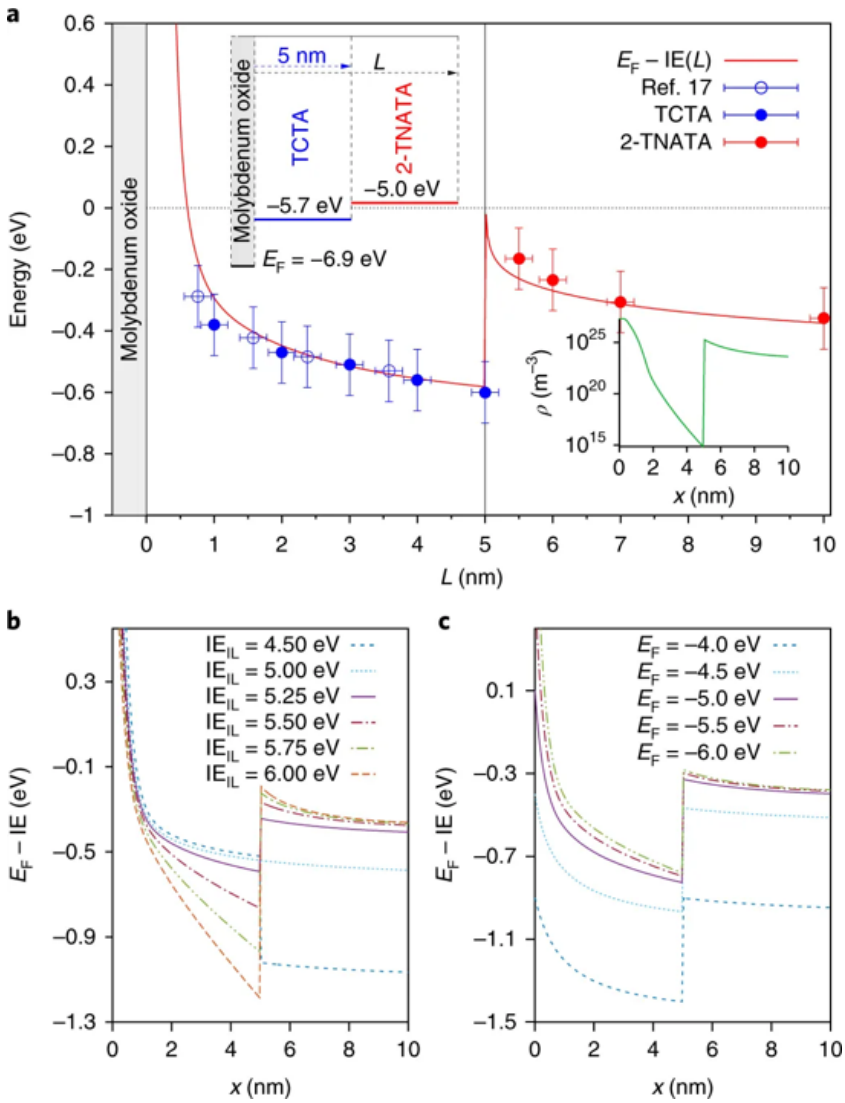

Figure 3.4.: Experimental and calculated IE profiles across interlayer/hole-transport layer structures. **a,** IE onset with respect to the Fermi level obtained by UPS layer by layer across a MoO_3/TCTA(5 nm)/2-TNATA(5 nm) structure (filled symbols), augmented with data of the universal IE profile of organic semiconductors on metal oxides [97] (open symbols). The error bars indicate an estimated error of ±0.1 eV for the IE and ±0.2 nm for the layer thickness. The calculated IE position at the layer surface (red line), corresponding to the UPS measurements, is obtained by evaluating the band bending at $x = L$ for different L. The top inset shows the energy levels of the separate materials and the bottom inset shows the calculated charge density across the layers. **b,** Simulated band diagrams (IE as a function of position x across the layers) for different interlayer IEs, using a work function of 6.9 eV and a HTL IE of 5.0 eV. **c,** Band diagrams for different work functions, with an IE of 5.5 eV for the interlayer and 5.0 eV for the HTL.

reason for the observed injection barriers at the metal-oxide contact.

At the TCTA/2-TNATA interface, the calculations support alignment of the IE of 2-TNATA with the Fermi level, which is accompanied by the presence of a high hole density (inset Figure 3.4). The experimental IE profile of the 2-TNATA layer is consistently described by using a Gaussian DOS width of 0.1 eV, without additional broadening. This disorder value is also consistent with molecular dynamics simulations of layered structures and evaluated energetic disorder in the organic films using polarizable force fields, showing no distinct DOS broadening at the organic/organic interfaces, as described in the supplementary information [103]. In short, the interlayer realigns the Fermi level with the IE of the organic semiconductor, negating the barrier formation due to DOS broadening and the image potential by effectively decoupling the electrode and semiconductor electrostatically.

With the developed model, we can now explore the limiting cases for the formation of an Ohmic contact by simulating band diagrams. By varying the interlayer IE in Figure 3.4b, it is found that the IE in the HTL is close to the Fermi level for an interlayer offset of at least $\sim$ 0.3 eV, with larger offsets having no effect on the energetic position of the HTL, as confirmed experimentally in Figure 3.2 by the identical currents obtained for different interlayers with varying offsets. In a similar fashion, electrode work functions that are equal to or higher than the IE of the HTL are required (Figure 3.4c), which is the case in our injection experiments with the high-work-function metal oxides MoO_3,V_2O_5 and WO_3.

The UPS measurements and simulations indicate a high hole density at the organic/organic interface (inset Figure 3.4a), which plays the role of a virtual Ohmic hole contact, spatially separated from the electrode by the interlayer. However, charges still have to pass through the interlayer to contribute to the current. Considering the measured space-charge-limited currents with mobilities that are close to the time-of-flight values, even for thin transport layers of less than 100 nm, it can be concluded that the interlayer does not add a significant resistance. In addition, as can be seen from the experimental currents in reverse bias, where the current is injected from the PEDOT:PSS electrode, the presence of the interlayer does not reduce the current, even for large IE offsets between the transport material and the interlayer, which normally imposes a hole-extraction barrier. This indicates that the interlayer is virtually transparent for holes.

Since the measured current is the same regardless of the interlayer material, it appears that the transport properties of different interlayers do not affect the injected current. However, at interlayer thicknesses above 5 nm, the current is reduced and depends on the interlayer material as shown in Figure B.6 and B.7, suggesting that transport through and injection into the interlayer becomes a limiting factor. This supports a scenario in which charges tunnel through the electrostatic barrier of the interlayer to the second layer. For thick interlayers, the charge density decreases and the tunnelling rates be-

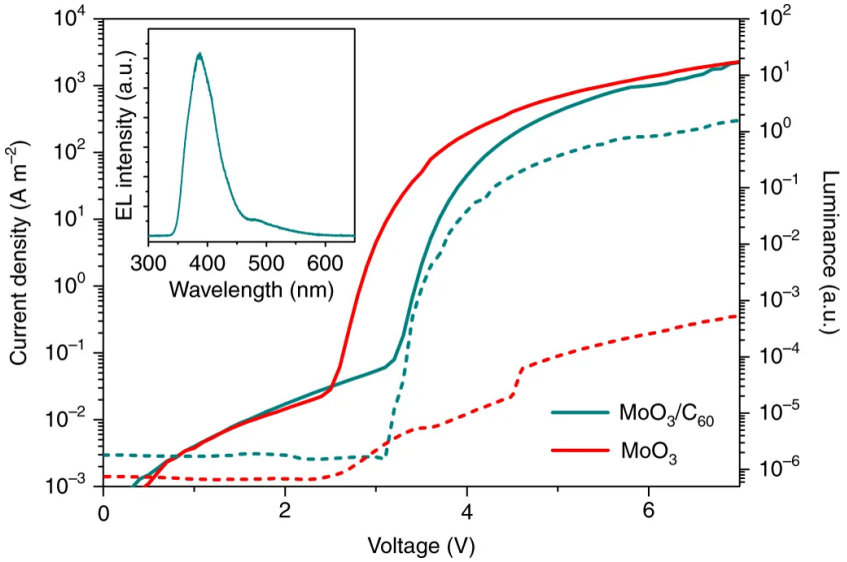

Figure 3.5.: UV-emitting TPBi OLEDs. Current density–voltage (solid lines) and luminance–voltage (dashed lines) characteristics of OLEDs with a MoO_3/[C_{60}(4 nm)]/TPBi(58 nm)/Ba/Al structure, with and without a C_{60} interlayer. The inset shows the electroluminescence spectrum corresponding to TPBi emission, with an onset at 340 nm and a maximum at 385 nm.

come negligible, thus explaining that the optimal interlayer thickness is below 5 nm. On the other hand, the optimum thickness of 3−5 nm helps to decrease the barrier due to the attractive image potential near the electrode interface, which is strongly reduced at these length scales.

As an ultimate proof, we demonstrate our hole injection strategy in a light-emitting diode based on the electron-transport material 1,3,5-tris(N-phenylbenzimidazol-2-yl) benzene (TPBi). Because of its high ionization energy of 6.3 eV, TPBi is frequently used as a hole-blocking material in OLEDs [102, 109]. Here, we use TPBi in an ultraviolet-emitting diode, consisting of TPBi sandwiched between a MoO_3 anode and a Ba cathode. As demonstrated in Figure3.5, adding an additional C_{60} interlayer between MoO_3 and TPBi results in a three orders of magnitude increased light output and efficiency. The increased light output is a direct consequence of the enhanced hole injection, showing that it is possible to directly inject holes even in materials that are normally used for hole-blocking purposes. Since TPBi is an electron transporter [109], the current through the OLED is mainly carried by electrons and does not increase by improving the hole contact. However, the J−V characteristics are shifted by 0.6 V along the voltage axis, which is the result of an increased built-in voltage due to the reduced barrier on the anode side, which in turn enhances the hole injection and light output.

3.3. Conclusion

In conclusion, we present a universal strategy for achieving Ohmic hole contacts on organic semiconductors with a high IE. In particular, the injected hole current is consistently improved by over an order of magnitude as compared to high-work-function transition-metal oxide electrodes. The barrier reduction is rationalized by electrostatic decoupling of the electrode from the organic semiconductor with an interlayer. This interlayer strongly reduces the effect of the attractive image potential near the electrode interface, and eliminates the DOS broadening present at the organic/electrode interface, while restoring Fermi-level alignment. As a proof of principle, we illustrate that the interlayer-enhanced contact can be used in an ultraviolet-emitting diode, providing direct hole injection into the hole-blocking material TPBi. The presented efficient hole injection into organic semiconductors with ionization energies beyond 6 eV extends the range of materials available for OLEDs and organic photovoltaic devices, which otherwise would suffer from high contact barriers.

Author contributions

- Naresh B. Kotadiya
  - Designed the experiments and developed processes for the deposition of organic small molecules and metal oxides
  - Fabricated all hole only devices and samples for UPS measurements
  - Performed electrical characterization of all devices
  - Processed and analyzed the experimental data together with G. Wetzelaer and P. Blom
  - Drawn chemical structures and wrote the experimental method section for the publication
  - Prepared figures for the experimental part of the publication along with G. Wetzelaer
- Hao Lu
  - Performed the UPS measurements
- Yutaka Ie
  - Synthesized 4CzIPN material and performed its purification
- Anirban Mondal
  - Performed molecular-dynamics simulations, quantum chemical calculations, and analytical energy-alignment calculations

- Denis Andrienko
  - Performed molecular-dynamics simulations and analytical energy-alignment calculations
- Paul W. M. Blom
  - Scientific guidance, discussion and supervision of the work
- Gert−Jan A. H. Wetzelaer
  - Proposed the project, Scientific guidance, discussion and supervision of the work
  - Reviewed the experimental design and helped with suggestions
  - Wrote the original publication with inputs from D. Andrienko and P. Blom

4. Hole Transport in Amorphous Organic Semiconductors

In this chapter, we have investigated the hole transport in a wide range of organic small molecules. Amorphous small-molecule hole-transporting materials are commonly used in organic light-emitting diodes and perovskite solar cells. Characterization of their main functionality, hole transport, has been complicated by the presence of large contact barriers. Using our ohmic charge injection strategy developed in chapter 3, we investigated the bulk hole transport in a series of molecules with a broad range of ionization energies from 5.0 to 6.0 eV. The temperature dependence of current-Voltage characteristics were measured and simulated using extended Gaussian disorder model (EGDM), from which charge-carrier mobility, energetic disorder and molecular site spacing were extracted. Excellent agreement is obtained between experimental data and EGDM simulations. [1]

4.1. Introduction and Background

Organic small molecules are omnipresent in hole-transport layers (HTLs) in thin-film optoelectronic devices, in particular in organic light-emitting diodes (OLEDs) and the emerging hybrid organic–inorganic perovskite solar cells [110, 94, 111]. The main function of this class of organic semiconductors is to transport holes between the active layer and the anode, while blocking electrons and excitons. To avoid barrier formation or voltage losses, the ionization energy (IE) of the hole-transport material must be well aligned with the IE of the active layer, while the electron affinity and energy gap must be sufficiently high to block excitons and electrons.

Apart from the appropriate energy-level alignment, the efficiency of hole transport depends on the charge-carrier mobility. This is a key quantity to be taken into account in optimizing the device architecture, as it impacts the device efficiency via the charge-extraction rate in solar cells and the operating voltage in OLEDs [112, 113, 80]. Proper characterization of charge transport in organic semiconductors is, however, not straightforward [114, 115]. Bulk charge transport is typically measured in single-carrier devices, in which a layer of organic semiconductor is sandwiched between two planar electrodes. The work functions of the electrodes are chosen such that only one type of carrier, electrons or holes, can be injected. When at least one of the electrodes forms an Ohmic contact, a space-charge-limited current (SCLC) is measured, from which the steady-state mobility can be extracted [47]. The formation of an Ohmic hole contact,

[1] This chapter is published as *Rigorous Characterization and Predictive Modeling of Hole Transport in Amorphous Organic Semiconductors*. Naresh B Kotadiya, Anirban Mondal, Shiyun Xiong, Paul W.M. Blom, Denis Andrienko, and Gert-Jan A.H. Wetzelaer. Advanced Electronic Materials, 4(12):1800366, 2018. N.B.K. and A.M Contributed equally to the work.

however, has proven to be quite problematic, especially for hole-transport materials with high ionization energies. When the work function of the electrode is lower than the IE of the HTL, an injection barrier is formed. In the presence of an injection barrier, the analysis of the current–voltage characteristics becomes much more complicated [116], which can easily lead to significant errors in the determined mobility.

The problem of Ohmic contact formation can be circumvented by using an alternative method to characterize charge transport in organic small molecules, the time-of-flight technique [117]. In this commonly used technique, the transit time of photogenerated charge carriers through micrometer-thick organic layers is measured as a function of the applied electric field between two non-injecting electrodes. The transit time is then used to calculate the charge-carrier mobility. However, while relatively straightforward, this technique has several limitations. As a result of energetic disorder, charge carriers may not equilibrate to deeper states during transit [33], which leads to an overestimation of the mobility [118, 119, 120]. The dispersive nature of charge transport is typically amplified at lower temperatures [121]. It has also been observed that the transit time is insensitive to deep traps [96], which may severely hinder charge transport in actual devices. Another drawback of the time-of-flight technique is that the dependence of the mobility on charge concentration cannot be evaluated, which is important in thin and electrically doped films, as frequently used in devices [80].

Alternatively, charge-carrier mobilities are also frequently determined from organic field-effect transistor characteristics [122, 39]. In such a device layout, transport takes place in a horizontal direction at the organic/dielectric interface, whereas for OLEDs and solar cells, vertical bulk transport is of main interest. Furthermore, field-effect transistors operate at much higher charge-carrier densities (10^{19} cm^{-3}) as compared to OLEDs and solar cells (10^{17} cm^{-3}). These high carrier densities mask the effects of traps and energetic disorder on the charge transport. As a result, rigorous experimental data of the charge-transport properties of hole-transport materials is often unavailable, even for widely used materials.

Using the ohmic hole injection strategy developed in chapter 3, we have fabricated hole only devices. Subsequently, measured the space-charge-limited hole currents as a function of temperature and layer thickness in a series of hole-transport molecules spanning a wide range of ionization energies. Device simulations are used to describe the hole transport as a function of temperature, electric field, and charge concentration, which yields values for the mobility, energetic disorder, and site spacing of these materials.

4.2. Results and Discussion

We have experimentally investigated the bulk hole transport in vacuum-deposited organic small molecules commonly used as hole-transport or host materials, namely 2-

TNATA, TCTA, Spiro-TAD, and CBP. Chemical structures of these materials are shown in Figure 4.1. These materials cover a broad range of ionization energies between 5.0 and 6.0 eV, which is relevant for matching the IE of the hole-transport material to the IE of the active layer in a device, or for matching the energy levels to the emitter when the material is used as a host in an OLED. The hole transport in these materials was investigated by means of temperature- and thickness-dependent current density-voltage characteristics of single-carrier devices.

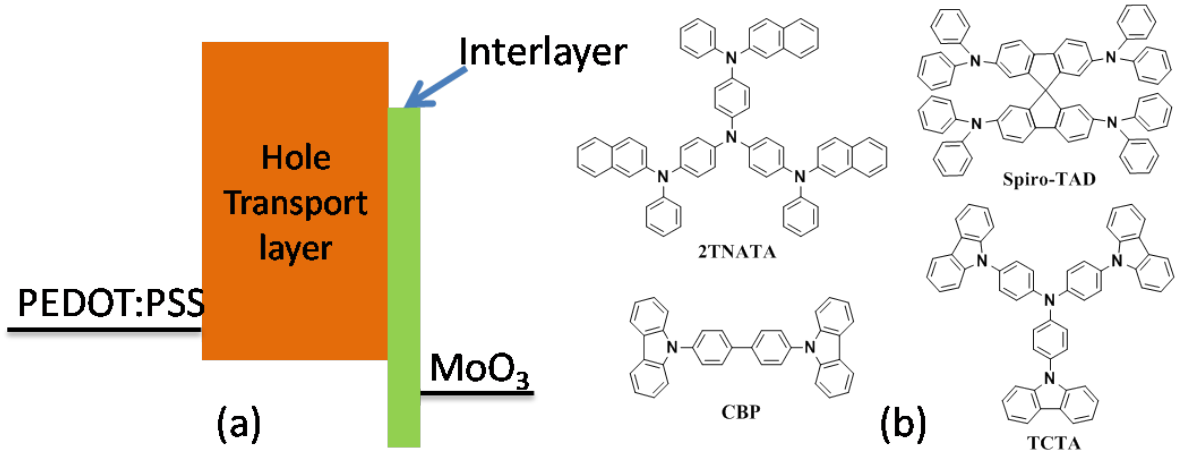

Figure 4.1.: (a) Hole only device layout, a thin interlayer with the HOMO deeper than the device layer forms the ohmic contact with MoO_3. **(b)** Chemical structures of the studied compounds, $4,4',4''$-tris[2-naphthyl(phenyl)amino] triphenylamine (2-TNATA), and $2,2',7,7'$-tetrakis(N,N-diphenylamino)-9,9 -spirobifluorene (Spiro-TAD), tris(4-carbazoyl-9-ylphenyl)amine (TCTA) and $4,4'$-bis(N-carbazolyl)-$1,1'$-biphenyl (CBP).

In these hole-only devices, it is critical that the injecting electrode is an Ohmic hole contact. To form an Ohmic hole contact, we inserted a thin interlayer (3−5 nm) of an organic semiconductor between the MoO_3 electrode and the transport layer. This interlayer has a higher IE than the transport material. Using this method, we have recently demonstrated barrier-free hole injection [103]. Since the current in a device scales exponentially with the injection barrier, the formation of an Ohmic charge-injecting contact is crucial. Otherwise, the measured current can be much lower and the calculated mobility can be severely underestimated.

The hole-only devices in this study consist of a single layer of either of the hole-transport materials, sandwiched between an ITO/PEDOT:PSS bottom electrode and an interlayer-enhanced MoO_3/Al top electrode. For hole-only devices of 2-TNATA, Spiro-TAD, TCTA was used as the interlayer. For TCTA and CBP devices, interlayers of CBP and BST ($4,4''$-bis(triphenylsilanyl)) were used, respectively.

In a single-carrier device with an Ohmic injecting contact, the current will be limited by the transport in the bulk of the semiconductor, commonly known as an SCLC. The

current density (J) in a space-charge-limited device is described by the Mott-Gurney square law [123],

$$J = \frac{9}{8}\varepsilon\mu\frac{(V - V_{bi})^2}{L^3} \tag{4.1}$$

where, ε is the permittivity, μ is the charge-carrier mobility, V is the voltage, V_{bi} is the built-in voltage due to asymmetric work functions of the electrodes, and L is the layer thickness. In this equation, the current density depends on the square of the applied voltage and scales inversely with layer thickness to the third power. By fitting the SCLC equation to experimental $J - V$ characteristics, the charge-carrier mobility can be determined. However, the mobility in disordered materials depends on the charge-carrier density and the electric field [40], resulting in a voltage−dependent mobility [124]. In addition, the mobility is temperature dependent, with the field and density dependence becoming more pronounced at lower temperatures.

In order to characterize charge transport more accurately, the use of numerical simulations is required. A well-established mobility model that includes the effects of temperature, charge concentration, and electric field on the mobility is the extended Gaussian disorder model (EGDM) [40]. This model describes the mobility in the situation of hopping transport in a system with a Gaussian DOS distribution. Previously, the EGDM has been successfully applied to describe charge transport in disordered organic semiconductors [124, 125, 32, 126, 127].

In the EGDM, the phenomenological expression for the mobility reads

$$\mu_0(T, p, E) = \mu_p(T, p) \exp\left[0.44\left(\bar{\sigma}^{1.5} - 2.2\right) \times \sqrt{1 + 0.8\left(\frac{Eea}{\sigma}\right)^2} - 1\right] \tag{4.2}$$

Where,

$$\mu_p(T, p) = \mu_0(T) \exp\left[\frac{1}{2}\left(\bar{\sigma}^2 - \bar{\sigma}\right)\left(2pa^3\right)^{\delta}\right] \tag{4.3}$$

provides the dependence on the charge-carrier density p, and

$$\mu_0(T) = \mu_0 C_1 \exp\left[-C_2\bar{\sigma}^2\right] \tag{4.4}$$

gives the temperature dependence of mobility in the limit of zero charge-carrier density and electric field. In our case, $C_1 = 1.8 \times 10^{-9}$ and $C_2 = 0.42$ are constants, μ_0 is the mobility prefactor, $\bar{\sigma} = \frac{\sigma}{k_B T}$ is the dimensionless width of the density of states, k_B is Boltzmann's constant, T is the temperature, a is the lattice constant, and $\delta = 2\frac{\ln(\bar{\sigma}^2 - \bar{\sigma}) - \ln(\ln 4)}{\bar{\sigma}^2}$.

In the EGDM, there are three free parameters that are used to fit the experimental data: μ_0, σ, and a. The mobility prefactor only influences the magnitude of the mobility, whereas σ mainly affects the temperature and density dependence, with these two

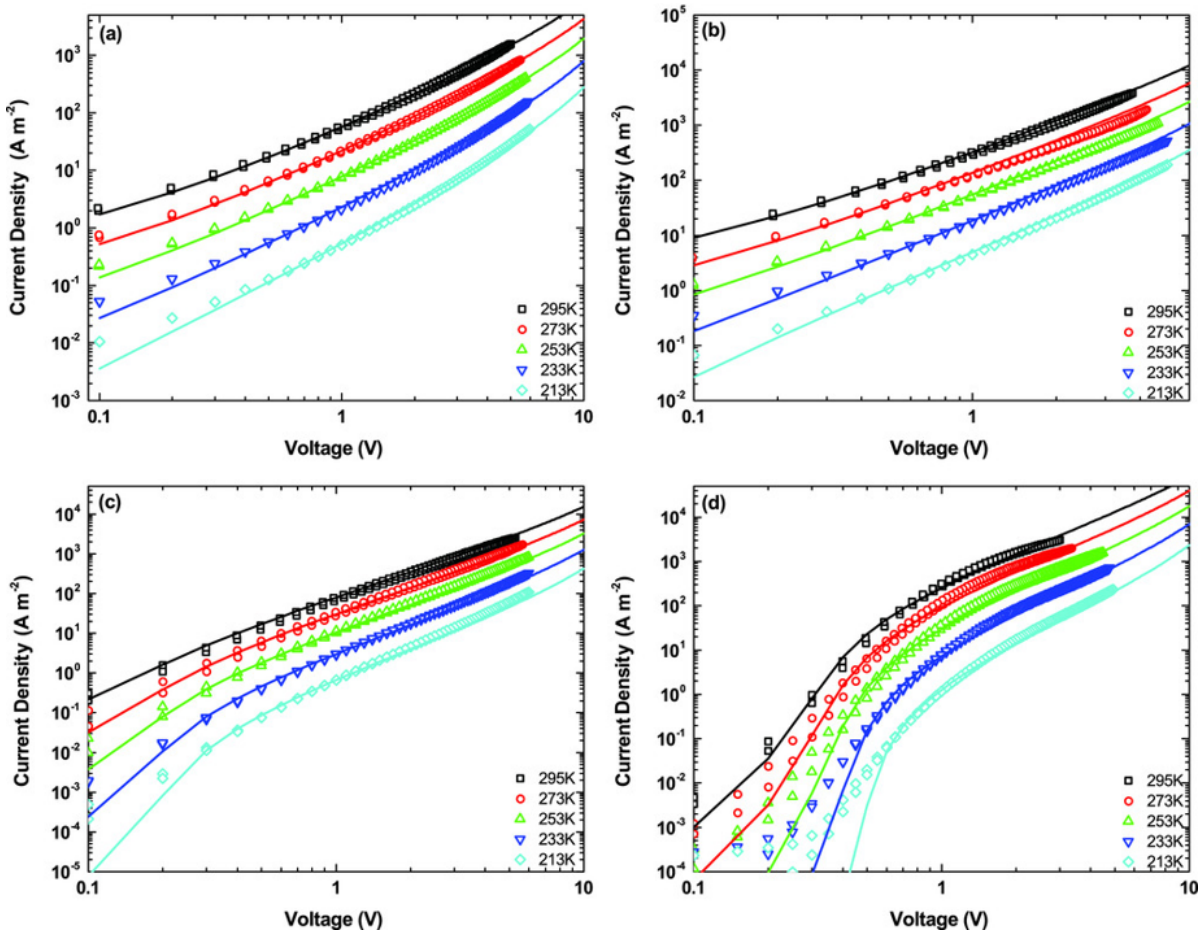

Figure 4.2.: Current density-voltage characteristics at different temperatures for a) 2-TNATA (151 nm), b) Spiro-TAD (179 nm), c) TCTA (179 nm), and d) CBP (138 nm). Symbols represent experimental data and lines are simulations with a drift-diffusion model with the mobility described by the EGDM. An interlayer-enhanced MoO_3/Al electrode was used as Ohmic injecting hole contact.

effects increasing for larger disorder. The lattice constant a predominantly controls the electric field dependence of the mobility.

To simulate $J - V$ characteristics, the EGDM mobility function is incorporated in a 1D drift-diffusion solver [128]. The simulated current densities are then fitted to the experimentally obtained current density-voltage characteristics. Figure 4.2 shows the temperature-dependent current density-voltage characteristics measured for 2-TNATA, Spiro-TAD, TCTA, and CBP. The simulated J–V characteristics are shown as solid lines. In the drift-diffusion simulations, the barrier at the injecting contact was set to zero, corresponding to an Ohmic hole contact. The barrier at the extracting contact increases with increasing IE of the organic semiconductor because of the increased offset between the IE and the work function (≈5.2 eV) of the PEDOT:PSS extracting electrode. This gives rise to a shift in the built-in voltage with increasing IE of the

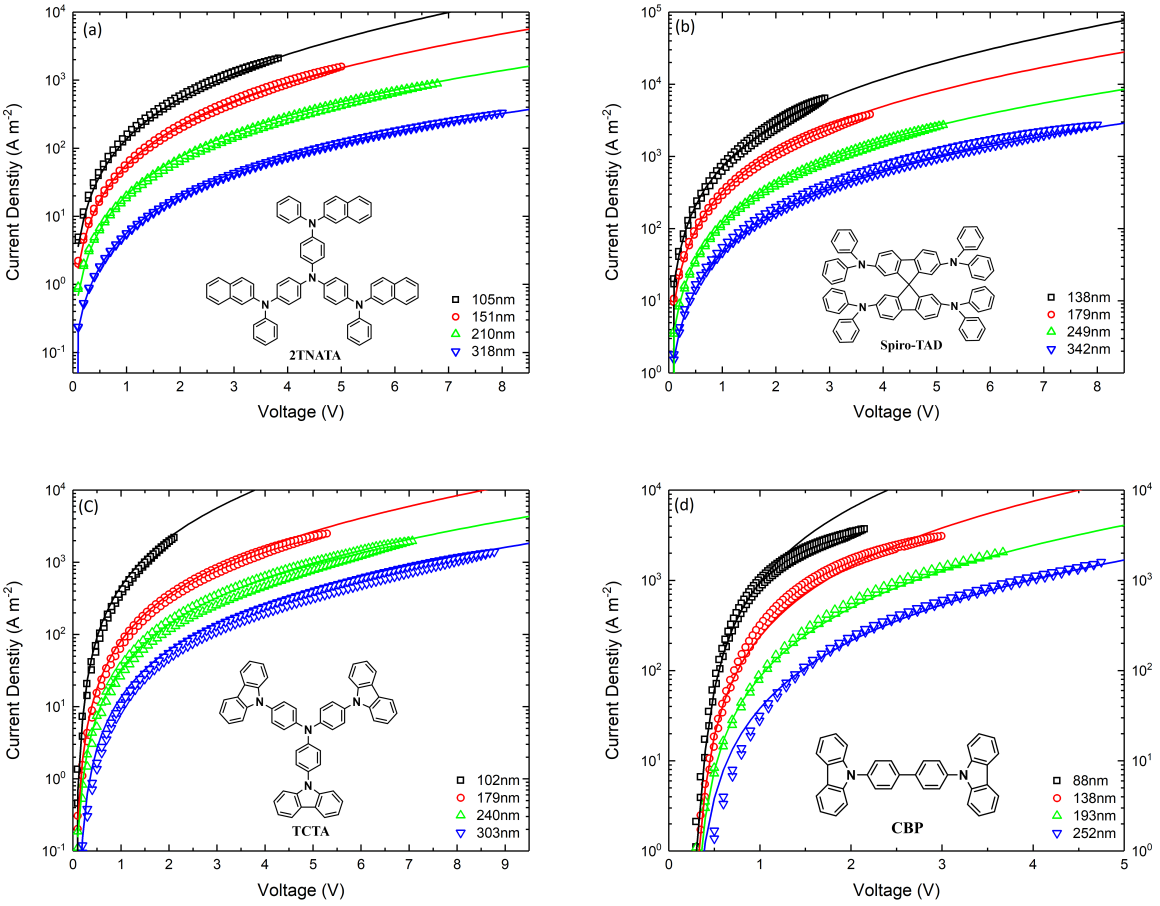

Figure 4.3.: Room temperature current-voltage characteristics for different thickness of 2-TNATA **(a)**, Spiro-TAD **(b)**, TCTA **(c)** and CBP **(d)**. The EGDM simulations (lines) shows excellent agreement with the experimetal data (symbols) for the wide range of thicknesses.

hole-transport material.

For all hole-transport materials, a good agreement between the experimental data and the model is observed. Note that the same set of parameters was used for each temperature. To further confirm the accuracy of the obtained parameters, the same set of parameters were also used to describe the current-voltage characteristics for a range of layer thicknesses, as shown in 4.3. The parameters used in the simulations are listed in Table 4.1. Despite the difference in chemical structures and ionization energies, a similar value for the energetic disorder σ of $0.09 - 0.10$ eV was found for all molecules. The similarity in energetic disorder is also reflected in similar mobilities at room temperature in the range of 1×10^{-8} $\mathrm{m^2V^{-1}s^{-1}}$. For all five materials, EGDM simulations were obtained without using any additional trapping parameters.

Property	**2-TNATA**	**Spiro-TAD**	**TCTA**	**CBP**
IE(eV)	5.0 [98]	5.3 [94]	5.7 [99]	6 [99]
σ**(eV)**	0.10	0.09	0.10	0.10
a[nm]	1.30	1.40	1.40	1.20
$\mu_{\mathbf{0}}[\mathbf{10^3 m^2 V^{-1} s^{-1}}]$	1	3.3	3.3	8
$\mu_{\mathbf{TOF}}[\mathbf{10^{-8} m^2 V^{-1} s^{-1}}]$	0.3 [98]	3 [99]	2 [100]	5 [101]
$\mu_{\mathbf{295K}}[\mathbf{10^{-8} m^2 V^{-1} s^{-1}}]$	0.271	3.07	0.893	2.17

Table 4.1.: Ionization energy (IE), energetic disorder (σ), effective lattice contact (a), room temperature hole mobility (μ), time-of-flight mobility (μ_{TOF}).

4.3. Conclusions

We have experimentally and theoretically investigated the bulk hole-transport properties of 2-TNATA, Spiro-TAD, TCTA, and CBP, which have ionization energies ranging from 5 to 6 eV. By using a recently developed method to form Ohmic hole contacts, temperature-dependent space-charge-limited hole currents were obtained in hole-only devices. The hole mobility and its dependence on charge concentration, electric field, and temperature were obtained by modeling the experimental current-voltage characteristics. The presented results are expected to be useful in the analysis and design of OLEDs and solar cells. The relatively similar mobilities obtained for a series of hole-transport materials over a range of ionization energies allows for the selection of a hole-transport layer with an IE that is best suited to work in conjunction with the active layer. The dependence of the mobility on charge-carrier density is an important factor that has to be considered when doping the hole-transport materials.

Author Contributions

- Naresh B. Kotadiya
  - Designed the experiments and fabricated all hole only devices
  - Performed electrical characterization and temperature dependent measurements of all devices
  - Performed EGDM simulations of all devices
  - Processed and analyzed the experimental data, prepared figures for the experimental part of the publication

- Anirban Mondal
  - Performed force field parameterization, molecular dynamics simulations of the organic molecules, quantum chemical calculations
  - Performed theoretical charge transport simulation
- Shiyun Xiong
  - Performed force field parameterization for molecular simulations
- Denis Andrienko
  - Supervision of the multiscale simulation work
- Paul W. M. Blom
  - Scientific guidance, discussion and supervision of the work
- Gert−Jan A. H. Wetzelaer
  - Scientific guidance, discussion and supervision of the work
- N. Kotadiya, A. Mondal, D. Andrienko and G. Wetzelaer wrote the original publication
- N. Kotadiya and A. Mondal contributed equally to the original publication

5. Trap-free Hole Transport in a Fullerene derivative

In this chapter, we have investigated charge transport in a fullerene derivative. Fullerenes and their derivatives are well-known electron-transporting materials used in organic solar cells and transistors. However, the extent to which fullerenes are able to transport holes is heavily disputed. Using selective Ohmic contacts developed in chapter 3, we study the bulk hole and electron transport in a bisadduct fullerene derivative. Trap-free space-charge-limited hole and electron currents are measured, with a hole mobility equivalent to the electron mobility. Our results identify the bisadduct fullerene as an organic semiconductor with balanced bipolar bulk transport with excellent electron and hole mobilities. [1]

5.1. Introduction and Background

Fullerenes and their derivatives are widely used in organic solar cells, in n-channel transistors, and as n-type thermoelectric materials, owing to their excellent electron-transport capabilities [129, 130]. For the same reason, fullerenes have been successfully applied as electron-transport layers in hybrid perovskite photovoltaic cells [131]. By functionalizing fullerenes, such as C_{60} and C_{70}, with side groups, their solubility and energy levels can be tuned, enabling their use in solution-processed electronic devices [132, 133, 134].

With regard to electron transport, fullerenes exhibit mobilities that are among the highest in organic semiconductors [135] and exceptionally long electron diffusion lengths have recently been observed [136]. The electron- transporting character of fullerenes has led to their classification as "n-type" materials [129], though it has been shown that films of C_{60} can also support radical cations [137]. The extent to which fullerenes are able to transport holes, on the other hand, is less clear. From a theoretical perspective, the intrinsic electron and hole mobilities are comparable in many organic semiconductors [28], which would also be expected to hold for fullerenes. However, experimentally, unipolar charge transport is often observed in organic semiconductors due to charge trapping [138, 50].

Evidence of a balanced electron and hole mobility in fullerenes has been reported for vapor-phase-grown C_{60} single crystals, measured with the photocurrent time-of-flight technique [139]. However, deep trapping sites for holes were also observed, which have

[1] This chapter is published as *Trap Free Space Charge Limited Hole Transport in a Fullerene Derivative.* Naresh B. Kotadiya, Paul W.M. Blom, and Gert-Jan A.H. Wetzelaer. Physical Review Applied, 11(2):024069, 2019

negligible influence on the measured transit time [96], but can greatly hinder steady-state charge transport. In films of C_{60}, the hole mobility has been reported to be many orders of magnitude lower than the electron mobility [140, 141, 142]. In later work, a field-effect transistor using a solution-processed layer of the fullerene derivative [60][6,6]-phenyl C_{61} butyric acid methyl ester (PCBM) was fabricated, exhibiting balanced electron and hole mobilities at high gate bias [143]. However, at low gate bias, a very low hole current was observed, which was ascribed to the presence of a large hole-injection barrier. In a field-effect transistor at high gate bias, charge-carrier densities are high, which obscures the presence of bulk traps or tail states to a certain degree [39]. By contrast, at low carrier densities in a diode configuration, measurements of the bulk mobility in [60]PCBM and [70]PCBM showed highly unipolar transport, with hole mobilities more than six-orders of magnitude lower than the electron mobilities [144], comparable to what has been observed for C_{60} thin films [140, 141, 142]. It should be noted that for charge-transport characterization in a diode configuration, Ohmic contacts are of critical importance.

In this chapter, we demonstrate trap-free space-charge-limited hole and electron currents in diodes based on a solution-processed bisadduct fullerene derivative. The bulk hole and electron mobilities are balanced and both are higher than 10^{-3} $cm^2V^{-1}s^{-1}$. Numerical modeling of the current-density voltage characteristics shows that the energetic disorder for holes and electrons is similar. These measurements demonstrate that fullerenes can be excellent hole-transporting materials. The absence of charge trapping for both types of charge carriers reveals the intrinsic bipolar character of charge transport in organic semiconductors, as would be theoretically expected, but is rarely observed experimentally.

5.2. Results and Discussion

For our charge-transport measurements, the fullerene derivative indene-C_{60} bisadduct (ICBA) is chosen (Figure 5.1). ICBA is a bisadduct fullerene, exhibiting a highest occupied molecular orbital (HOMO) and lowest unoccupied molecular orbital (LUMO) that are raised by 0.2 eV as compared to PCBM [135]. The shallower HOMO (-5.9 eV) is expected to alleviate hole-injection issues, and should allow for Ohmic hole-contact formation using a recently developed technique [103]. Hole-only devices are prepared, with ICBA spin coated from a chloroform solution on top of glass substrates with patterned indium-tin-oxide electrodes, covered with a 40-nm layer of poly(3,4-ethylenedioxythiophene)-poly (styrenesulfonate) (PEDOT:PSS), which has a work function of approximately 5.2 eV. To establish an Ohmic hole contact, a top electrode comprising C_{60}(4 nm)/MoO_3(10 nm)/Al(100 nm) is thermally evaporated in which the C_{60} interlayer is inserted to obtain Fermi level alignment between MoO_3 and ICBA [103].

The interlayer-based contact engineering technique [103] allows us to inject holes directly from the top electrode into the HOMO of ICBA. For the case of an Ohmic contact

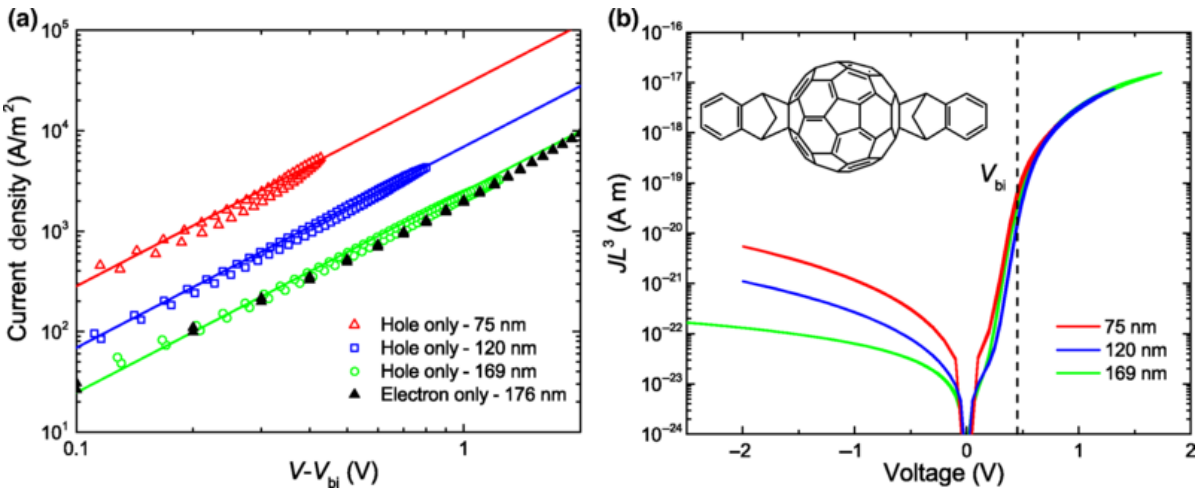

Figure 5.1.: (a) Current density-voltage characteristics of ICBA single-carrier devices. Hole-only devices of different layer thicknesses are shown (open symbols), with the voltage corrected for the built-in voltage (0.40−0.45 V) and the electrode series resistance. The solid lines are fits with Equation 5.1 using a mobility of 3×10^{-3} $cm^2V^{-1}s^{-1}$ for all layer thicknesses. A 176-nm-thick electron-only device is plotted for comparison (closed symbols). The error (standard deviation) in the thickness is determined to be 3−4 nm for all films. (b) Thickness-scaled current density (JL^3) vs voltage for ICBA hole-only devices. The built-in voltage, which marks the transition from the exponential diffusion regime to the quadratic drift regime, is indicated by the dashed line at 0.45 V. The chemical structure of ICBA is shown in the inset.

on a trap-free, intrinsic semiconductor, the injected current is limited by space charge, as described by the Mott-Gurney square law, which is [65]

$$J = \frac{9}{8}\varepsilon\mu\frac{(V - V_{bi})^2}{L^3} \tag{5.1}$$

where J is the current density, ε is the permittivity, μ is the charge-carrier mobility, V is the voltage, V_{bi} is the built-in voltage due to asymmetric work functions of the electrodes [145], and L is the layer thickness. In Figure 5.1(a), the measured hole-current density is plotted against voltage for three different layer thicknesses. Remarkably, the hole current depends on the square of the voltage and scales inversely with layer thickness to the third power, as demonstrated in Figure 5.1(b), which is characteristic of a bulk trap-free space-charge-limited current. This also confirms the formation of an Ohmic hole contact on ICBA. Furthermore, the hole-only devices do not show electroluminescence, confirming the absence of electron injection (as shown in Appendix C.2). As a result, the current is carried by holes only. Because of the mismatch between the work function of PEDOT:PSS and the HOMO of ICBA, a small built-in voltage of approximately 0.45 V is present and the current in reverse bias is injection limited, as shown in Figure 5.1(b). When fitting Equation 5.1 to the forward J-V characteristics, as shown in Figure 5.1(a), a hole mobility of 3×10^{-3} $cm^2V^{-1}s^{-1}$ is obtained for all layer thicknesses, using the experimentally determined relative permittivity of 3.9 [146].

This hole mobility is similarly high as the electron mobility in the ubiquitous fullerene derivative PCBM [147]. Interestingly, the ICBA bulk-hole mobility is even superior to that of typical hole-transport molecules and polymers [103, 148, 149, 150].

To compare the hole transport directly to the electron transport, the electron current is measured in ICBA electron-only devices with an Al(35 nm)/ICBA/TPBi(5 nm)/Ba(5 nm)/Al(100 nm) structure, where TPBi [2,2′,2″-(1,3,5-Benzinetriyl)-tris(1-phenyl-1-H-benzimidazole)] is evaporated as a buffer layer. As can be observed in Figure 5.1, the electron current is very similar to the hole current for a device with similar layer thickness. The electron mobility obtained by fitting the $J-V$ characteristics with Equation 5.1 amounts to 2.7×10^{-3} $\mathrm{cm^2V^{-1}s^{-1}}$, which is very close to the determined hole mobility.

Since Equation 5.1 is a drift-only approximation, we also evaluate the electron and hole mobility with a numerical drift-diffusion solver [128] as shown in Appendix C.3. The drift-diffusion simulations can fit the full J-V characteristics, simultaneously fitting the exponential diffusion current below the built-in voltage and the quadratic drift current above the built-in voltage. The built-in voltage is determined by both the barrier at the hole-extracting cathode and band bending at the Ohmic hole-injecting anode. The band bending typically amounts to approximately 0.3 eV for an Ohmic contact [145]. In the drift-diffusion simulations, the barrier at the cathode is determined to be about 0.75 eV, consistent with the difference between the ICBA HOMO (−5.9 eV) and the work function of PEDOT:PSS (5.1–5.2 eV). Combined with band bending, this barrier is also consistent with the built-in voltage of 0.45 V, as discussed in detail in Appendix C.3. For both electron- and hole-only devices, the thickness-dependent $J-V$ characteristics can be fitted with a mobility of 2×10^{-3} $\mathrm{cm^2V^{-1}s^{-1}}$, without incorporating electron or hole traps. This mobility is slightly lower than the value estimated with Equation 5.1, which does not consider the diffusion contribution to the current. The charge transport measurements demonstrate that ICBA is a material with balanced hole and electron transport, which has not been shown before for an organic semiconductor in a diode configuration.

To explore the charge transport in more detail and evaluate the energetic disorder, we investigate the temperature dependence of the hole and electron currents. The mobility in disordered semiconductors exhibiting hopping transport depends on temperature, charge concentration, and electric field [39, 40]. For a system with Gaussian disorder, these mobility characteristics can be described by the extended Gaussian disorder model (EGDM) [40], which uses three input parameters: the width of the density-of-states distribution σ, the lattice constant a, and a mobility prefactor μ_∞. The mobility prefactor determines the magnitude of the mobility, σ mainly controls its temperature and charge-concentration dependence, and a predominantly affects its field dependence. In the EGDM, the temperature-dependent mobility at zero field and density is a function of the energetic disorder and is given by [40]

$$\mu_0(T) = \mu_\infty C_1 \exp\left[C_2(\frac{\sigma}{k_B T})^2\right] \tag{5.2}$$

with $C_1 = 1.8 \times 10^{-9}$, $C_2 = 0.42$, k is the Boltzmann constant, and T is the temperature. As can be seen from Equation 5.2, the temperature dependence of the mobility at low fields and densities is controlled by two input parameters, the mobility prefactor and the energetic disorder. To obtain the current density-voltage characteristics, the full EGDM mobility function, including the dependence on temperature, density, and field, is incorporated in the drift-diffusion solver [128].

Figure 5.2(a) shows the temperature-dependent current density-voltage characteristics of an ICBA hole-only device. The experimental data is fitted with drift-diffusion simulations incorporating the EGDM, using an energetic disorder σ of 0.10 eV and a lattice constant a of 2 nm. The mobility for vanishing carrier density and electric field at room temperature, $\mu_0(295\ \mathrm{K})$, amounts to 1.4×10^{-3} $\mathrm{cm^2V^{-1}s^{-1}}$. This number is slightly lower than the mobility extracted with Equation 5.1 and from drift-diffusion simulations with a constant mobility, which is due to the presence of a non zero space-charge density due to diffused carriers from the contacts of typically approximately 10^{16} $\mathrm{cm^{-3}}$ in the measurements [64]. We estimate the error in the energetic disorder to be within 0.01 eV, where higher or lower energetic disorder results in too strong or weak temperature dependence of the current density, respectively. We have checked that the measured temperature range falls within the validity window of the EGDM.

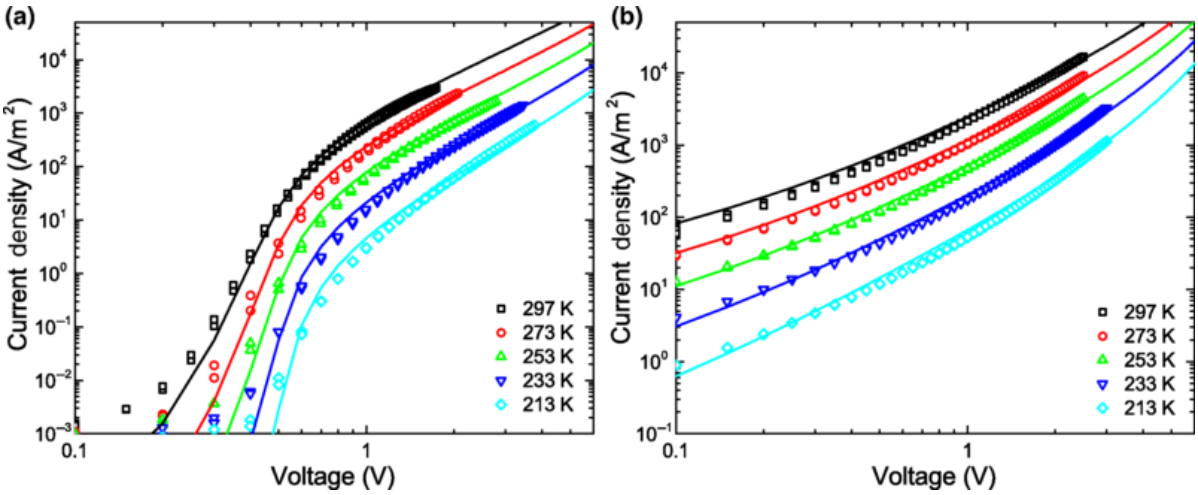

Figure 5.2.: Temperature-dependent current density-voltage characteristics of ICBA hole-only (a) and electron-only (b) devices, with ICBA layer thicknesses of 169 and 176 nm, respectively. Experimental data is plotted as symbols, the solid lines are fits with drift-diffusion simulations incorporating the temperature-, field-, and density-dependent mobility according to the EGDM. Due to the built-in voltage in the hole-only device, the steep diffusion-limited current is visible at low voltages [see Figure 5.1(b)].

A similar analysis is performed for the electron transport, as shown in Figure 5.2(b). The temperature-dependent J-V characteristics are again fitted using the EGDM, yielding an energetic disorder σ of 0.09 eV and a lattice constant a of 3 nm. The electron mobility μ_0(295 K) of 1.4×10^{-3} $\mathrm{cm^2V^{-1}s^{-1}}$ is very similar to the hole mobility, demonstrating balanced bipolar charge transport in ICBA, which is also reflected in the similar values obtained for the energetic disorder. The obtained charge-transport parameters are consistent for electron- and hole-only devices of different layer thicknesses as shown in Figure C.1.

The hole- and electron-transport simulations are performed without the need for incorporating additional trapping sites. Trap-free charge transport for both electrons and holes is quite exceptional in organic semiconductors, which frequently exhibit electron trapping [50, 151, 152, 153]. While near-balanced charge transport in a poly(p-phenylene vinylene) derivative has been claimed [154], the thickness dependence of the current was not reported and parasitic hole injection from the used TiN bottom electrode in the electron-only device cannot be excluded [155]. Other studies have demonstrated highly unbalanced charge transport in this polymer [156, 157]. As an exception to most conjugated polymers, trap-free electron and hole transport has been found in the copolymer N2200, however, hole transport was substantially inferior to electron transport due to highly unbalanced intrinsic mobilities [44]. The high and balanced bulk mobilities observed for ICBA are an experimental confirmation of the intrinsic bipolar character of organic semiconductors, which previously could only be assessed by deactivation of charge trapping either by doping [153, 158], blending with an insulator [157], or by measuring at carrier densities much higher than the concentration of bulk traps [138].

The observation of balanced electron and hole transport in ICBA raises the question of whether a bipolar device can be fabricated in which electrons and holes are injected simultaneously. Bipolar injection, resulting in subsequent recombination, has been observed previously in devices of the fullerene derivative [60]PCBM with electrically detected magnetic resonance [159]. It has been observed by Gadisa et al. that bipolar injection into a similar [60]PCBM device leads to electroluminescence [160]. Although these observations cannot evidence the presence of balanced electron and hole transport, they do support that bipolar injection and recombination are possible in fullerenes.

To confirm electron-hole recombination in ICBA, a bipolar device is fabricated in which an ICBA layer is sandwiched between a PEDOT:PSS bottom electrode and a TPBi(5 nm)/Ba/Al top electrode. The barrier at the non-Ohmic PEDOT:PSS electrode can be reduced by electrical conditioning in a bipolar device, enabling hole injection [161]. As observed in Figure 5.3, the device exhibits electroluminescence, effectively operating as a light-emitting diode. The measured light output shows the presence of both electrons and holes in the device. In the hole-only device, that is, under unipolar injection conditions, electroluminescence cannot be detected (as shown in Appendix C.2). The external quantum efficiency for electroluminescence in the bipolar device is determined to be 1.8×10^{-5}, which indicates relatively efficient electron-hole recombina-

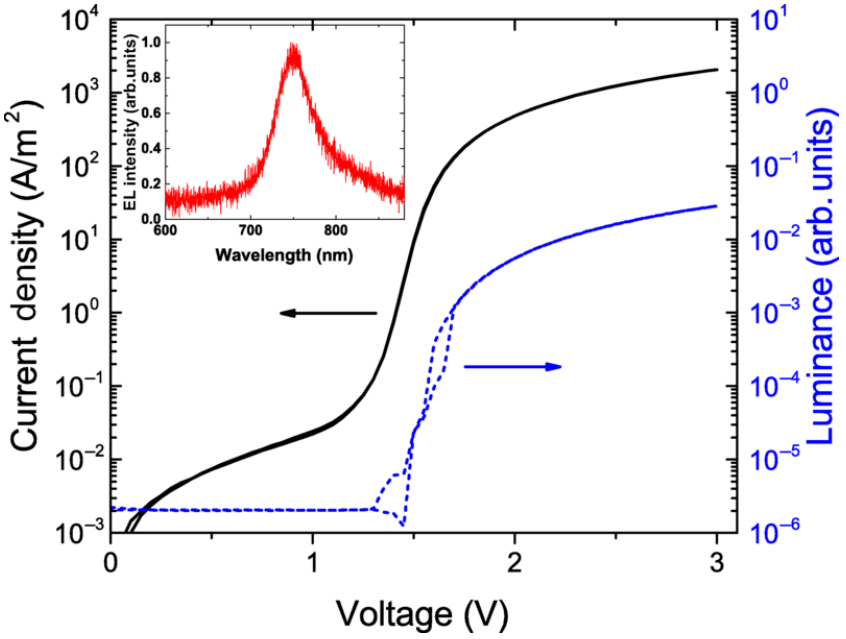

Figure 5.3.: Current density and luminance vs voltage for an ICBA organic light-emitting diode (OLED) with an ICBA layer thickness of 118 nm. The electroluminescence spectrum is shown in the inset. El, electroluminescence.

tion when considering the low-fluorescence quantum yield of fullerenes (approximately 7×10^{-5} for MoO_3 films at 300 K [162]).

5.3. Conclusion

In conclusion, trap-free space-charge-limited hole currents are measured in the fullerene derivative ICBA. The determined bulk hole mobility of 1.4×10^{-3} $cm^2V^{-1}s^{-1}$ at zero field is equally as high as the bulk electron mobility, and similar to the electron mobility of the widely-used fullerene derivative PCBM, highlighting the fact that fullerenes can be excellent hole-transporting materials. Both the electron and hole transport exhibit trap-free characteristics, resulting in the unique observation of an organic semiconductor with trap-free and balanced electron and hole transport.

Author Contributions

- Naresh B. Kotadiya
  - Designed the experiments and Fabricated all devices
  - Performed electrical characterization and temperature dependent measurements of all devices

  - Performed EGDM simulations of all devices
  - Processed and analyzed the experimental data, prepared figures for the publication

- Paul W. M. Blom
  - Scientific guidance, discussion and supervision of the work

- Gert−Jan A. H. Wetzelaer
  - Scientific guidance, discussion and supervision of the work
  - Wrote the original publication

6. Trap-free Charge Transport Window in Organic Semiconductors

In chapter 4 and chapter 5 we have shown trap free hole transport in organic semiconductors, however electron trapping is often observed in conjugated polymers. In this chapter, [1] we have investigated charge trapping in a wide range of organic semiconductors. In many cases, organic semiconductors exhibit highly unipolar charge transport, meaning that they predominantly conduct either electrons or holes [138, 50]. A fundamental question is what causes this unipolarity. To answer this question, we identify an energetic window inside which organic semiconductors do not experience charge trapping for device-relevant thicknesses in the range of 100 to 300 nm, leading to trap-free charge transport of both carriers. It is demonstrated that when the ionization energy (IE) of a material surpasses 6 eV, hole trapping will limit the hole transport, whereas an electron affinity (EA) lower than 3.6 eV will give rise to trap-limited electron transport. When both energy levels are within this window, charge transport for both types of carriers is trap free, enabling bipolar charge transport. Based on simulations, water clusters are proposed to be the source of hole trapping. The implication for devices such as OLEDs, organic solar cells, and organic ambipolar transistors is that the energy levels of the organic semiconductors are ideally situated within this energetic window of around 2.4 eV. However, for blue-emitting OLEDs, for which the required energy gap is 3 eV, this poses significant challenge to remove or disable charge traps.

6.1. Introduction and Background

Theories of charge transport in organic semiconductors predict that for most materials the charge-carrier mobility should be similar for electrons and holes [28]. In experiments, however, the transport of one type of carrier is usually clearly superior. In field-effect transistor geometries, this has been ascribed to the limited injection capabilities of commonly-used electrodes [163] and charge trapping at the semiconductor/dielectric interface [138]. However, there seems to be a more fundamental factor causing unipolarity in the bulk transport of organic semiconductors, not related to interfaces at the electrodes or gate insulator. For example, bulk hole transport is dominant in most solution-processed conjugated polymers, being orders of magnitude higher than electron transport. By systematically varying the electron affinity of these polymers, it was found that electron trapping in the bulk is the reason for the low electron mobilities [50]. The trap depth reduces with increasing electron affinity, suggesting the presence of a general impurity acting as the electron trap, with an electron affinity of around 3.6 eV. For this

[1] This chapter is published as *A window to trap-free charge transport in organic semiconducting thin films.* Naresh B. Kotadiya, Anirban Mondal, Paul W.M. Blom, Denis Andrienko, and Gert-Jan A.H. Wetzelaer. Nature materials,18(11):11821186, 2019.

reason, polymers with electron affinities higher than 3.6 eV can exhibit trap-free electron transport, which is a design rule for the realization of n-type conducting polymers [50].

Here, we first generalize this concept of electron trapping for organic semiconductors by including measurements on vacuum-deposited small-molecular semiconductors. We then demonstrate that not only electron transport becomes trap limited when the electron affinity is below 3.6 eV, but that also hole transport will be hindered by trapping when the ionization energy of the material exceeds 6 eV, implying that trap-free charge transport is only observed within this energetic window.

6.2. Results and Discussion

Hole transport in materials with ionization energies above 6 eV could previously not be measured, because of the lack of electrode materials with a sufficiently high work function to form an Ohmic hole contact. When measuring the hole current through an organic semiconductor in a hole-only device structure, it is essential that the injecting electrode does not exhibit an injection barrier. Otherwise, the measured current will be predominantly controlled by the injection rate, rather than the charge transport inside the organic semiconductor. Recently, we have developed a technique to create Ohmic hole contacts on organic semiconductors with ionization energies beyond 6 eV [103].

Enabled by this technique, we have here characterized the hole and electron transport for a large variety of organic semiconductors, both polymers and small molecules, by measuring the current density-voltage characteristics of hole- and electron-only devices. In the case of trap-free charge transport, the current depends on the square of the voltage, according to the Mott-Gurney square law for space-charge-limited currents [166] However, when charge transport is trap limited, the current exhibits stronger voltage dependence, according to a power law$J \propto V^m$ with $m > 2$ [45]. The slope m of the J-V characteristics on a double-logarithmic scale can therefore be used as a fingerprint of trap-limited transport.

Figure 6.1 shows the slope (m) of the current density-voltage characteristics of single-carrier devices plotted versus the ionization energy or electron affinity of the investigated materials. Results for electron transport in conjugated polymers [50] are included. For electron transport, as observed for both conjugated polymers and small molecules, a slope higher than 2 is measured when the electron affinity of the organic semiconductor is lower than $\sim$ 3.6 eV, indicating trap-limited electron transport in this regime. Remarkably, for ionization energies higher than 6 eV also the hole transport becomes trap limited. Consequently, for both electron- and hole-only devices, trap-free charge transport ($m = 2$) is measured when the electron affinity (electron transport) or ionization energy (hole transport) lies between 3.6 and 6.0 eV. As such, an energetic window for trap-free charge transport in organic semiconductors spanning approximately 2.4 eV can

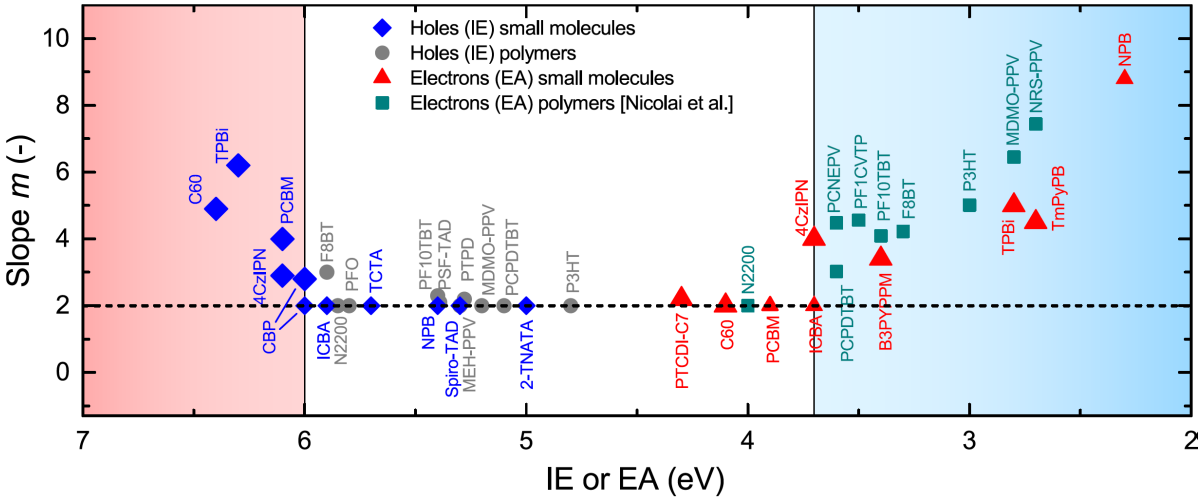

Figure 6.1.: Slope of the hole or electron current vs ionization energy and electron affinity of the organic semiconductor, respectively. The symbols are divided in groups representing either electron or hole transport in either small molecules or polymers. Larger symbols represent data measured in this study as shown in Figures D.2,D.3, D.4, D.5, D.6 in the Appendix D. small symbols are slopes determined from J-V characteristics from literature [50, 103, 146, 44, 164, 63, 47, 165, 39]. The dashed line marks a slope of 2, characteristic of a trap-free space-charge-limited current. Trap-limited currents ($m > 2$) for electrons and holes are marked by the red and green shaded areas, respectively. The chemical structures of the investigated molecules are displayed in the Figure D.1 and slopes are listed in **Table** D.1.

be identified.

The absence of trapping for materials inside the trap-free window has been confirmed with thickness-dependent measurements [103, 146, 44, 164, 63, 47, 165, 167, 168], typically covering a thickness range of 100 to 300 nm, and transient transport measurements further confirmed the obtained steady-state mobilities [167, 169] (also as shown in Figure D.7). In most cases, the trap-limited currents were observed even for relatively thin layers of close to 100 nm, in which the charge-carrier density is comparatively high: when Ohmic contacts are applied, charge carriers will diffuse from the contact into the semiconductor in order to align the Fermi level. The thinner the semiconductor film, the more diffused carriers will fill the traps. The fact that we observe trap-limited currents even for thin layers demonstrates that trapping is severe and important for device-relevant layer thicknesses. Consequently, a trap-filled limit, in which all trap are filled by injected charge carriers, was generally not observed, except for PCBM and CBP as discussed in detail below.

An interesting class of materials to exemplify the onset of the universal hole trapping are fullerenes, which are commonly known for their good electron-transport properties. As shown in Figure 6.2, for the fullerene derivatives C_{60} and PCBM with IEs of 6.4

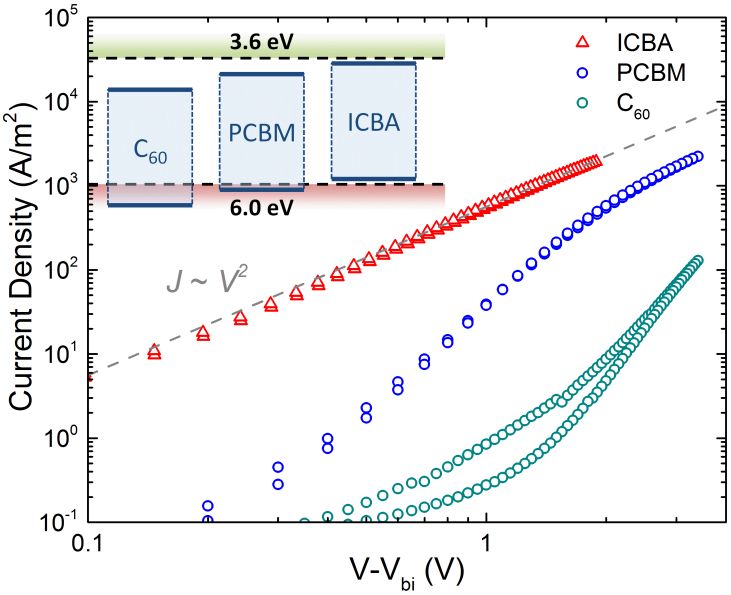

Figure 6.2.: Hole transport in C_{60}, PCBM, and ICBA. Current density vs voltage characteristics of ICBA (213 nm), PCBM (222 nm), and C_{60} (227 nm) hole-only devices, corrected for the built-in voltage (V_{bi}). The grey dashed line indicates a quadratic voltage dependence ($m = 2$). The inset shows a schematic energy diagram, indicating the IE and EA of the fullerene derivatives with respect to the trap-free window (dashed lines)

and 6.1 eV, respectively, the current has a strong voltage dependence, with slopes of 4.9 and 4.0, respectively, which is a sign of trap-limited hole transport. By contrast, for the fullerene derivative ICBA, which has a lower IE of 5.9 eV, a high hole current is observed that depends quadratically on voltage, indicative of trap-free charge transport. As a result, we demonstrate that the inferior hole transport in C_{60} and PCBM is a direct result of hole trapping. For ICBA with an ionization energy that falls within the previously-identified window, the hole transport is trap free. Since the electron affinity of ICBA, 3.7 eV, is also situated in this energetic window, the electron and hole transport are both trap free and nearly balanced [146]. Similarly, trap-free transport for both electrons and holes has been observed in the polymer N2200 and a diketopyrrolopyrrole-based polymer, which also fall within the trap-free window [170].

The ICBA hole mobility of 1.4×10^{-3} $cm^2V^{-1}s^{-1}$ extracted from space-charge-limited currents is very similar to the trap-free electron mobility [146], as would be expected theoretically for organic semiconductors. For PCBM, the hole transport can also be described with a high hole mobility similar to the electron mobility, but with the addition of a hole-trap concentration of 1.1×10^{16} cm^{-3} as shown in Figure D.2a. At high voltages, a transition to a less steep slope of the J−V characteristics is observed (Figure 6.2), which indicates that the current approaches the trap-filled limit, reaching a hole mobility of approximately 10^{-3} $cm^2V^{-1}s^{-1}$. The high hole mobility of PCBM is confirmed for a thin (75 nm) hole-only device, in which the higher charge density fills most of the traps,

leading to almost trap-free hole transport. This shows that the intrinsic hole mobility of PCBM is not low, but that the hole transport is hindered by possibly extrinsic hole traps.

From these results, it is clear that hole transport in organic semiconductors with an IE higher than 6 eV is trap limited. Similarly, electron transport becomes trap limited for materials with an electron affinity lower than 3.6 eV. For electron transport, molecular oxygen [171, 172] and water-oxygen complexes [50, 173] have been identified as a possible candidate for the electron traps. The presence of water has in fact been linked to the formation of shallow hole traps, due to an energetic broadening of occupied states of the semiconductor in the presence of water molecules [19]. Similar effects have been reported for clusters of water [174]. To investigate if water or oxygen itself could also be responsible for hole trapping, the ionization energies of these species were evaluated. The gas-phase IE of water (12.65 eV) [175] or oxygen (12.06 eV) [176] are, however, much too high to cause hole trapping, even when considering the stabilization by the dielectric medium. This implies that isolated water or oxygen molecules in an organic semiconductor cannot function as hole traps.

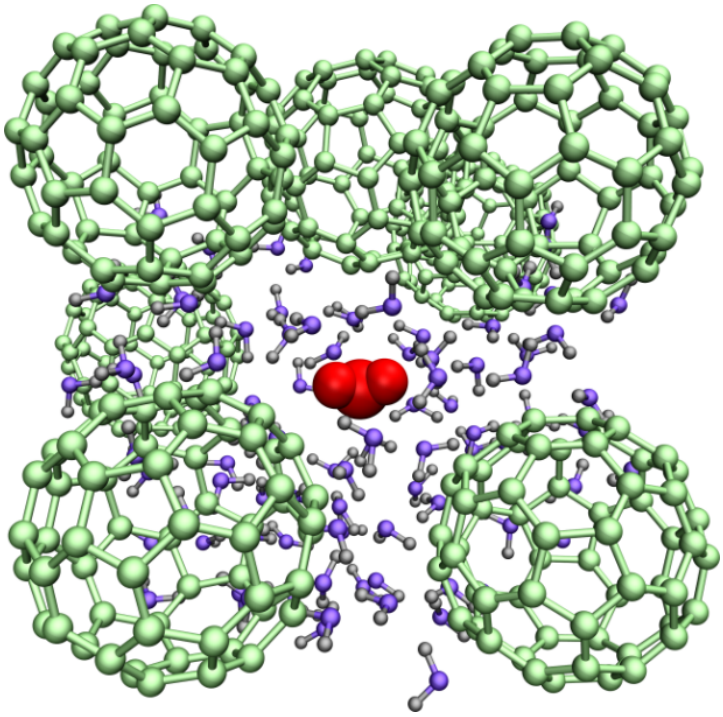

Figure 6.3.: Snapshot from molecular dynamics trajectory. C_{60} with water molecules filling the intermolecular voids. Red water molecule has ionization energy of ≈ 6 eV and is therefore a trap for crystalline C_{60}.

This situation changes when clusters of water are considered. If a water molecule is surrounded by an H_2O shell, its ionization energy can drastically decrease if dipole moments of the surrounding water coherently stabilize the charge on the water molecule.

In fact, the very same mechanism is responsible for the difference in the optical and low-frequency relative permittivities of water (1.8 and 80). Statistically, there always exist clusters with water orientations leading to potential traps (recall that the actual trap density is tiny, however sufficient to cause a large reduction in charge transport).

To justify our proposition, we show that "empty pockets" in organic materials are large enough to provide electrostatic stabilization capable of lowering the gas-phase ionization energy from 12 eV to 6 eV. To this end, we have evaluated the ionization energies of water clusters in amorphous morphologies of representative organic molecules, with a broad variation of IEs and different molecular packings. Molecular dynamics simulations of amorphous films and perturbative calculations of ionization energies were performed as described in details in the methods section of [177]. We note that these simulations represent a more realistic situation than the system of a single organic molecule surrounded by water [174], which does not include the stabilization effect of the surrounding organic molecules. A part of a snapshot of molecular dynamics simulations is shown in Figure 6.3 for amorphous C_{60}. It is clear that 20-40 molecules can fit such a pocket. For the other materials, the distributions of cluster sizes are shown in the Figure D.10.

Figure 6.4 shows corresponding densities of states of organic materials and water clusters. We can see that the ionization energy of a water cluster can be lower than the ionization energy of C_{60} (6.4 eV), implying that clusters indeed can act as hole traps. This is in agreement with the experimentally observed trap-limited hole transport in C_{60} and its energy position outside of the trap-free window. For CBP with its IE (6.0 eV) at the border of the trap-free window, some clusters would still act as hole traps according to the simulations, which is also observed experimentally. For relatively thin layers of CBP, hole transport appears to be trap free. However, for thicker CBP layers, some hole trapping is observed, which is due to the lower charge-carrier density in thick samples. The hole-trap density is determined to be 7×10^{15} cm^{-3} as shown in Figure D.2b, which is smaller than the charge-carrier density in thin samples, implying that all traps are filled in thin samples and are consequently not observed. For NPB and TCTA, which have lower IEs of 5.4 eV and 5.7 eV, located inside the trap-free window, hole trapping by water clusters would not be expected based on the simulations. This is in agreement with the experimental observation of trap-free hole transport in these materials.

A water-induced shift in energy of the occupied states of the organic semiconductor leading to shallow traps, as proposed recently [174], was not observed. This is due to the fact that stabilization already occurs due to the surrounding organic molecules. Therefore, we would not expect water-related trapping inside the trap-free window. The absence of trapping is confirmed experimentally by the thickness- and time dependence of the transport [103, 146, 44, 164, 63, 47, 165, 167, 168, 169] (see also Figure D.7). Note that the trap-free window for charge transport is observed for diodes fabricated and characterized in inert atmosphere. This indicates that the traps observed outside the window are already present in the material after synthesis or deposition, and are not

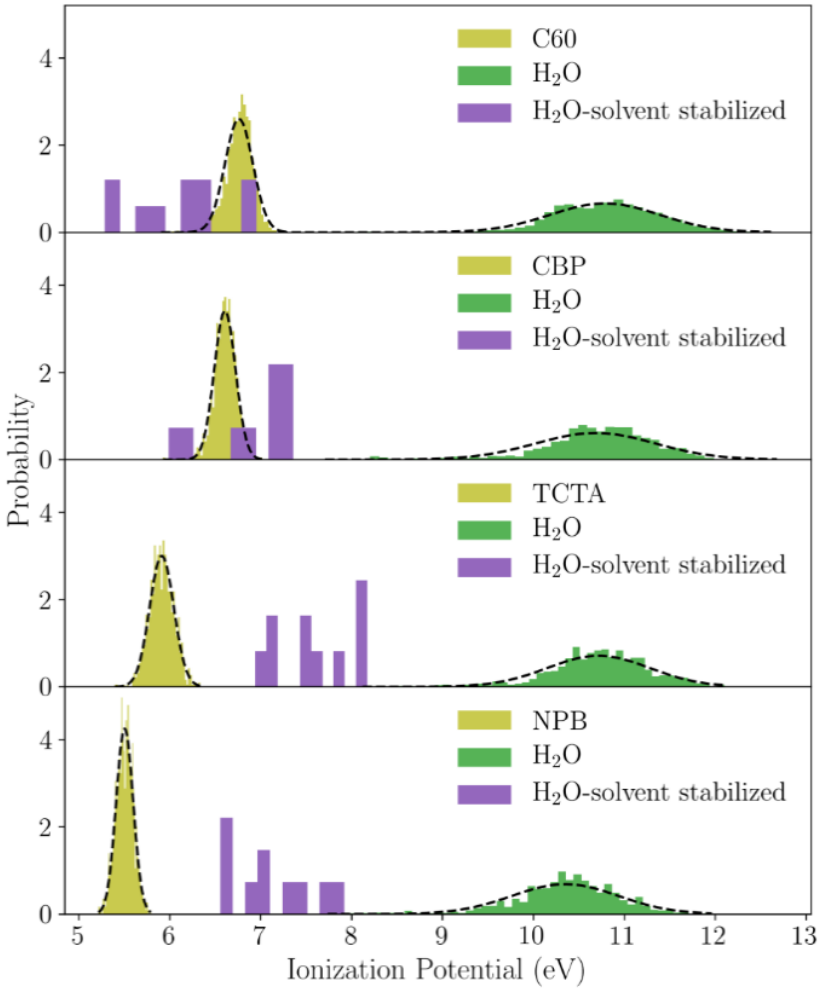

Figure 6.4.: Calculated densities of states of water clusters in four organic films. The dark yellow distributions are the calculated density-of-states distributions of the organic semiconductors. Broad green distributions are clusters with random orientations of water molecules, violet peaks correspond to a few clusters were the water shell leads to a large dielectric screening of the charge. The larger is the cluster, the stronger is the stabilization.

necessarily related to ambient exposure [178]. We have carried out ambient-exposure experiments, which show only minor but consistent effects on the device currents. However, the interpretation of these results is nontrivial, since it is not clear how much water is actually absorbed upon air exposure and how this would translate in the amount of additional traps, as shown in detail in Figure D.8. We additionally demonstrate that hole traps in PCBM can be partially removed by thermal annealing, while the transport in the trap-free ICBA control device was unaffected as shown in Figure D.9.

6.3. Conclusion

In conclusion, we have identified an energetic window inside which organic semiconductors exhibit trap-free charge transport. This was shown to apply to both small-molecule and polymeric organic semiconductors. In addition to the frequently-observed electron trapping in organic semiconductors with an electron affinity below 3.6 eV, it was found that also hole trapping occurs in materials with an ionization energy beyond 6 eV, even in vacuum-deposited films of small molecules. Theoretical calculations reconcile this behaviour with water clusters acting as hole traps. This study on a large number of materials with a large variation in chemical structures shows that the labelling of organic semiconductors as being n-type, p-type, or bipolar is directly related to the position of their energy levels with respect to the trap-free window. Balanced charge transport in devices such as organic solar cells and OLEDs requires the energy levels of the organic semiconductors to be situated within this energetic window of around 2.4 eV, which is a design rule for efficient organic devices.

Author contributions

- Naresh B. Kotadiya
  - Designed the experiments and fabricated all small molecule based hole only and electron only devices
  - Carried out air exposure and temperature dependent measurements
  - Performed electrical characterization of all devices
  - Processed and analyzed the experimental data together with G. Wetzelaer
  - Drawn chemical structures and wrote the experimental method section for the publication
  - Prepared figures for the experimental part of the publication along with G. Wetzelaer
- Anirban Mondal
  - Devised and performed molecular-dynamics simulations, force field parameterization, quantum chemical calculations and energy alignment simulations
- Denis Andrienko
  - Devised and performed molecular-dynamics simulations
- Paul W. M. Blom
  - Scientific guidance, discussion and supervision of the work
- Gert−Jan A. H. Wetzelaer

- Proposed the project, Scientific guidance, discussion and supervision of the work
- Reviewed the experimental design and helped with suggestions
- Wrote the original publication with inputs from D. Andrienko and P. Blom

7. Efficient and Stable Single-layer TADF OLED

Using the knowledge from previous chapters on charge injection and transport, we have developed a novel organic light emitting diode, presented in this chapter. From a design, optimization and fabrication perspective, an organic light-emitting diode consisting of only one single layer of a neat semiconductor would be highly attractive. Here, we demonstrate an efficient and stable organic light-emitting diode based on a single layer of a neat thermally activated delayed fluorescence emitter. By employing ohmic electron and hole contacts, charge injection is efficient and the absence of heterojunctions results in an exceptionally low operating voltage of 2.9 V at a luminance of $10,000$ cdm^{-2}. Balanced electron and hole transport results in a maximum external quantum efficiency of 19% at 500 cdm^{-2} and a broadened emission zone, which greatly improves the operational stability, allowing a lifetime to 50% of the initial luminance of 1,880 h for an initial luminance of 1000 cdm^{-2}. As a result, this single-layer concept combines high power efficiency with long lifetime in a simplified architecture, rivalling and even exceeding the performance of complex multilayer devices. [1]

7.1. Introduction and Background

After the discovery of electroluminescence in thin films of evaporated organic small molecules [6] and conjugated polymers [179], tremendous efforts have been made to utilize these materials in electronic devices such as organic light-emitting diodes (OLEDs). Devices based on conjugated polymers were considered attractive due to their simple device structure (one organic layer sandwiched between two electrodes), opening up applications such as printable large-area flexible displays. To ensure efficient hole injection from conventional electrodes such as indium tin oxide (ITO) or poly(3,4-ethylenedioxythiophene):polystyrene sulfonate (PEDOT:PSS), the ionization energies of the organic semiconductors were designed not to be higher than ∼5.3 eV. As a result, depending on the emission colour, the electron affinities then typically ranged from 2 to 3 eV. This choice in the design of organic semiconductors turned out to have a number of unfavourable consequences. First, the high electron affinity requires the use of highly reactive cathodes such as calcium or barium for efficient electron injection, putting high demands on the quality of the OLED encapsulation. Furthermore, the electron and hole transport were found to be highly unbalanced with differences up to several orders of magnitude [47]. This was found to be the result of a universal trap level situated at a depth of 3.6 eV below vacuum, leading to heavily trap-limited electron transport in

[1] This chapter is published as *Efficient and stable single-layer organic light-emitting diodes based on thermally activated delayed fluorescence.* Naresh B. Kotadiya, Paul W.M. Blom, and Gert-Jan A.H. Wetzelaer. Nature Photonics, 13(11):765769, 2019.

organic semiconductors with low electron affinities [50]. Electron trapping confines the emission zone close to the cathode, leading to efficiency losses due to exciton quenching, as well as non-radiative trap-assisted recombination [74].

The way to overcome some of these limitations was to increase the amount of organic layers, which could easily be done using thermally evaporated molecules. In 1987, a double-layer structure consisting of a hole-transport layer and an emissive layer was used to separate the recombination zone from the electrodes [6]. In subsequent years, the efficiency of OLEDs was further improved by using more extensive multilayer structures for better tuning of the injection, charge transport and positioning of the recombination zone [180].

Another important step forward was achieved in the emissive layer by employing phosphorescent heavy-metal complexes to harvest triplet excitons [21, 22], which decay non-radiatively in fluorescent emitters. These phosphorescent molecules were applied as dopants (typically 8-10 wt%) in a large-gap host to avoid concentration quenching. As a next step, it was found that the hole- and electron-transport layers can additionally be doped electrically with p- or n-type dopants, resulting in increased conductivity and, as a result, a reduced operating voltage [78, 80, 79]. The resulting p–i–n devices furthermore required the use of additional undoped exciton- and charge-blocking layers to prevent exciton quenching by the dopants, resulting typically in a five-layer device. Given that these undoped blocking layers do not necessarily consist of the same material as the host or the doped transport layers, a multilayer OLED can easily contain up to eight different organic compounds [79].

Recently, it was demonstrated that high electroluminescence quantum yields could also be obtained with metal-free organic emitters by using the concept of thermally activated delayed fluorescence (TADF) [23]. Here, the small gap between the energy of the singlet and triplet excited state allows thermally activated back transfer of the non-radiative triplet excitons to the fluorescent singlet state. Most research has been devoted to the design and fabrication of TADF OLEDs with high external quantum efficiency (EQE) [181]. However, an unresolved problem in TADF multilayer OLEDs is their limited operational stability. A notable increase in operational lifetime was achieved by using n-type hosts, resulting in a broadened recombination zone [182].

As is the case for phosphorescent OLEDs, TADF devices make use of similar complex multilayer device architectures. This complicates their design, as the properties of the charge-transport, host and blocking layers all need to be tuned to the emitter with regard to energy levels, triplet energies and charge-transport properties. The complexity further hinders interpretation of the efficiency and stability of these devices. Ideally, an OLED would consist of only one active organic semiconducting layer, in which charges are efficiently injected. Subsequently, both types of carrier are transported efficiently towards each other, after which the electrons and holes recombine through excitons with a high radiative yield via the TADF mechanism. An advantage of TADF emitters is that

they are able to harvest triplet excitons even in undoped films, so a host-guest emissive layer is not always required [183]. Balanced transport can be achieved by using an organic semiconductor with an electron affinity of ~ 3.6 eV (or higher) to strongly reduce or even eliminate electron trapping [50]. This would not only reduce the non-radiative recombination losses due to exciton quenching and trap-assisted recombination [74], but would also allow the use of non-reactive electron-injection layers, thereby enhancing the air stability of the device and the starting materials. A major challenge to overcome is then that a deeper lowest unoccupied molecular orbital (LUMO) of approximately -3.6 eV also leads to a lowering of the highest occupied molecular orbital (HOMO), even beyond -6 eV, to maintain the energy gap for visible light emission. Such a deep HOMO poses a significant challenge for hole injection that currently cannot be solved by p-type doped transport layers. Recently, we have developed a strategy to overcome this problem [103]. By using high-work-function transition metal oxides, such as MoO_3, in combination with an organic interlayer with a high ionization energy, ohmic hole contacts were formed on organic semiconductors with a HOMO at -6 eV and deeper. A similar strategy to create truly ohmic electron contacts would be highly desirable to enable efficient bipolar injection into an OLED device.

Here, we demonstrate that high efficiency, low operating voltage and high stability can be realized in a simplified TADF OLED comprising only a single layer of neat emitter sandwiched between ohmic electron and hole contacts. The efficient charge injection and the absence of heterojunctions lead to barrier-free flow of electrons and holes towards each other, yielding exceptionally low operating voltages. Balanced transport is achieved by choice of the energy levels of the emitter. The resulting broadened recombination zone gives rise to a greatly enhanced operational stability. Notably, the ohmic electron contact is formed without the requirement for air-sensitive dopants or injection layers, resulting in an OLED with improved air stability.

7.2. Device concept

As a candidate for the active material to be used in a single-layer OLED, we selected the TADF emitter CzDBA 9,10-bis(4-(9H-carbazol-9-yl)-2,6-di-methylphenyl)-9,10-diboraanthracene; Figure 7.1b). This emitter has its HOMO at -5.93 eV and its LUMO at -3.45 eV [184], which should be sufficiently low to alleviate the impact of electron traps on electron transport. The donor moieties of CzDBA consist of carbazole, which is a known hole-transport unit. However, the electron transport and hole transport in CzDBA have not been investigated so far. Furthermore, CzDBA showed excellent EQEs in conventional doped multilayer stack OLEDs, as well as exhibiting high photoluminescence quantum yields in both doped ($\sim$ 100% in 4,4′-bis(N-carbazolyl)-1,1′-biphenyl; CBP) and neat films (90.6%) [184].

In Figure 7.1a, the device layout of our single-layer OLED is shown. For hole injec-

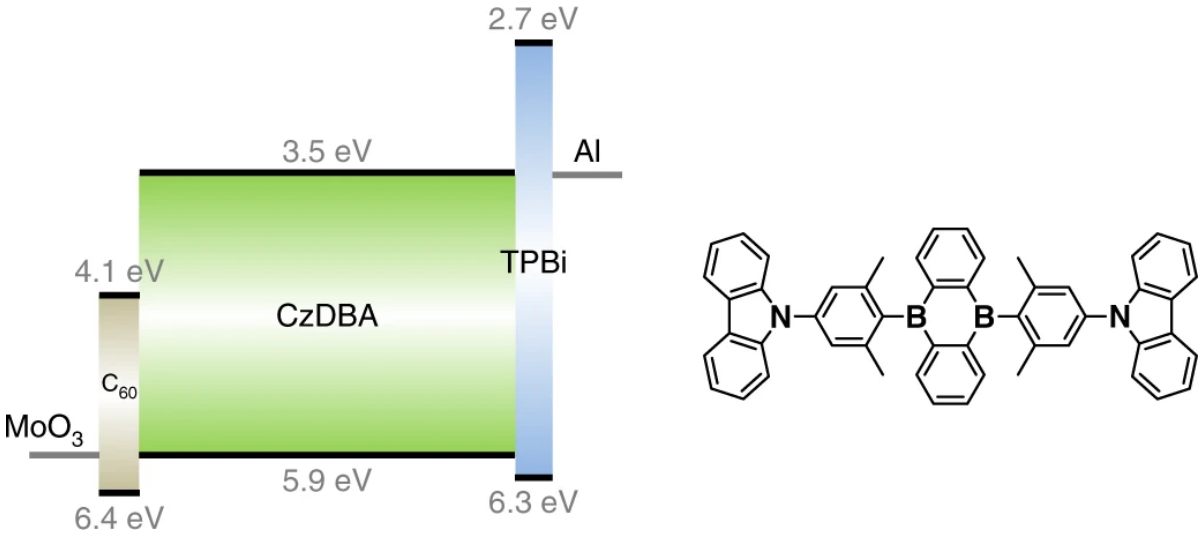

Figure 7.1.: Device layout and molecular structure of the TADF emitter CzDBA. Left: schematic energy band diagram of the single-layer OLED. A CzDBA layer is sandwiched between a MoO_3 bottom anode and an Al top cathode, using a thin C_{60} and TPBi interlayer for the formation of an ohmic hole and electron contact, respectively. Right: chemical structure of CzDBA.

tion, we use an interlayer of C_{60} to form an ohmic hole contact in combination with MoO_3, as we have demonstrated in earlier work [103]. For electron injection, we do not use a conventional reactive injection layer, such as LiF, calcium or barium. Instead, we use a thin (4 nm) interlayer of the electron-transport material TPBi (1,3,5-tris(N-phenylbenzimidazol-2-yl)benzene), which has a higher LUMO (−2.7 eV) than CzDBA, following a concept similar to the interlayer strategy for hole injection. TPBI is capped wiht a 100 nm Al layer, which has an effective work function of 3.4 eV at organic/evaporated metal interfaces [185].

The concept of ohmic contact formation with the help of a thin organic interlayer is based on Fermi level alignment of the electrode with the HOMO or LUMO of the active organic semiconductor. The interlayer acts as a spacer, eliminating the electrostatic interactions between electrode and organic semiconductor that result in barrier formation. The interlayer is virtually transparent for charges and thus does not result in any additional electrical resistance [103]. The interlayer can thus be regarded as part of the electrode, rather than as a charge-transport layer. As demonstrated previously for the formation of ohmic hole contacts, we now show that a similar strategy can also be applied for electron injection.

7.3. Results and discussion

To find out if CzDBA exhibits good charge transport, as well as to investigate electron injection from the TPBi/Al top electrode, we fabricated single-carrier devices. Electron-only devices consisted of an Al/CzDBA/TPBi(4 nm)/Al layout and hole-only devices were fabricated with a layer of CzDBA sandwiched between two ohmic C_{60}(3 nm)/MoO_3 hole contacts. The current density-voltage characteristics are displayed in Figure 7.2a. The electron and hole currents are very similar, indicating balanced bipolar charge transport in CzDBA. For both electron- and hole-only devices, it is observed that the current density has a close to quadratic dependence on voltage at voltages higher than ~ 1 V, characteristic of a trap-free space-charge-limited current. However, at lower voltages, the current depends slightly stronger on voltage. Such behaviour corresponds to trap filling [186]. After reaching the trap-filled limit, where the voltage depends on the trap density [186], a transition to trap-free transport is observed.

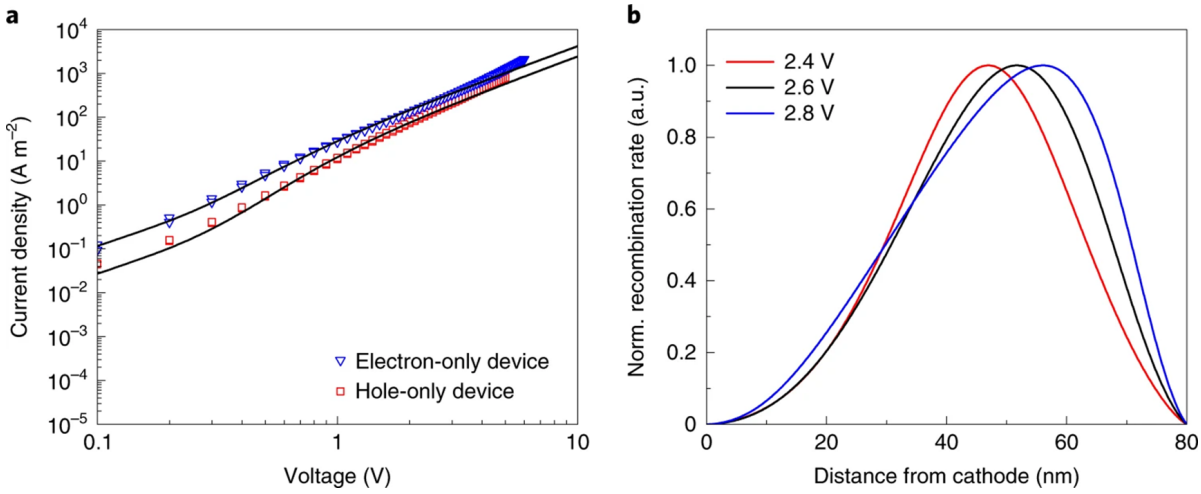

Figure 7.2.: Charge transport in CzDBA and simulated recombination profile. **a,** Current density–voltage characteristics of CzDBA electron- and hole-only devices (symbols) with a CzDBA layer thickness of 155 nm. Solid lines are fits with a numerical drift-diffusion model. **b,** Normalized recombination profile simulated for an 80 nm CzDBA OLED at different driving voltages.

To obtain quantitative charge-transport parameters, the electron and hole currents were fitted with numerical drift-diffusion simulations [128]. First, the mobility was determined at higher voltages in the trap-filled limit. The electron mobility amounted to 5×10^{-5} cm^{2}V^{-1}s^{-1}, where as the hole mobility had a slightly lower value of 3×10^{-5} cm^{2}V^{-1}s^{-1}. Subsequently, the full J-V characteristics of the electron- and hole-only devices were fitted by including an electron-trap density of 1.4×10^{16} cm^{-3} and a hole-trap density of 1.7×10^{16} cm^{-3}, respectively. These are remarkably low numbers of trap states, which are frequently an order of magnitude higher in organic semiconductors [50]. The obtained mobility and trapping parameters were verified for different layer

thicknesses, yielding excellent agreement between simulation and experiment as shown in Figure E.1. In the simulations, injection barriers were assumed to be absent. The fact that the same charge-transport parameters are obtained for different layer thicknesses shows that the newly designed TPBi/Al electrode is indeed an ohmic electron contact, notably without the use of reactive metals or n-type dopants. The obtained mobilities, although good, are not unusually high for organic semiconductors [110]. It is mainly the low trap densities for both electron and holes in combination with ohmic contacts that result in high and balanced electron and hole currents.

The balanced electron and hole mobility should also result in a broad recombination zone. This is indeed observed in the recombination profile simulated for the CzDBA OLED (Figure 7.2b). The bimolecular recombination was assumed to follow the Langevin mechanism, as is typical for single-layer OLEDs [32]. Because the electron mobility is slightly higher than the hole mobility, the recombination maximum is situated closer to the anode. The recombination zone broadens with voltage due to an increased overlap between the electron and hole density, with the maximum shifting in the anode direction. A broad recombination zone is expected to be beneficial for the operational stability of OLEDs, reducing exciton-polaron interactions associated with degradation [187, 188, 189, 190].

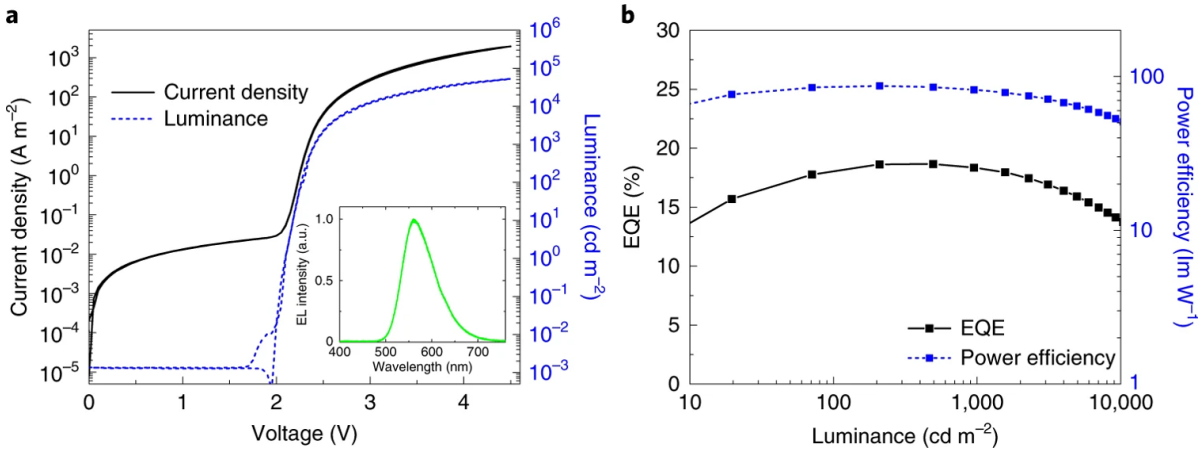

Figure 7.3.: Device performance of single-layer CzDBA OLEDs. **a,** Current density-voltage and luminance-voltage characteristics of a CzDBA single-layer OLED with a CzDBA thickness of 75 nm. Inset: the electroluminescence (EL) spectrum, with its maximum at a wavelength of 560 nm. **b,** Corresponding EQE and power efficiency as a function of luminance.

Having verified nearly balanced electron and hole transport, we fabricated an OLED with the structure displayed in Figure 7.1a. The measured current density and luminance as a function of voltage are shown in Figure 7.3a, with the EQE displayed in Figure 7.3b. The EQE reaches 19%, which is high for a single-layer OLED, but not unusual for multilayer TADF OLEDs. We note that a similar EQE has been reached

previously for a multilayer stack employing a neat emissive layer instead of a host-guest system [183]. However, the corresponding single-layer device in that study yielded an EQE of only $\sim 0.1\%$. We anticipate that the much higher value in our case is a combination of more balanced transport in combination with improved charge injection. In the case of ohmic injecting contacts, large densities of electrons and holes are located at the cathode and anode, respectively, as shown in the Figure E.2a, which prevents the charge carriers from reaching the opposite electrode. This effectively results in a built-in charge-blocking effect. Insertion of an additional electron- and exciton-blocking layer (CBP) between the C_{60} interlayer and CzDBA indeed did not improve the EQE as shown in Figure E.3, confirming that blocking layers are not required when using ohmic contacts. Furthermore, without special measures to enhance optical outcoupling, the outcoupling losses of OLEDs are estimated to be $\sim 70 - 80\%$ [191], meaning that our device has a high internal quantum efficiency. The light distribution pattern was measured to follow that of an ideal Lambertian source as shown in Figure E.2b.

Remarkably, the single-layer CzDBA OLED already reaches a luminance of $1,000$ cdm^{-2} at 2.41 V and $10,000$ cdm^{-2} at 2.89 V. In addition, the turn-on voltage of 2.10 V, measured at 1 cdm^{-2}, is considerably lower than the optical gap of 2.48 eV reported for CzDBA [184] and lower than the photon energy of 2.21 eV at the emission maximum, which is possible due to recombination of diffused carriers injected below the built-in voltage [145, 192]. These low operating voltages are even slightly superior to state-of-the-art phosphorescent OLED stacks [78, 80, 193, 194]. In our case, the low driving voltages are obtained without dedicated hole- and electron-transport layers and without electrical doping. Owing to the relatively high hole and electron mobility of CzDBA and in particular the low trap densities, charge transport on the emitter itself is efficient. In combination with the used ohmic contacts and the absence of further barriers induced by heterojunctions, this results in exceptionally low driving voltages. In particular at high luminance, the obtained operating voltages are markedly lower than previously reported for TADF multilayer OLEDs [195, 102].

The low operating voltage also results in a high power efficiency of 82 lmW^{-1} at $1,000$ cdm^{-2}, with a maximum of 87 lmW^{-1} (Figure 7.3b). Power efficiencies in excess of 100 lmW^{-1} at $1,000$ cdm^{-2} have been reported for multilayer TADF OLEDs due to a higher EQE [184, 195]. However, it is important to note that the operational stability of these highly efficient TADF devices has not been reported, and extended lifetimes are usually obtained at the expense of device efficiency. As we will demonstrate below, our single-layer OLED combines high power efficiency with long lifetime.

As shown in Figure 7.2b, a fairly broad emission zone is expected due to balanced bipolar transport and the absence of blocking layers. Previous research has shown that broadening of the emission zone results in increased operational stability [188, 189] due to a decrease in exciton-polaron interactions [187, 188, 189, 190]. We have performed lifetime measurements on our single-layer CzDBA OLEDs in a nitrogen atmosphere at constant current density, with initial luminance of $1,000$ cdm^{-2} and $5,000$ cdm^{-2}. As

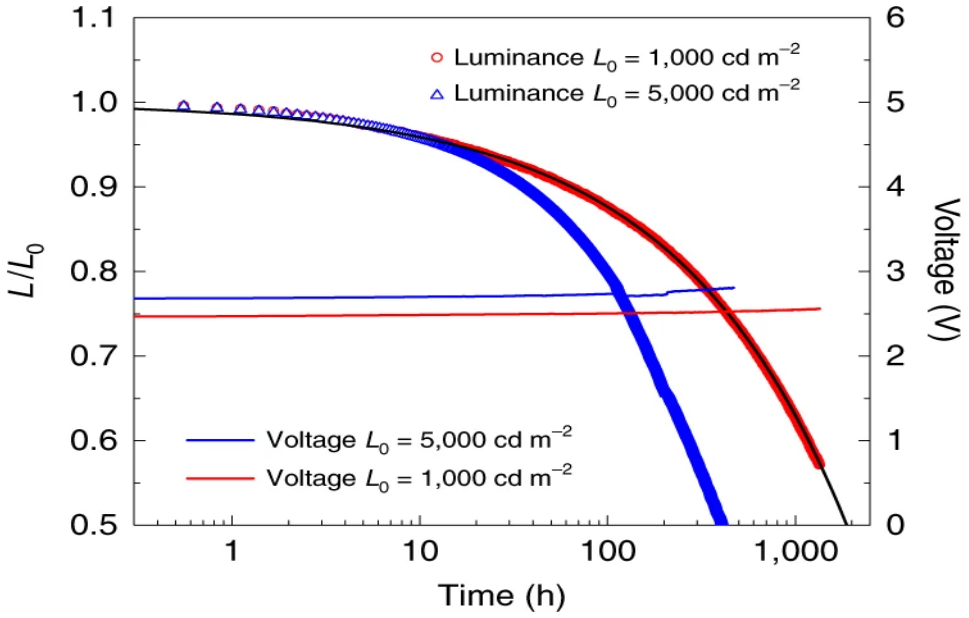

Figure 7.4.: Operational lifetime of single-layer CzDBA OLEDs. Normalized luminance (symbols, left axis) and driving voltage (lines, right axis) as a function of operation time in a nitrogen atmosphere, with an initial luminance of $L_0 = 1,000$ cdm^{-2} and $L_0 = 5,000$ cdm^{-2} at constant driving current. The luminance decay was fitted (black line) with a function $\frac{L}{L_0} = 1 - At^{(\frac{1}{\alpha})}$ with $\alpha = 2.1$ (ref. [196]) to extrapolate to LT_{50} for $L_0 = 1,000$ cdm^{-2}.

demonstrated in Figure 7.4, lifetimes to 50% of the initial luminance (LT_{50}) of 1,880 h and 414 h are obtained, respectively. Interestingly, these lifetimes are markedly longer than the lifetime reported for the same CzDBA emitter in a more complex multilayer configuration. For the multilayer structure used in the degradation test in the reference [184], which has a similar power efficiency to our device at 1,000 cdm^{-2}, the LT_{50} at 1,000 cdm^{-2} reached only 97 h [184]. This demonstrates that a single-layer OLED configuration can not only match the stability of a multilayer stack, but can even greatly extend the lifetime, retaining similar power efficiencies. The operational lifetimes at 5,000 cdm^{-2} are comparable to those obtained for the stable green TADF emitter 4CzIPN(1,2,3,4-tetrakis(carbazol-9-yl)-5,6-dicyanobenzene) in multilayer structures with n-type hosts, with similar EQE but lower operating voltage in our case, resulting in an approximately doubled power efficiency at 1,000 cdm^{-2} compared to reference [182]. It should be noted that there is a slight difference in the emitted wavelength. In addition, the driving voltages were observed to be very stable, increasing only marginally to 2.56 V after 1,350 h of aging at 1,000 cdm^{-2} and to 2.80 V after reaching LT_{50} at 5,000 cdm^{-2} (Figure 7.4), In addition, the electroluminescence spectrum was unaltered after stressing as shown in Figure E.5a. Besides the high operational stability, these single-layer architectures would greatly simplify a quantitative study of the cause of degradation in small-molecule OLEDs, which is a subject of further study.

These measurements show that single-layer OLEDs can be a viable or even superior alternative to multilayer stacks in terms of efficiency and operational stability. Another noteworthy feature of our OLED is the absence of reactive electron-injection layers or n-type doping. These layers are the most prominent cause of the rapid degradation of OLEDs in ambient atmosphere [197, 198]. Therefore, we expect our OLED to be more stable in air. In Figure 7.5, photographs are presented of an unencapsulated device operating in ambient conditions after being stored in air for set periods of time. The photographs are captured with the OLED biased at 2.15 V, corresponding to an initial luminance of $\sim$ 4 cdm^{-2}. A low luminance was used to minimize flare in the photographs, aiding the visibility of the appearance of black spots. After storage in air for 4 h, the emission remains practically uniform. After 24 h of storage in air, black spots have appeared. These black spots are usually associated with oxidation or delamination of the cathode [197, 198, 199]. The black spots are still comparatively small, considering that complete device failure after a day of storage in air has been reported for some OLEDs [199, 200]. After 5 days of storage in air, the black spots have grown in size, although 95% of the area still emits light. The ambient stability in air for various hours without encapsulation helps to provide flexibility in the OLED production process. An alternative example of a single-layer device with air-stable electrodes is the light-emitting electrochemical cell; however, such devices typically suffer from low operational stability and high operating voltages [201].

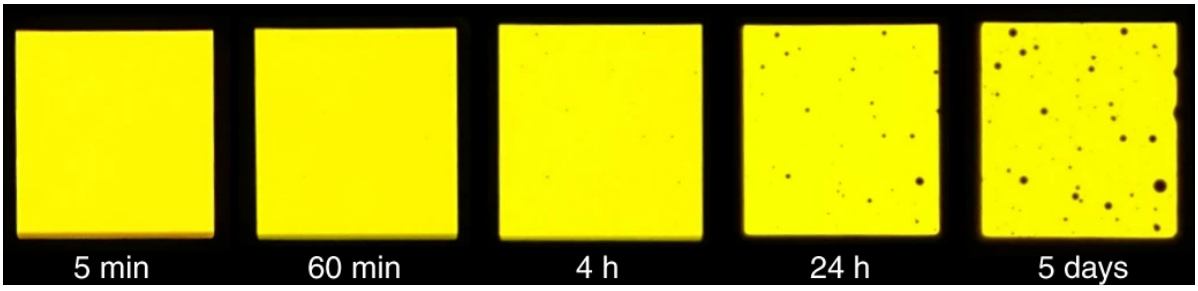

Figure 7.5.: Ambient stability of a single-layer CzDBA OLED. Photographs of an unencapsulated CzDBA OLED operating in ambient conditions as a function of time while stored in air. The OLED has an active area of 1×1 cm^2.

As a design rule for efficient OLEDs with low operating voltages, our study shows that it is more important to create ohmic contacts and use materials with a low trap density than focus on charge-carrier mobility. Although a high mobility remains important to obtain high currents at low voltages, the current is far more sensitive to injection and trapping; the latter phenomenon has received surprisingly little attention in the design of charge-transport materials and OLED stacks. Here, we have demonstrated that it is even possible to combine excellent bipolar charge-transport properties and emitter characteristics in a single organic semiconductor, providing a concept for stable and efficient single-layer OLEDs. These emitter requirements, shown here for a yellow emitter, are identical for blue- or red-emitting devices, with high photoluminescence quantum yields

having been reported for many TADF emitters in neat films [202]. Furthermore, the crucial formation of ohmic contacts has been demonstrated for a wide energy range, even enabling near-ultraviolet emission with direct charge injection [103]. For the widely used green TADF emitter 4CzIPN, the presence of ohmic contacts still ensures decent device performance in a single-layer architecture as shown in Figure E.6, in spite of strongly unbalanced electron and hole transport (Figure E.5b). The combination of transport and light emission in a single material and the use of ohmic contacts obviates the need for developing host, transport and blocking layers with matching energy levels and triplet energies, which is a great challenge, especially in the design of stable blue OLEDs with low operating voltages.

7.4. Conclusion

In summary, we have demonstrated that efficient and stable OLEDs can be achieved in a structure with a single layer of a TADF emitter sandwiched between two ohmic contacts. The TADF emitter showed excellent bipolar charge transport with low trap densities, which, in combination with truly ohmic electron and hole contacts, resulted in remarkably low operating voltages. The obtained driving voltages both at low and high luminance were lower than reported for multilayer phosphorescent and TADF OLEDs featuring dedicated electron- and hole-transport layers, or p-i-n doped structures, yielding high power efficiencies. As a result of a broadened recombination zone, the operational stability could be greatly improved in comparison with a conventional multilayer OLED structure. Furthermore, the newly designed ohmic electron contact does not feature air-sensitive interlayers or n-type doping, resulting in enhanced air stability of the TADF OLED.

Author contributions

- Naresh B. Kotadiya
  - Proposed the CzDBA as an efficient emitter for single layer OLEDs
  - Designed the experiments and Fabricated all devices
  - Performed electrical and lifetime characterization of all devices
  - Processed and analyzed the experimental data along with G. Wetzelaer
  - Prepared figures the publication along with G. Wetzelaer
- Paul W. M. Blom
  - Scientific guidance, discussion and supervision of the work
- Gert−Jan A. H. Wetzelaer

  - Proposed the project and performed simulations
  - Scientific guidance, discussion and supervision of the work
  - Reviewed the experimental design and helped with suggestions
- G. Wetzelaer and P. Blom wrote the original publication

8. Summary

8.1. Summary

The aim of this thesis was to understand the fundamental charge transport properties of small molecule-based organic semiconductors, to identify the factors limiting charge transport in organic semiconductors and to develop novel device architectures for organic and hybrid optoelectronic devices.

To design efficient organic optoelectronic devices, one needs to have ohmic contacts. So, in chapter 3 we have developed a charge injection strategy for making ohmic hole contacts in organic semiconductors. By adding an interlayer between high work function metal oxides and organic semiconductors, ohmic contacts were realized for a range of organic small molecules with ionization energies up to 6 eV.

Using this charge injection strategy, in chapter 4, we have studied experimentally and theoretically the bulk hole-transport properties of 2-TNATA, Spiro-TAD, NPB, TCTA, and CBP, which have ionization energies between 5 to 6 eV. Experimental current-voltage characteristics were investigated using the extended Gaussian disorder model, from which the energetic disorder, molecular site spacing and hole mobilities were evaluated. Despite the difference in chemical structures and ionization energies, a similar value for the energetic disorder σ of 0.09−0.10 eV and a trap free hole transport was found for all molecules. This similarity in energetic disorder is also reflected in similar mobilities at room temperature in the range of 1×10^{-4} $\mathrm{cm^2V^{-1}s^{-1}}$. In addition, molecular multiscale simulations were performed, which gave similar values of energetic disorder, Ionization energy (IE), site spacing, and mobility as obtained from the experimental results. This opens up new possibilities to predict the charge transport properties using molecular multiscale simulations.

In chapter 5, we have extended our charge transport studies to the fullerene derivative ICBA. Fullerene derivatives are well known as electron-transporting materials commonly used in organic solar cells and organic transistors. However, we have found that ICBA also has excellent hole transporting properties. We determined the bulk hole mobility to be 1.4×10^{-3} $\mathrm{cm^2V^{-1}s^{-1}}$ which is the same as the bulk electron mobility. In addition both electron and hole transport have trap free characteristics. Such trap free and balanced bipolar charge transport with high charge carrier mobilities is quite uncommon in organic semiconductors.

In chapter 6 we have investigated charge transport and trapping in a large number of vacuum deposited organic small molecules. We found that, similar to organic polymers, there exists electron trapping in organic small molecules when the electron affinity (EA) is lower than 3.6 eV. In addition, we found that there exists hole trapping when the

ionization energy is higher than 6 eV. When both energy levels are between 3.6 and 6 eV, charge transport for both types of carriers is trap free. In short, we have identified an energetic window of about 2.4 eV, inside which organic semiconductors exhibit trap-free charge transport. Based on simulations, water clusters are proposed to be the source of hole trapping. The implication for devices such as OLEDs, organic solar cells, and organic ambipolar transistors is that the energy levels of the organic semiconductors are ideally situated within this energetic window of around 2.4 eV. However, for blue-emitting OLEDs, for which the required energy gap is 3 eV, this poses significant challenge to remove or disable charge traps.

Combining the knowledge on charge injection and charge trapping, in chapter 7 we have designed an efficient and stable single layer OLED based on a neat thermally activated delayed fluorescence (TADF) emitter. By employing ohmic electron and hole contacts, charge injection is efficient and the absence of heterojunctions results in an exceptionally low operating voltage of 2.9 V at a luminance of $10,000$ cdm^{-2}. The obtained driving voltage is lower than reported for multilayer phosphorescent and TADF OLEDs featuring dedicated electron- and hole-transport layers, or p-i-n doped structures, yielding high power efficiency of 87 lmW^{-1}. Balanced electron and hole transport results in a maximum external quantum efficiency of 19% at luminance of 500 cdm^{-2} and a broadened emission zone, which greatly improves the operational stability, allowing a lifetime to 50% of the initial luminance of 1,880 h for an initial luminance of 1000 cdm^{-2}. Furthermore, the newly designed ohmic electron contact does not feature air-sensitive interlayers or n-type doping, resulting in enhanced air stability of the TADF OLED.

8.2. Zusammenfassung

Das Ziel dieser Arbeit war es, die grundlegenden Ladungstransporteigenschaften organischer, aus kleinen Molekülen bestehender Halbleiter zu verstehen, die den Ladungstransport limitierenden Faktoren zu identifizieren und neuartige Architekturen für organische sowie hybride optoelektronische Bauelemente zu entwickeln.

Um effiziente organische optoelektronische Bauelemente zu entwerfen, müssen ohmsche Kontakte bestehen. In Kapitel 3 haben wir daher eine Strategie zur Ladungsinjektion zum Herstellen ohmscher Lochkontakte in organischen Halbleitern entwickelt. Durch Hinzufügen einer Zwischenschicht zwischen Metalloxiden mit hoher Austrittsarbeit und den organischen Halbleitern wurden ohmsche Kontakte für eine Reihe kleiner organischer Moleküle mit Ionisierungsenergien von bis zu 6 eV hergestellt.

Unter Verwendung dieser Ladungsinjektionsstrategie haben wir in Kapitel 4 experimentell und theoretisch die Bulk-Lochtransporteigenschaften von 2-TNATA, Spiro-TAD, NPB, TCTA und CBP untersucht, die Ionisierungsenergien zwischen 5 und 6 eV aufweisen. Die experimentellen Strom-Spannungs-Eigenschaften wurden unter Ver-

wendung des erweiterten Gaußschen Unordnungsmodells untersucht, anhand dessen die energetische Unordnung, der Abstand zwischen den lokalisierten, molekularen Zuständen und die Lochbeweglichkeiten ermittelt wurden. Trotz der unterschiedlichen chemischen Strukturen und Ionisierungsenergien wurde für alle Moleküle ein ähnlicher Wert für die energetische Unordnung σ von 0,09 bis 0,10 eV und ein defektfreier Lochtransport gefunden. Diese Ähnlichkeit bei der energetischen Störung spiegelt sich auch in ähnlichen Beweglichkeiten bei Raumtemperatur im Bereich von 1×10^{-4} $cm^2V^{-1}s^{-1}$ wider. Zusätzlich wurden molekulare Multiskalensimulationen durchgeführt, die ähnliche Werte der energetischen Unordnung, der Ionisierungsenergie, des Abstand der lokalisierten Zustände und der Mobilität ergaben, wie sie aus den experimentellen Ergebnissen erhalten wurden. Dies eröffnet neue Möglichkeiten zur Vorhersage der Ladungstransporteigenschaften mithilfe molekularer Mehrskalensimulationen.

In Kapitel 5 haben wir unsere Ladungstransportstudien auf das Fullerenderivat ICBA ausgeweitet. Fullerenderivate sind als elektronentransportierende Materialien bekannt, die üblicherweise in organischen Solarzellen und organischen Transistoren verwendet werden. Wir haben jedoch festgestellt, dass ICBA auch hervorragende Lochtransporteigenschaften aufweist. Wir ermittelten die Bulk-Loch-Beweglichkeit zu $1,4 \times 10^{-3}$ $cm^2V^{-1}s^{-1}$, was der Bulk-Elektronenmobilität entspricht. Darüber hinaus weisen sowohl der Elektronen- als auch der Lochtransport defektfreie Eigenschaften auf. Ein derartiger defektfreier und ausgeglichener bipolarer Ladungstransport mit hohen Ladungsträgerbeweglichkeiten ist bei organischen Halbleitern ungewöhnlich.

In Kapitel 6 haben wir den Ladungstransport und das Einfangen von Ladungen in einer großen Anzahl von vakuumabgeschiedenen organischen kleinen Molekülen untersucht. Wir fanden heraus, dass ähnlich wie bei organischen Polymeren Elektronen in organischen kleinen Molekülen Ladungen eingefangen werden, wenn die Elektronenaffinität (EA) niedriger als 3,6 eV ist. Darüber hinaus haben wir festgestellt, dass Lochdefekte vorhanden sind, wenn die Ionisierungsenergie höher als 6 eV ist. Wenn beide Energieniveaus zwischen 3,6 und 6 eV liegen, ist der Ladungstransport für beide Arten von Ladungsträgern defektfrei. Kurz gesagt, wir haben ein energetisches Fenster von etwa 2,4 eV identifiziert, in dem organische Halbleiter einen defektfreien Ladungstransport zeigen. Basierend auf Simulationen wird vorgeschlagen, dass Wassercluster die Quelle für das Einfangen von Löchern sind. Die Implikation für Geräte wie OLEDs, organische Solarzellen und organische, ambipolare Transistoren ist, dass sich die Energieniveaus der organischen Halbleiter ideal innerhalb dieses energetischen Fensters von etwa 2,4 eV befinden. Für blau emittierende OLEDs, für die eine Energielücke von 3 eV erforderlich ist, stellt dies jedoch eine erhebliche Herausforderung dar, um Ladungsdefekte zu entfernen oder zu deaktivieren.

In Kapitel 7 haben wir das Wissen über Ladungsinjektion und Ladungsdefekte kombiniert und eine effiziente und stabile einschichtige OLED entwickelt, die auf einem thermisch aktivierten Emitter mit verzögerter Fluoreszenz (TADF) basiert. Durch die Verwendung von ohmschen Elektronen- und Lochkontakten ist die Ladungsinjektion ef-

fizient und das Fehlen von Heteroübergängen führt zu einer außergewöhnlich niedrigen Betriebsspannung von 2,9 V bei einer Leuchtdichte von 10.000 cdm^{-2}. Die erhaltene Ansteuerspannung ist niedriger als für mehrschichtige phosphoreszierende und TADF-OLEDs mit speziellen Elektronen- und Lochtransportschichten oder p-i-n-dotierten Strukturen angegeben, was eine hohe Leistungseffizienz von 87 lmW^{-1} ergibt. Ein ausgeglichener Elektronen- und Lochtransport führt zu einem maximalen externen Wirkungsgrad von 19% bei einer Leuchtdichte von 500 cdm^{-2} und einer verbreiterten Emissionszone, was die Betriebsstabilität erheblich verbessert und eine Lebensdauer von 1.880 h unter Reduktion zu 50% der anfänglichen Leuchtdichte von 1000 cdm^{-2} ermöglicht. Darüber hinaus verfügt der neu entwickelte ohmsche Elektronenkontakt nicht über luftempfindliche Zwischenschichten oder eine n-Dotierung, was zu einer verbesserten Luftstabilität der TADF-OLED führt.

A. Appendix: Experimental Techniques

A.1. Materials

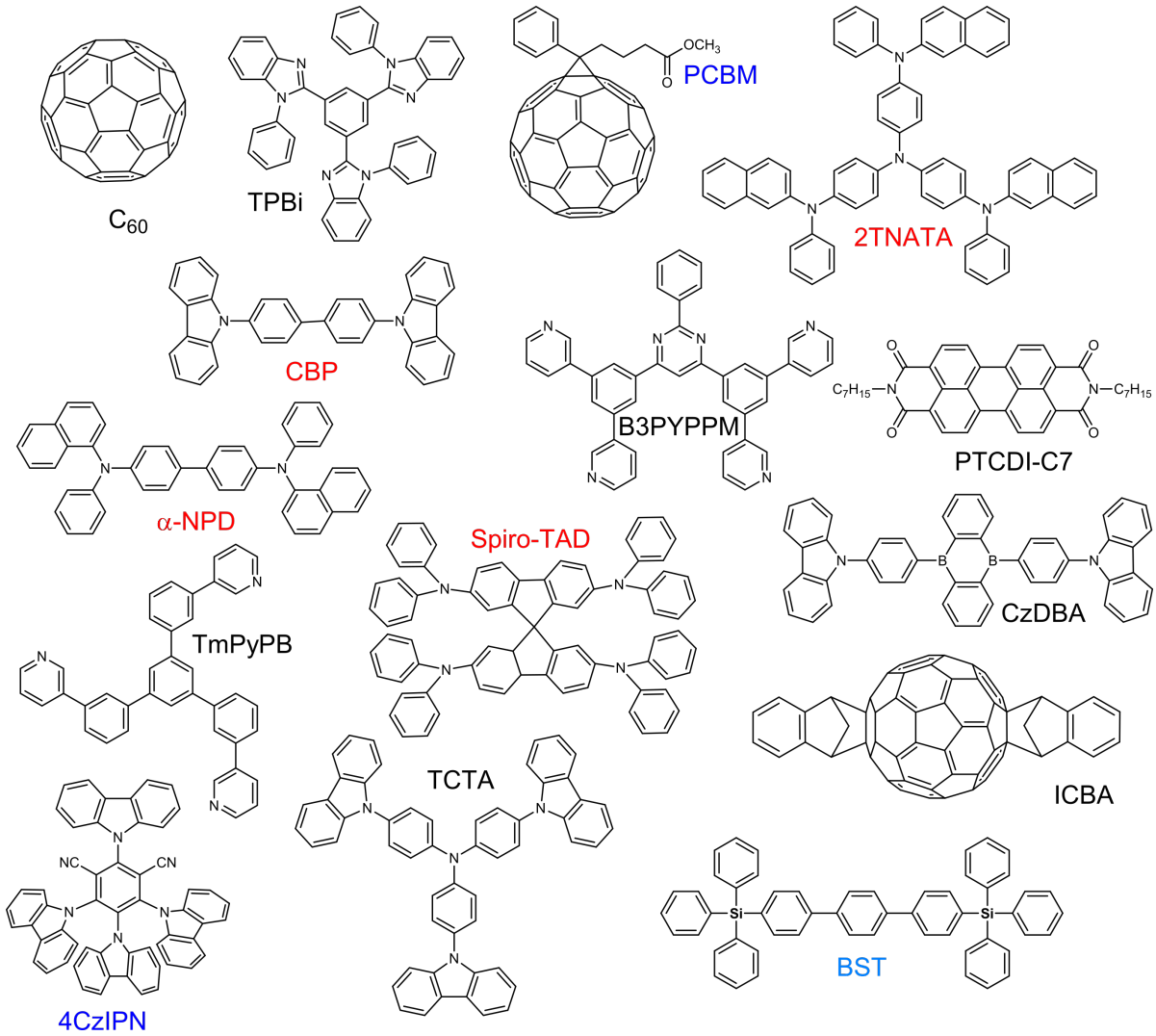

Figure A.1.: Chemical structures of organic small molecules used in this thesis

Figure A.1 shows the chemical structures of the organic small molecules investigated in this thesis. Their full names are as follows
$4,4',4''$-tris[2-naphthyl(phenyl)amino] triphenylamine **2-TNATA**, $2,2',7,7'$-tetrakis (N,N-diphenylamino)-9,9 -spirobifluorene **Spiro-TAD**, N,N'-Di(1-naphthyl)-N,N' -diphenyl-$1,1'$-biphenyl)-$4,4'$-diamine **α-NPD**, tris(4-carbazoyl-9-ylphenyl)amine

TCTA, $4,4^{'}$-bis(N-carbazolyl)-$1,1^{'}$-biphenyl **CBP**. these molecules are typically used as a host material or hole transport layer in OLEDs or orgnic photovoltaics (OPVs).

Buckminsterfullerene or Fullerene-C_{60} $\mathbf{C_{60}}$, [6,6]-Phenyl C_{61} butyric acid methyl ester **PCBM**, $1^{'}$,$1''$,$4^{'}$,$4''$-Tetrahydro-di[1,4]methanonaphthaleno[1,2:$2^{'}$,$3^{'}$,56,60:$2''$,$3''$][5,6] fullerene-C_{60} **ICBA**, N,$N^{'}$-Diheptyl-3,4,9,10-perylenedicarboximide **PTCDI-C7**, 1,3,5-Tri(m-pyridin-3-ylphenyl)benzene,1,3,5-Tris(3-pyridyl-3-phenyl)benzene **TmPyPB**, $2,2^{'}$, $2''$-(1,3,5-Benzinetriyl)-tris(1-phenyl-1-H-benzimidazole) **TPBi**, 4,6-Bis(3,5-di(pyridin-3-yl)phenyl)-2-(pyridin-3-yl)pyrimidine **B3PyPPM** are typically used as an eletron transport layer or electron acceptor materials.

1,2,3,5-tetrakis(carbazol-9-yl)-4,6-dicyanobenzene (4CzIPN) and 9,10-bis(4-(9H-carbazol-9-yl)-2,6-di-methylphenyl)-9,10-diboraanthracene (CzDBA) are thermally activated delayed fluorescence (TADF) emitters typically used to make efficient OLEDs. $4,4''$-bis(triphenylsilanyl)-($1,1^{'}$,$4^{'}$,$1''$)-terphenyl (BST) was used as an interlayer for hole injection in the present work.

4CzIPN was synthesized using the procedure described in the literature [23] and purified by vacuum sublimation. poly(3,4−ethylenedioxythiophene):polystyrene sulfonate (PEDOT:PSS) was purchased from Heraeus, BST and B3PyPPM, were purchased from Luminescence Technology Corp. and all other materials were purchased from Sigma-Aldrich and were used as received.

A.2. Device Fabrication

Hole-only devices were fabricated on glass substrates pre-patterned with indium-tin oxide (ITO). Substrates were thoroughly cleaned by washing with detergent solution and ultrasonication in acetone and isopropyl alcohol, followed by UV-ozone treatment. Next, a 35 nm layer of PEDOT:PSS [CLEVIOS^{TM} P VP AI 4083] was spin coated on it and annealed at 140 ℃, for 10 min in air. The substrates were then transferred into a nitrogen-filled glove box and were not exposed to air in the subsequent steps. Majority of organic small molecule layers were thermally deposited at a rate of $0.3-1.0\mathring{A}s^{-1}$ and at a base pressure of $4-5\times10^{-7}$ mbar, while fullerene derivatives were spin coated from the chloroform solvent in a nitrogen atmosphere. Subsequently, a MoO_3(10 nm)/Al(100 nm) top electrode was thermally evaporated to complete the device. The final device structure was glass/ITO/PEDOT:PSS/hole-transport layer/interlayer/MoO_3/Al.

For some hole-only devices instead of MoO_3 WO_3 or V_2O_5 were used as top electrode along with 100 nm Al as a capping layer. The symmetric Hole-only devices were also fabricated in a similar way, except that the device structure then becomes glass/ITO/PEDOT:PSS/metal oxide/interlayer/hole-transport layer/interlayer/metal oxide/Al.

For electron-only devices, glass/Al(35 nm)/organic semiconductor/TPBi(5 nm)/ Ba(5 nm)/Al(100 nm) architecture was used, where the fabrication procedure for organic layer and metal contacts remains same as above.

For Organic light emitting diodes, either glass/ITO/PEDOT:PSS/MoO_3/interlayer/ Emitter/interlayer/Al or glass/ITO/PEDOT:PSS/Emitter/interlayer/Al(or Ba/Al) device architecture was used. Again the fabrication procedure remains same as above.

A.3. Device Charcaterization

Electrical characterization of all devices were performed in a nitrogen atmosphere ($O_2 < 0.1\ ppm\ H_2O < 0.1\ ppm$) using a Keithley 2400 source meter. Between fabrication and characterization, the devices were not exposed to air. For low temperature measurements the devices were cooled using a cold nitrogen gas supply, which was cooled by passing through the liquid nitrogen tank (or reservoir). To measure the EQE and power efficiency of OLEDs, the light output was measured using a calibrated Si photodiode and procedure described in [203] was followed. Electroluminescence spectrum of OLEDs were measured with a USB4000-UV-VIS-ES spectrometer. The angular dependence of electroluminescence was measured with a home-built set-up based on a goniometer and a Si photodiode.

A.4. UPS characterization

For UPS studies, ultrasonically cleaned silicon wafers were used as substrates. To avoid any charging during the measurement, substrates were coated by thermal evaporation with 2 nm of chromium as an adhesive layer and the 50 nm of gold as a conductive layer. Subsequent layers (MoO_3 and organic molecules) were thermally evaporated in the same way as the hole-only devices. For the measurement of IE profiles, separate samples were prepared with different organic layer thickness, so no cumulative irradiation damage occurs during the acquirement of the valence-band spectra.

UPS measurements were conducted at a base pressure of 10^{-9} mbar on Si/Cr(2 nm)/Au(50 nm)/MoO_3(10 nm)/organic substrates with a Kratos Axis Ultra-DLD spectrometer (Kratos, Manchester, UK). During UPS measurement, the sample was held at a bias of -9 V with respect to the spectrometer. Illumination at 21.22 eV was provided by the He(I) emission line from a helium discharge lamp. Photoelectron emission was collected at 0° from the surface normal of the samples. The spectra were taken in three different spots to confirm their reproducibility and the irradiation exposure time was kept under one minute.

A.5. Molecular simulations and density of states evaluation

All morphology simulations were performed using the GROMACS package and re-parameterized OPLS-AA force-field, Density of states was evaluated using the VOTCA package [204, 205] and polarizable force-field (Thole model). The detailed procedures can be found in the supporting information of the original publications [103], [167] and [177].

B. Appendix: Chapter 3 Hole Injection

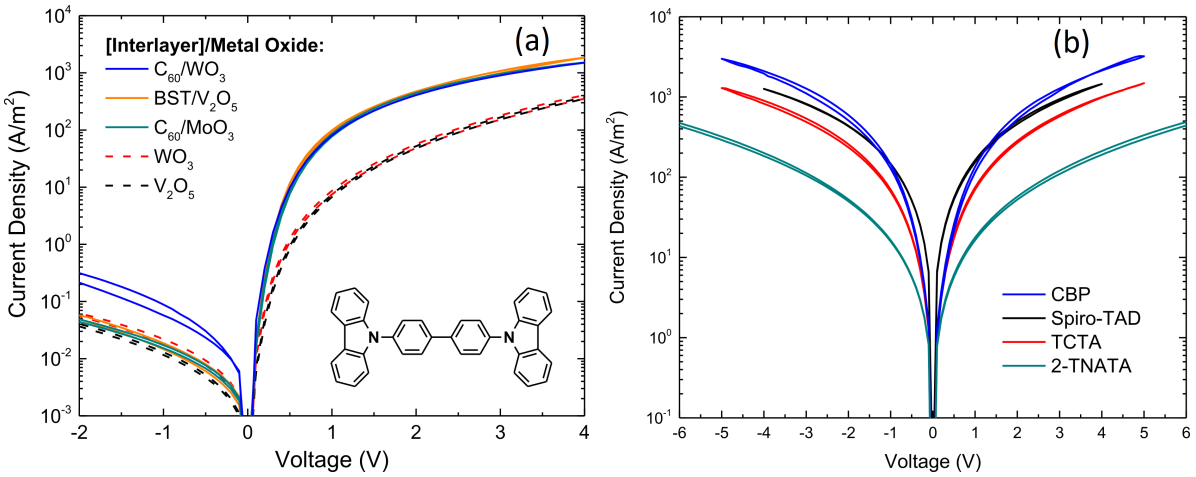

Figure B.1.: Current density−voltage characteristics **(a)** of CBP (190 nm) hole-only devices with MoO_3, WO_3 and V_2O_5, showing that ohmic contact can be formed with all three high work function metal oxides. **(b)** of symmetric hole-only devices, having MoO_3 along with same interlayers as bottom and top electrodes. The interlayers used were TCTA for 2−TNATA (222 nm) and Spiro-TAD (227 nm), CBP for TCTA (211 nm), and C_{60} for CBP (197 nm). The identical currents in forward and reverse bias show that ohmic contacts can also be formed for a bottom-anode configuration. It also shows that diffusion of MoO_3 into the organic layers (which occurs only when MoO_3 is deposited on top of the organic layer), is not responsible for the ohmic-contact formation.

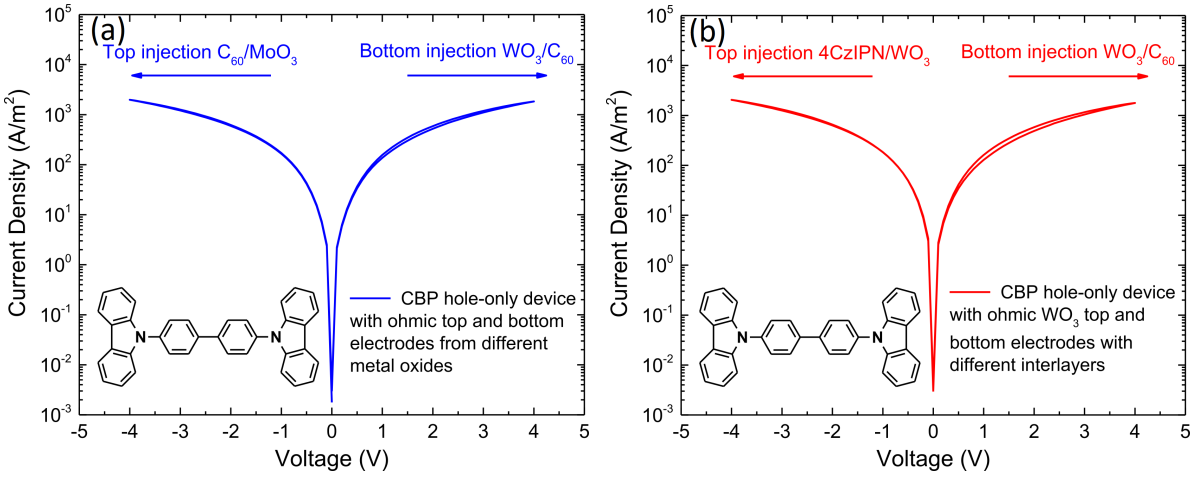

Figure B.2.: (a) Current density-voltage characteristics of a CBP (200 nm) hole-only device with a WO_3 bottom electrode and a MoO_3 top electrode, with C_{60} interlayers on both sides. The current is identical in forward (bottom injection) and reverse (top injection) bias, indicating that an ohmic hole contact with CBP can be formed also with a WO_3 bottom electrode. **(b)** Similar to the case of MoO_3, injection from other metal oxides can also be rendered ohmic with different interlayers.

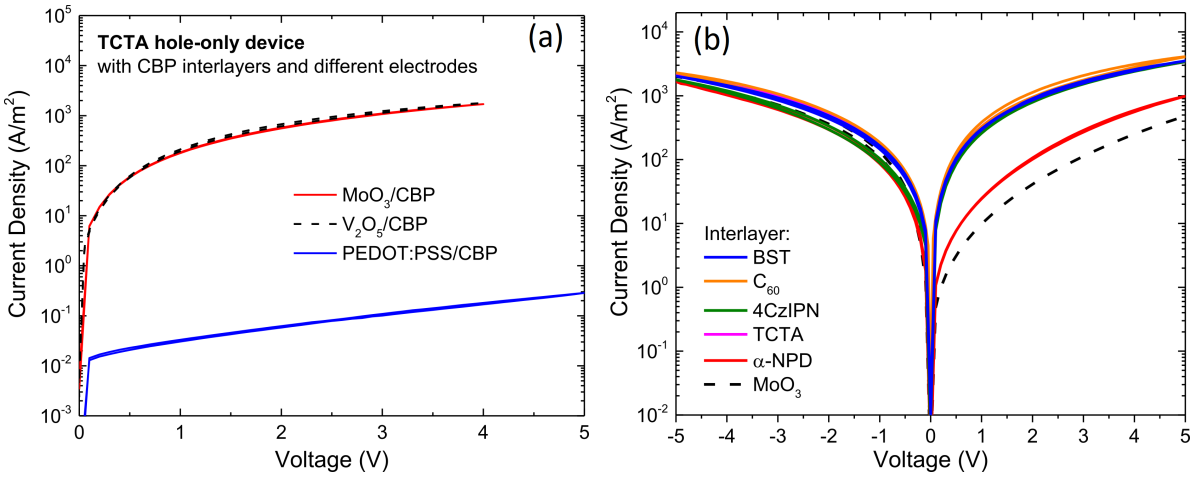

Figure B.3.: (a) Current density-voltage characteristics of TCTA (173 nm) hole-only devices with CBP interlayer and different bottom electrodes. The figure shows that for the high work-function electrodes MoO_3 and V_2O_5, ohmic contacts and identical high currents are obtained. For a PEDOT:PSS electrode with a work function of 5.0−5.2 eV, which is lower than the IE of TCTA (5.7 eV), the injected current is orders of magnitude lower, showing that the interlayer only enhances injection of electrodes with a sufficiently high work function. This result is expected from the band-diagram simulations in Figure 3.4c, which show that the work function has to be at least the same as the IE of the HTL. **(b)** Current density-voltage characteristics of a PEDOT:PSS/Spiro−TAD/MoO_3 hole-only device with different interlayers between the Spiro−TAD (163 nm) transport layer and MoO_3. The offset between α−NPD (5.4 eV) and Spiro−TAD (5.3 eV) is not sufficient for formation of an ohmic contact, but the minor positive offset results in a noticeable improvement of the injected hole current with respect to the MoO_3 reference.

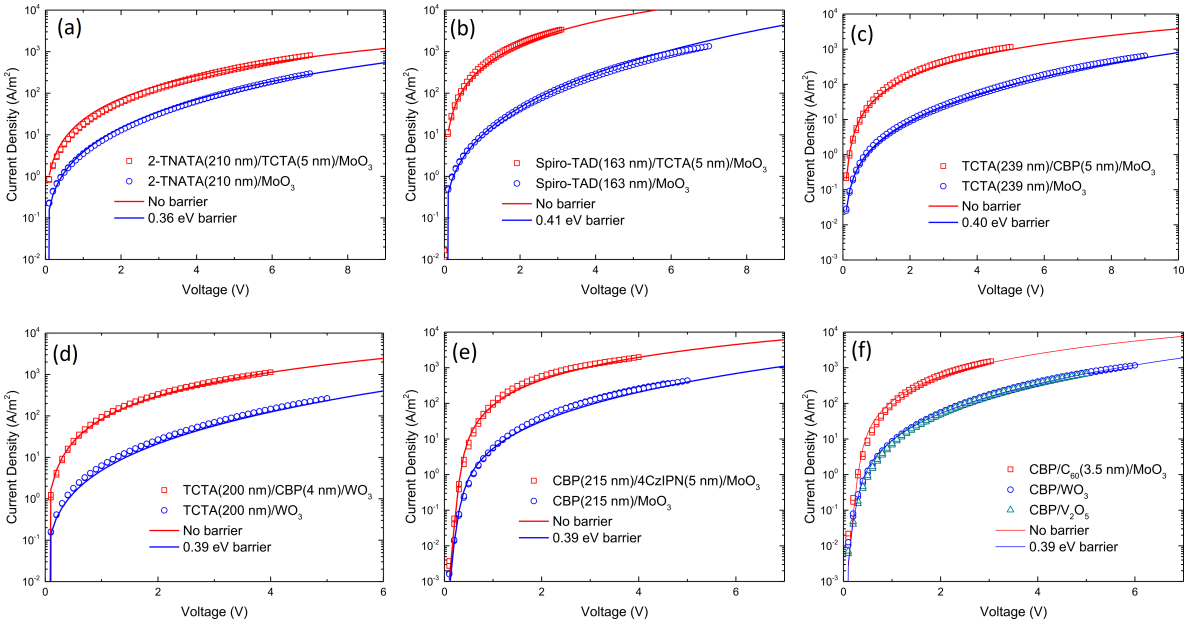

Figure B.4.: Drift-diffusion simulation [128] of hole−only device of **(a)** 2−TNATA, **(b)** Spiro−TAD, **(c, d)** TCTA and **(e, f)** CBP, using charge injection contact fabricated with and without interlyer, between organic semiconductor and metal oxide (MoO_3, WO_3 or V_2O_5) as electrode. A charge injection barrier of about ∼0.4 eV is observed in all cases, when metal oxide is directly used as an electrode without an interlyer. The injection model includes barrier lowering due to the image charges [206].

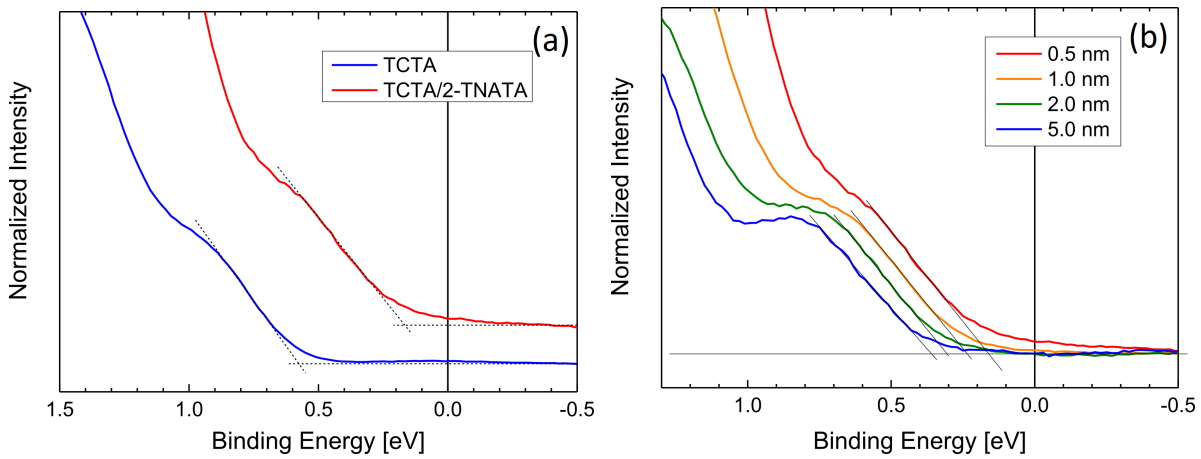

Figure B.5.: (a) Photoemission spectra obtained by UPS for TCTA (5 nm) and TCTA(5 nm)/2−TNATA(0.5 nm) on top of MoO_3 (10 nm). The onset of the ionization energy (IE) is determined at the intersection of the dashed lines, which is at 0.58 eV for TCTA(5 nm) and at 0.16 eV for TCTA(5 nm)/2−TNATA(0.5 nm) w.r.t. the Fermi level, showing that near the interface the IE of 2−TNATA almost aligns with the Fermi level. **(b)** Onset of the IE for varying 2−TNATA thickness (see legend) on top of MoO_3/TCTA(5 nm), showing the separation of the valence states from the Fermi level due to band bending, which is a result of charge accumulation at the interface.

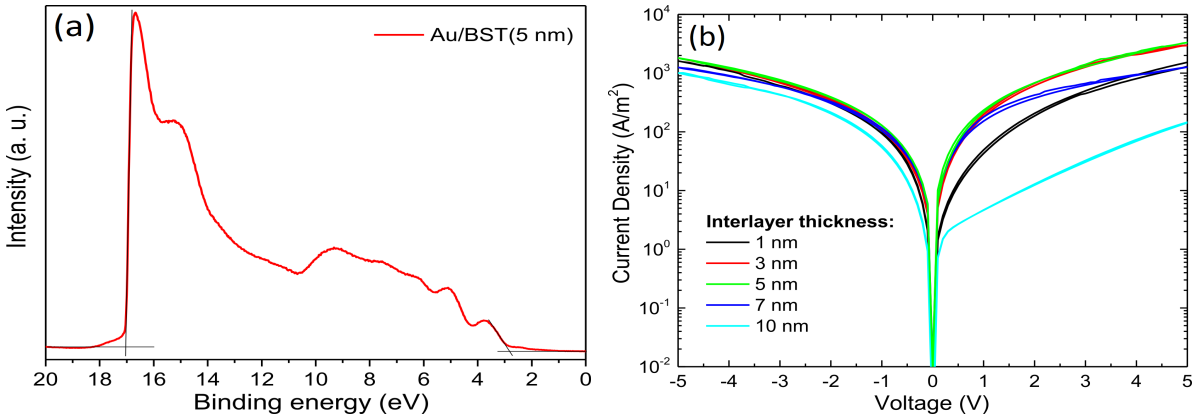

Figure B.6.: **(a)** UPS spectrum of BST on Au with an excitation energy of 21.22 eV. The onset of the ionization energy was determined to be 7.0 eV. **(b)** Current density−voltage characteristics of a Spiro−TAD (193 nm) hole-only device for different TCTA interlayer thicknesses. Enhanced injection (compared to a MoO_3 contact) is already observed for an interlayer of 1 nm, but injection is maximized for interlayers between 3 and 5 nm. An interlayer thickness of 1 nm of TCTA might not be sufficient to effectively decouple the Spiro−TAD from the oxide. In addition, the thickness may be insufficient to form a closed layer. For interlayers thicker than 7 nm, the current reduces, which indicates that the current is limited by injection in and transport through the interlayer.

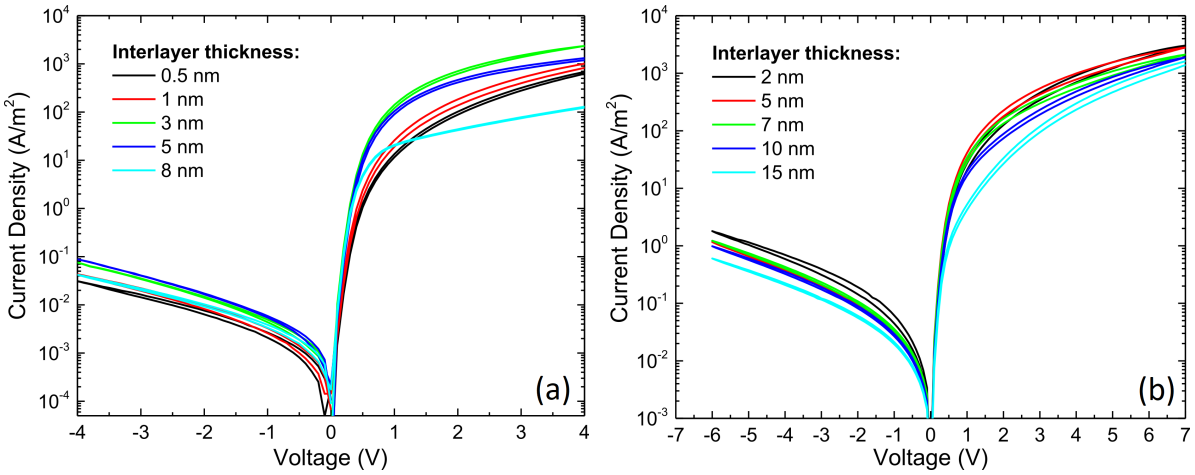

Figure B.7.: Current density−voltage characteristics of hole−only devices of **(a)** CBP (184 nm) for different BST interlayer thicknesses and of **(b)** TCTA(188 nm) for different CBP interlayer thicknesses. The thickness dependence of the interlayer is similar to the Spiro-TAD/TCTA system. However, In case of CBP/BST system a stronger reduction in current is observed at thicker BST layer, this could be due to inferior injection in and/or transport through the BST interlayer. And in case of TCTA/CBP system a higher injection current is observed even at thicker CBP layer, this could be explained by the higher hole mobility in the CBP interlayer.

C. Appendix: Chapter 5 ICBA

C.1. Additional hole-only and electron-only devices

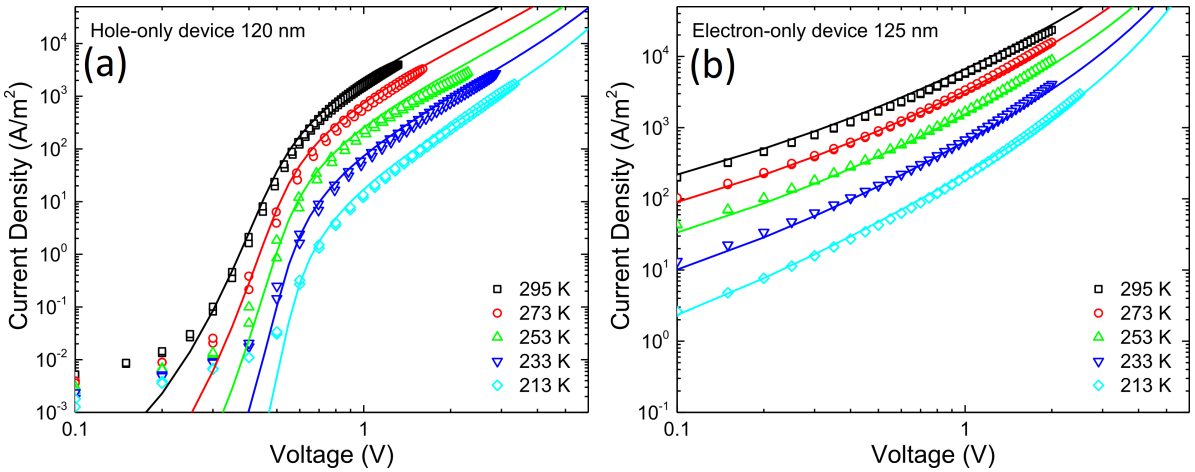

Figure C.1.: Temperature-dependent current density-voltage characteristics of an ICBA (a) hole-only device of 120 nm thickness and (b) electron-only device of 125 nm thickness. Symbols represents experimental results and solid lines drift-diffusion simulations using EGDM model. For both hole-only and electron-only device same set of parameters were used to fit the data as in the Figure 5.2.

C.2. Confirmation of Hole-Only Current

In Figure C.2(a), it is demonstrated that the current measured in the hole-only devices is carried by holes only and electron injection is absent. This can be confirmed by performing electroluminescence measurements, which we detect as a photocurrent from a silicon photodiode. Figure C.2(a) demonstrates that while electroluminescence is observed in the bipolar device above the built-in voltage following the injected current, there is no electroluminescence detected for the hole-only device, despite the large current density. This implies that electron injection from PEDOT:PSS in the hole-only device is not significant, confirming that the measured current is carried by holes only. In addition, Figure C.2(a) shows the current of the bipolar device in reverse bias. Only a leakage current is observed in reverse bias, demonstrating that electron injection from PEDOT:PSS and hole injection from TPBi/Ba/Al are not significant. As a result, electroluminescence is also absent in reverse bias. The low built-in voltage in the hole-only device once more confirms the unipolar character.

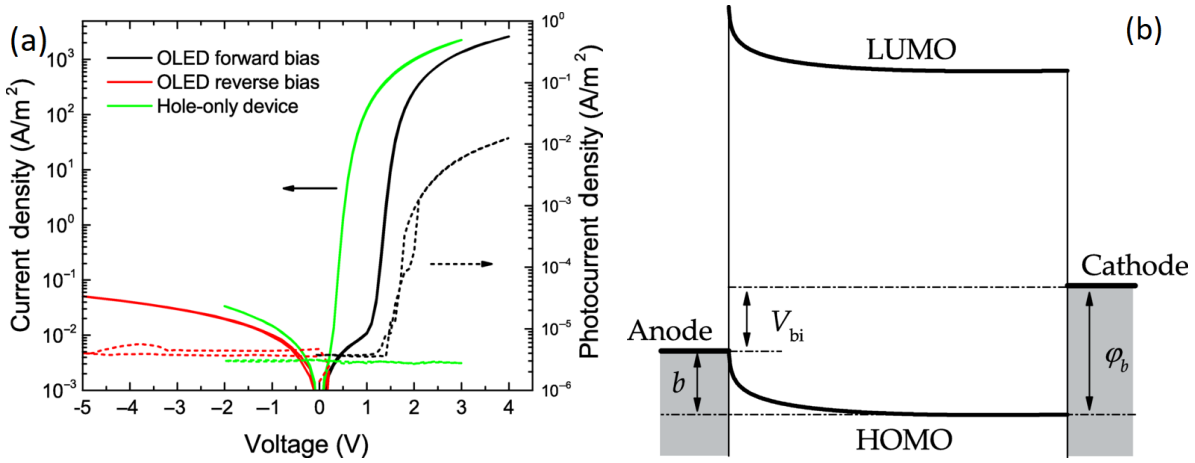

Figure C.2.: (a) Current density (solid lines) and light output (dashed lines) vs voltage for hole-only and bipolar (OLED) devices of ICBA. The light output is measured as a photocurrent by a silicon photodiode. (b) Schematic band diagram of an ICBA hole-only device with an Ohmic hole-injecting anode and a non-Ohmic hole-extracting cathode at the built-in voltage ($V = V_{bi}$).

C.3. Drift-Diffusion Simulations with a Constant Mobility

As discussed in [145], the current density in an asymmetric single-carrier device can be described by a diffusion-dominated current below the built-in voltage and a drift-dominated current above the built-in voltage. As illustrated in the energy band diagram in Figure C.2(b), the built-in voltage in a hole-only device can be described as the potential difference between the energetic barrier at the cathode φ_b, and the band-bending parameter b. Band bending is present at the Ohmic contact, which is the result of charges diffusing into the organic-semiconductor layer. The band-bending parameter b typically has a value of approximately 0.3 V and can be calculated as described in [145].

Figure C.3(a) shows the experimental data and the simulated drift-diffusion current for hole-only devices of different ICBA layer thicknesses. A constant mobility of 2×10^{-3} $\mathrm{cm^2V^{-1}s^{-1}}$ is used for all layer thicknesses. The barrier at the injecting contact is set to 0 V (Ohmic contact). The barrier at the extracting (PEDOT:PSS) contact φ_b (see Figure C.2(b)), which shifts the simulated curves horizontally along the voltage axis, is tuned to fit the exponential diffusion regime below V_{bi}. The values obtained for φ_b are 0.72, 0.78, and 0.78 V for layer thicknesses of 75, 120 and 169 nm, respectively. The variation in the barrier φ_b is small and the value is consistent with the difference between the ICBA HOMO (−5.9 eV) and the work function of PEDOT:PSS (5.1–5.2 eV). Since $V_{bi} = \varphi_b - b$, as shown schematically in Figure C.2(b), the value of the cathode barrier φ_b is in agreement with the built-in voltage in Figure 5.1, considering a typical

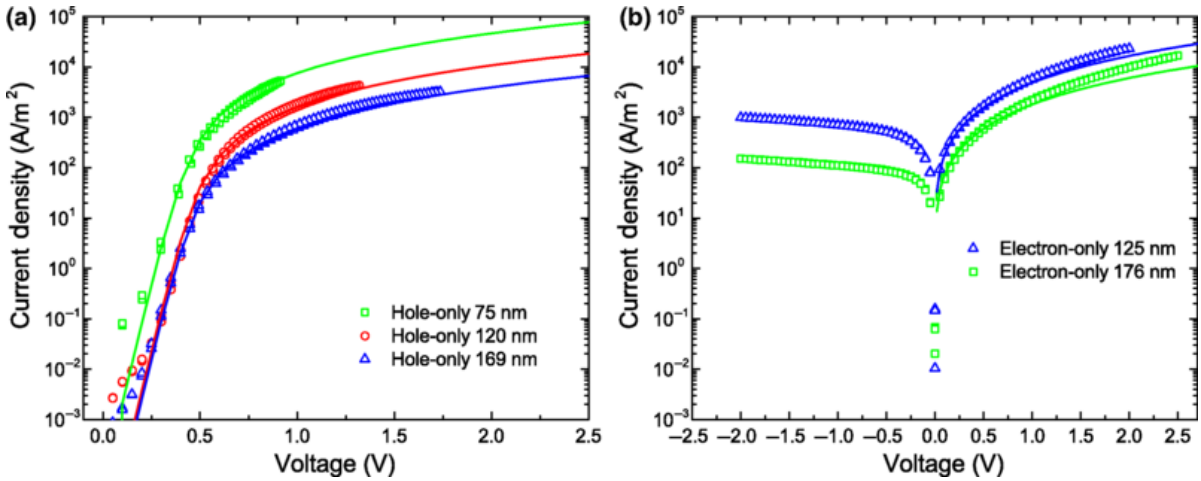

Figure C.3.: Current density-voltage characteristics of ICBA hole-only (a) and electron-only (b) devices of different layer thicknesses. The symbols represent experimental data, the lines are fits with drift-diffusion simulations using a constant mobility.

band-bending parameter b of approximately 0.3 V [145].

Figure C.3(b) shows the current density-voltage characteristics of ICBA electron-only devices and corresponding fits with drift-diffusion simulations. A constant mobility of 2×10^{-3} $\mathrm{cm^2V^{-1}s^{-1}}$ is used for both layer thicknesses. The deviation at higher voltage is due to the field dependence of the mobility, not included in this simulation. The simulations are performed without injection barrier and the barrier at the extracting contact φ_b is 0.25 V, thus a built-in voltage is consequently absent. The small barrier φ_b results in a slightly injection-limited current in reverse bias.

D. Appendix: Chapter 6 Trap-free Window

Full names of the organic polymer materials listed in the Table D.1 are as follows. **F8BT** Poly(9,9-dioctylfluorene-alt-benzothiadiazole), **PFO** Poly(9,9-di-n-octylfluorenyl-2,7-diyl), **N2200** Poly[N,N′-bis(2-octyldodecyl)-naphthalene-1,4,5,8-bis(dicarboximide)-2,6-diyl]-alt-5,5′-(2,2′-bithiophene), **PF10TBT** Poly[2,7-(9,9-didecylfluorene)-alt-5,5-(4,7-di-2-thienyl-2,1,3-benzothiadiazole)], **PSF-TAD** Polyalkoxyspirobifluorene-N,N, N′,N′-tetraaryldiamino biphenyl, **MEH-PPV** Poly[2-methoxy-5-(2-ethylhexyloxy)-1,4-phenylenevinylene], **MDMO-PPV** Poly[2-methoxy-5-(3′,7′-dimethyloctyloxy)-1,4-phenylenevinylene], **PCPDTBT** Poly[2,6-(4,4-bis-(2-ethylhexyl)-4H-cyclopenta [2,1-b;3, 4-b′]dithiophene)-alt-4,7(2,1,3-benzothiadiazole)], **PTPD** Poly[N,N′-bis(4-butylphenyl)-N,N′-bis(phenyl)-benzidine], **P3HT** Poly(3-hexylthiophene-2,5-diyl). Full names of the organic small molecules were mentioned earlier in the appendix A.

Material	IE (eV)	EA (eV)	$\mathbf{m_h}$	$\mathbf{m_e}$
F8BT	5.9[207]	3.3[50]	3[50]	4.2[50]
N2200	5.85[207]	4.0[50]	2[44]	2[50]
PFO	5.8[208]	-	2[164]	-
PF10TBT	5.4[209]	3.4[50]	2.3[50]	4.1[50]
PSF-TAD	5.39[210]	-	2.1[63]	-
MEH-PPV	5.3[211]	2.8[50]	2[63]	-
MDMO-PPV	5.2[212]	2.8[50]	2[47]	6.5[50]
PCPDTBT	5.1[213]	3.6[50]	2[50]	3.0[50]
PTPD	5.28[214]	-	2.2[63]	-
P3HT	4.8[215]	3[50]	2[39]	5[50]
C60	6.4	4.1[216]	4.9	2 *
TPBi	6.3	2.8[102]	6.2	5 *
PCBM	6.1[217]	3.9[134]	4 *	2[50]
4CzIPN	6.1	3.7[102]	2.9	4.0 *
CBP	6.0[103]	-	2.8	- *
ICBA	5.9	3.7[218]	2	2[146]
TCTA	5.7[103]	-	2[103]	-
α-NPD	5.4	2.3[95]	2	8.8[165]
Spiro-TAD	5.3[103]	-	2[103]	-
2T-NATA	5[103]	-	2[103]	-
PCDI-C7	6.3	4.3[219]	-	2.2 *
B3PYPPM	7.2	3.4[220]	-	3.4 *
TmPyPB	6.7	2.7[221]	-	4.5 *

Table D.1.: Materials studied in the chapter 6 and as displayed in Figure D.1 in the 6. The ionization energies and electron affinities are listed with literature references, together with the slope, m_h and m_e , inferred from the hole and electron current, respectively. The slopes were determined either from J-V characteristics measured in this work ($*$ as shown in the following figures), or from J-V data published in the literature. A hyphen indicates that the slope m was not determined.

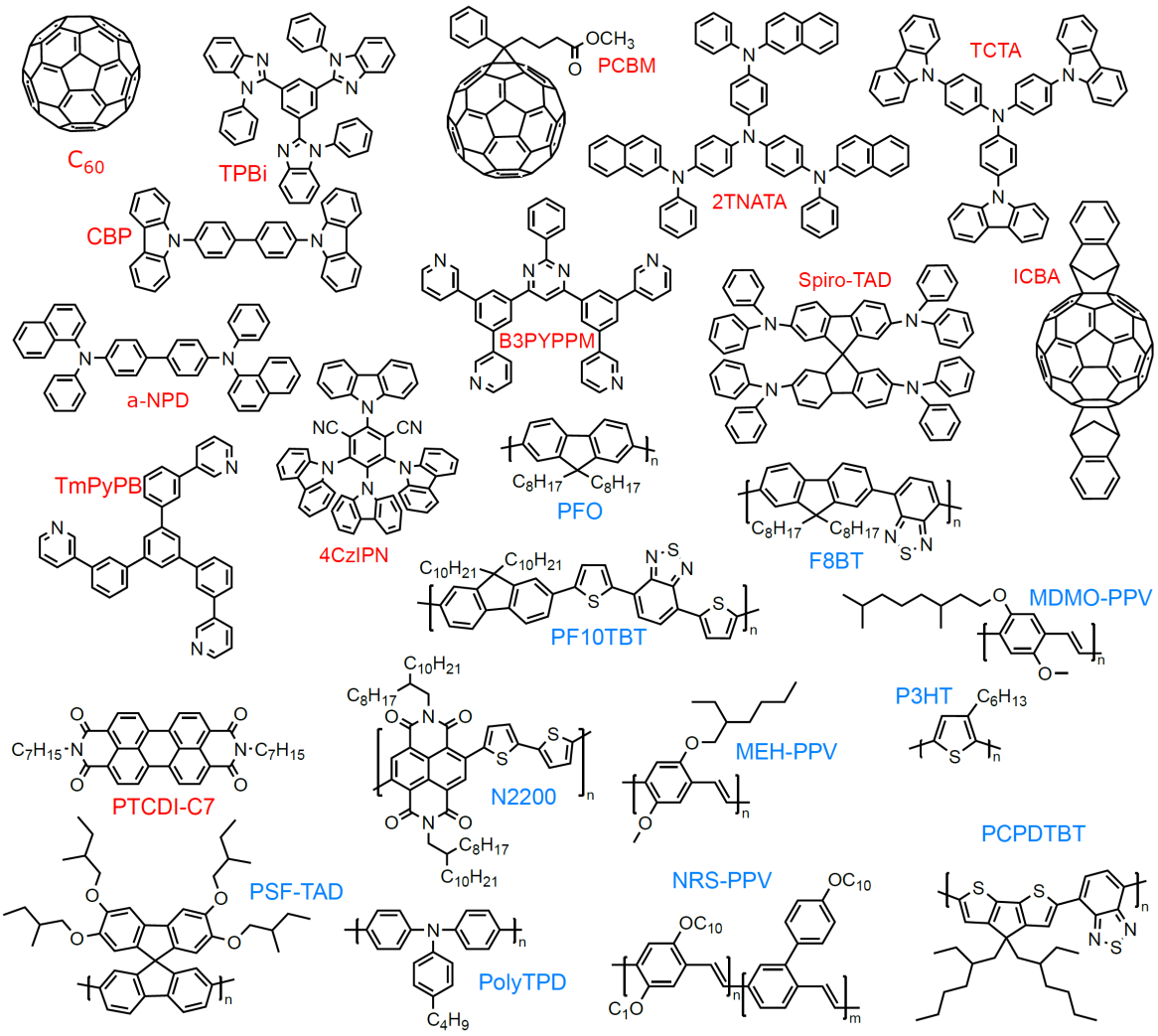

Figure D.1.: Chemical structures of the organic semiconductors whose slopes are plotted in the Figure 6.1. Their slopes are listed in **Table** D.1.

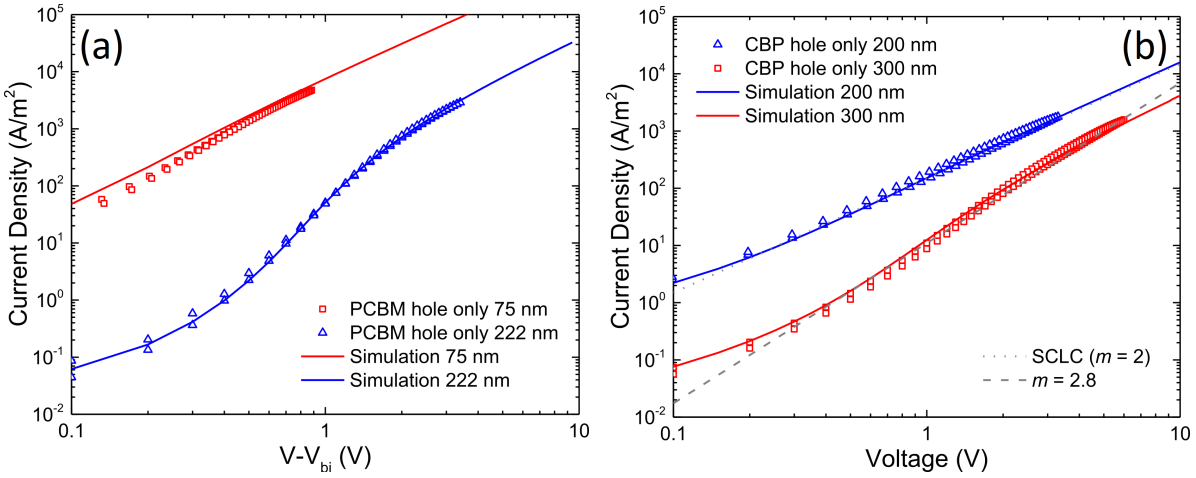

Figure D.2.: Current density-voltage characteristics of hole-only devices of (a) PCBM asymmetric and (b) CBP of different layer thickness. Experimentl data are represented by symbols and drift-diffusion simulations by lines. For PCBM, the simulations were performed with a hole mobility of 1.0×10^{-3} cm^{2}V^{-1}s^{-1} for the 75 nm device and 1.5×10^{-3} cm^{2}V^{-1}s^{-1} for the 222 nm device, with Gaussian hole traps with trap densitiy 1.1×10^{16} cm^{-3}, width σ=0.1 eV, and a trap depth 0.5 eV. At higher voltages, a transition to a quadratic voltage dependence is observed, indicating operation in the trap filled limit, which allows determination of the hole mobility. Due to the higher carrier density in the thinner device, the trap-filled limit is reached at lower voltage and the effect of trapping is considerably less severe as seen in both experiemts and simulations. For CBP simulations, the hole mobility of 4×10^{-4} cm^{2}V^{-1}s^{-1}, Gaussian trap densities of 7×10^{15} cm^{-3}, width σ=0.1 eV, and a trap depth 0.5 eV were used for for both thickness. Due to the low trap density, the traps are almost filled in the 200 nm device, leading to a quadratic voltage dependence of the current. As indicated by grey dotted line, which is the calculated SCLC current with a hole mobility of 4×10^{-4} cm^{2}V^{-1}s^{-1}. In the thicker 300 nm device the carrier density is lower, which leads to trap-filling behavior at low voltages and an increased slope m of 2.8, as indicated by the grey dashed line. The low trap density is in agreement with theoretical calculations that only a small fraction of water clusters act as hole traps in CBP.

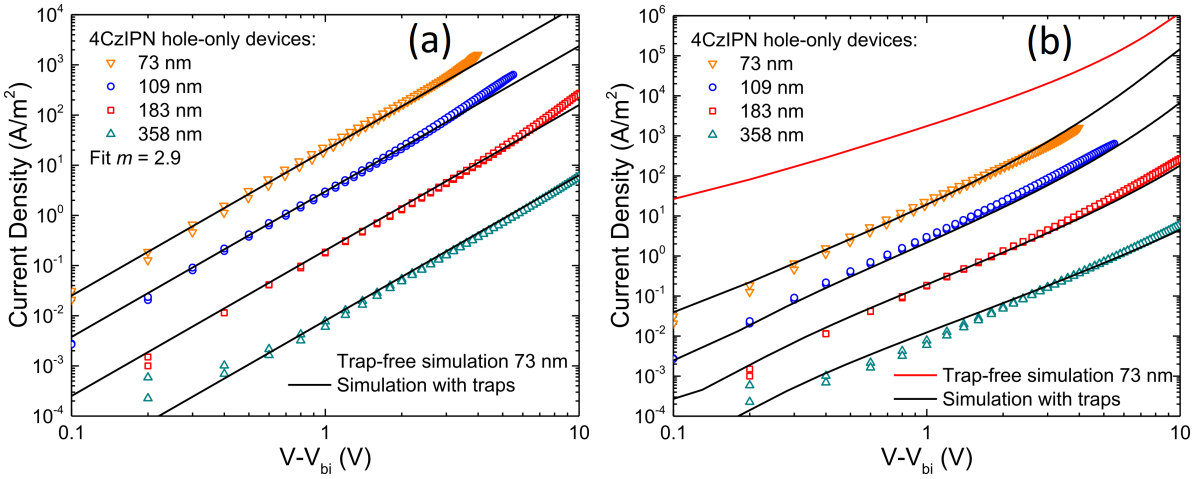

Figure D.3.: Current density-voltage characteristics of 4CzIPN hole-only devices of varying layer thickness, using a C_{60}(4 nm)/MoO_3 injecting electrode and a PEDOT:PSS extracting electrode. In (a) All solid lines represent a power law with the slope fixed at m =2.9. Similar to the other materials wiht hgher trap density, trap-filled limit was not observed over the complete investigated layer-thickness range, resulting in the slope which is relatively be relatively insensitive to the layer thickness. In (b) EGDM simulations were performed for the mobility of free charge carriers, using $\sigma = 0.1$ eV, a = 1.4 nm, and a mobility $\mu_0(295K) = 8 \times 10^{-5}$ $cm^2V^{-1}s^{-1}$, based on the time-of-flight value [222]. To fit the data, Gaussian traps with trap density of 1.6×10^{18} cm^{-3}, a distribution width of $\sigma = 0.1$ eV and a depth of 0.13 eV, were used. For all layer thicknesses, same fittig parameteres were used, For reference, the simulation excluding traps is also plotted for the 73 nm device. The strong thickness dependence of the J-V characteristics can only be described by including hole traps, confirming trap-limited hole currents. However, unlike in PCBM or CBP trap-filled limit is not observed. So, we can only use an estimated value for the mobility.

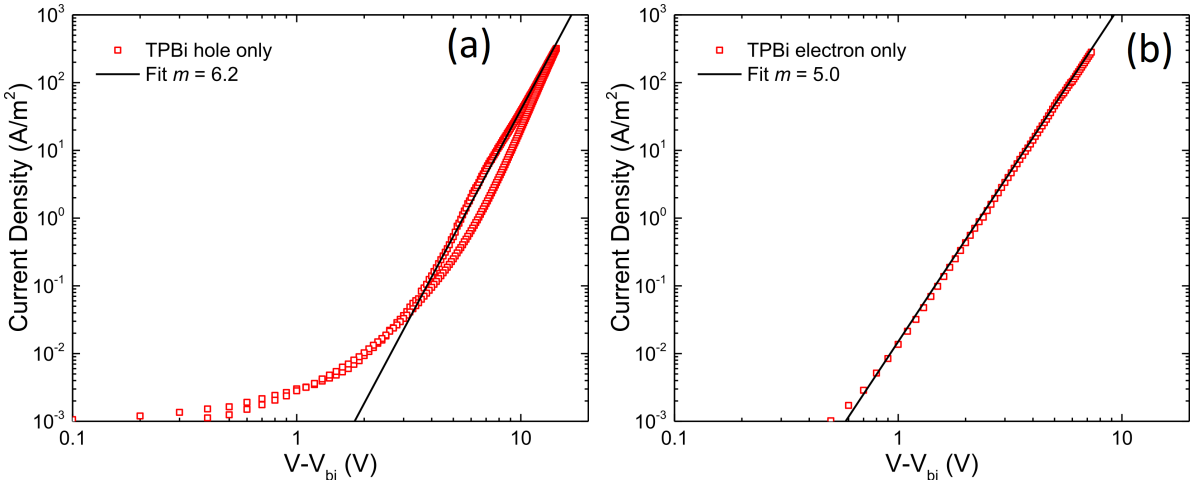

Figure D.4.: Current density-voltage characteristics of a TPBi (a) hole-only device (98nm), using a BST(3.5 nm)/MoO_3 injecting electrode and a PEDOT:PSS extracting electrode. (b) electron-only device (115 nm), using a Ba(5 nm)/Al(100nm injecting electrode and an Al extracting electrode. The built-in voltage was set to 0.6 V for hole-only and 0.7 V for electron-only device. The solid line represents a power law with slope m = 6.2. for hole-only and m = 5.0 for electron-only device respectively.

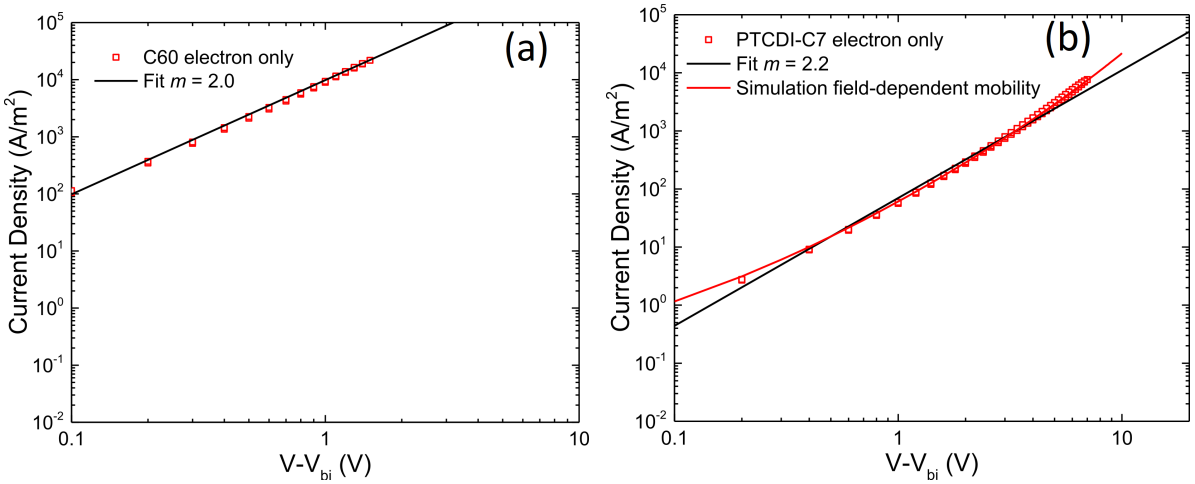

Figure D.5.: Current density-voltage characteristics of electron-only device of (a) C_{60} (230 nm) and (b) PTCDI-C7 (170 nm), using a TPBi(5 nm)/Ba(5 nm)/Al(100nm injecting electrode and an Al/TPBi(4 nm) extracting electrode. For both C_{60} and PTCDI-C7 the built-in voltage was set to 0 V. The solid line represents a power law with slope m= 2.0 for C_{60} and m = 2.2 for PTCDI-C7. In the case of PTCDI-C7, The deviation at higher voltages can be explained by the field and density dependence of the mobility. This is shown by the simulation, were we have used a field-dependent mobility for simplicity.

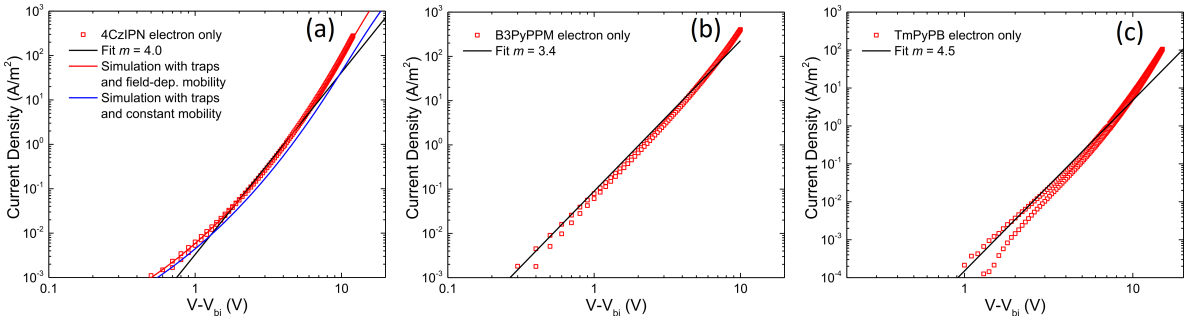

Figure D.6.: Current density-voltage characteristics of electron-only device of (a) 4CzIPN (101 nm), (b) B3PyPPM (120 nm) and (c) TmPyPB (200 nm), using a TPBi(5 nm)/Ba(5 nm)/Al(100nm injecting electrode and an Al/TPBi(4 nm) extracting electrode. For all the built-in voltage was set to 0 V. The solid line represents a power law with slope m= 4.0 for 4CzIPN, m = 3.4 for B3PyPPM and m = 4.5 for TmPyPB. In the case of 4CzIPN, The deviation at higher voltages can be again explained by the field and density dependence of the mobility, as shown by the simulations, which include 2×10^{18} cm^{-3} electron traps with a depth of 0.1 eV.

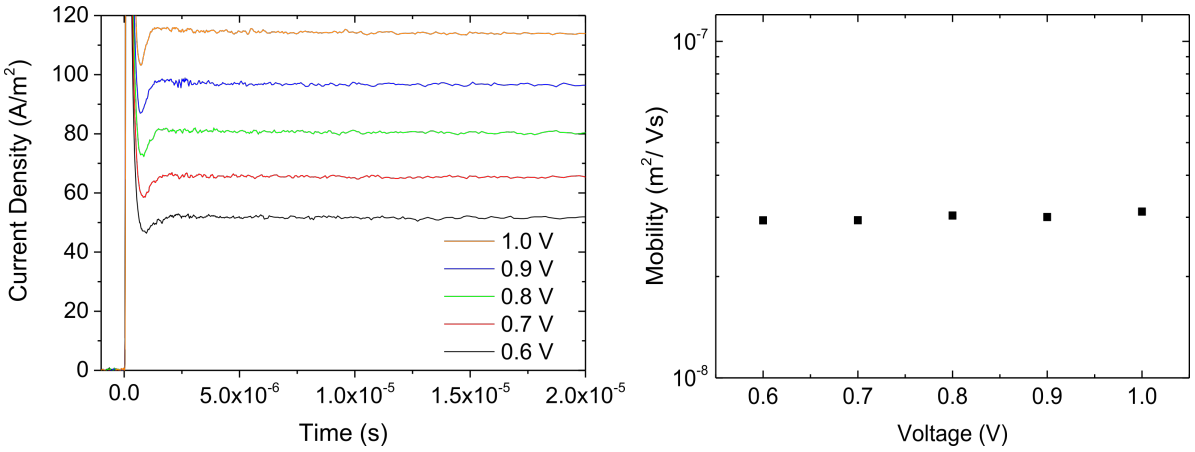

Figure D.7.: The hole mobility in Spiro-TAD was determined using dark-injection transients. The mobility obtained from the transit time at different voltages corresponds to the mobility obtained from the DC current, which is reached immediately after the transit time. This is an additional confirmation that the hole transport in Spiro-TAD is trap free, as is also concluded from the thickness-dependent current density-voltage characteristics and the agreement with the time-of-flight mobility [167]. If trapping were present, the DC current would be substantially lower than the calculated space-charge-limited current based on the transient mobility.

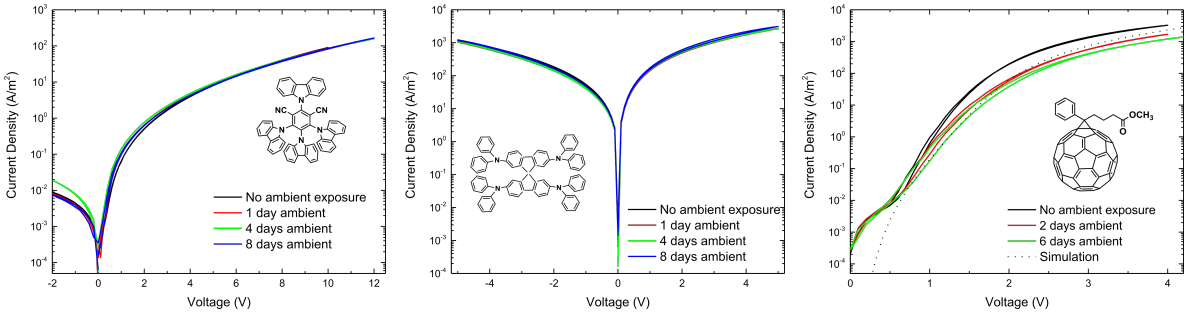

Figure D.8.: Hole-only devices of Spiro-TAD, 4CzIPN and PCBM as a function of time of exposure to air of the devices without top electrode. To investigate the effect of water and oxygen on the amount of traps, the unfinished devices were exposed to air in dark for varying periods of time. The exposure to air was performed without top electrode, since the air exposure affects the electrodes. When exposing the completed devices – including top electrode – to air, the top electrode degrades, which reduces the current in the device, making the investigation of potentially formed traps impossible. To eliminate degradation of the top electrode, the devices were exposed to air before evaporating this electrode. However, this also implies that the air-exposed layers are subsequently transferred to a high vacuum, which is required for deposition of the top electrode, which might affect the potentially absorbed oxygen and water concentration inside the layer. The results show that the trap-free current in Spiro-TAD is unaffected, implying that no extra traps have formed upon air exposure.By contrast, in PCBM having its ionization energy outside of the trap-free window, the air exposure did have an effect on the measured current, indicating that a small number of additional traps has been formed. A simulation is included in which the trap concentration is increased to 1.5×10^{16} cm^{-3}, as compared to 1.1×10^{16} cm^{-3} obtained for the as-fabricated device, keeping all other parameters the same. Prolonged air exposure did not further decrease the current, which could indicate saturation of the absorbed water and consequently the created hole traps. In contrast to PCBM, the trap-limited hole current in 4CzIPN is unaffected by air exposure. This can be either due to the fact that no extra water has been absorbed, or that the amount of extra traps formed is small compared to the large number of hole traps already present in the as-fabricated device (1.6×10^{18} cm^{-3}). If the amount of additionally formed traps in 4CzIPN would be similar to the amount of extra traps formed in PCBM upon air exposure, the current would remain unchanged due to the percentually minor increase in trap density. Such unchanged current is in agreement with the experimental observation. While these results are consistent with the hypothesis that water forms hole traps in materials with an ionization energy beyond 6 eV, it is unclear how much water is absorbed upon and hence how many traps are formed upon air exposure.

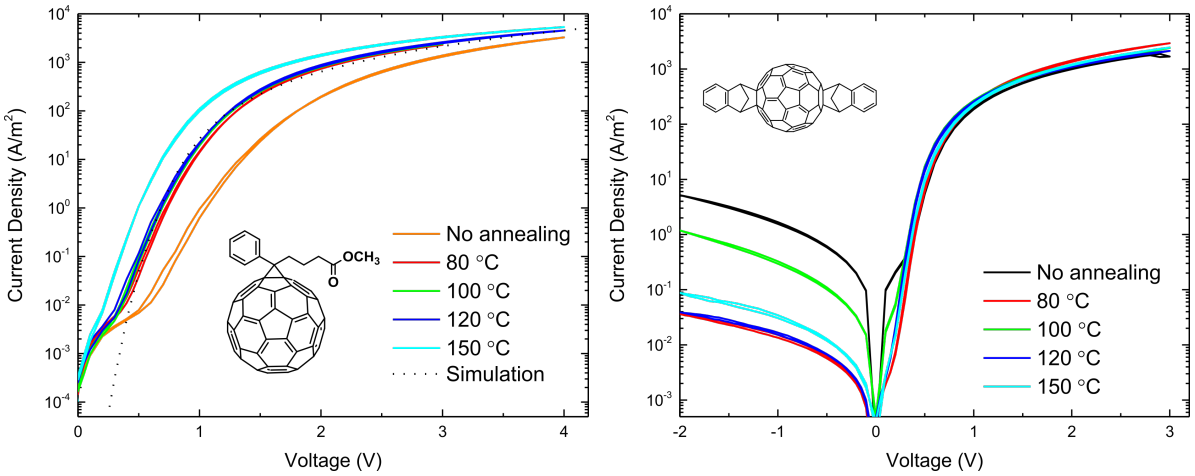

Figure D.9.: Current density-voltage characteristics of PCBM and ICBA hole-only devices as a function of annealing temperature. The annealing was performed in nitrogen atmosphere before deposition of the top electrode. It is observed that at low annealing temperatures the current improves, indicating the removal of hole traps. There is no apparent difference between annealing temperatures of 80 ℃, 100 ℃, and 120 ℃. The simulation estimates a reduction of traps to a concentration of 0.5×10^{16} cm^{-3}. After annealing at 150 ℃, an additional increase of the current is observed, which is possibly related to a change in morphology. By contrast, the reference ICBA device, which shows trap-free hole transport in the as-fabricated state, is unaffected by annealing. Note that small deviations or changes in leakage current may occur due to the fact that all curves represent different devices, since annealing is performed before deposition of the top electrode.

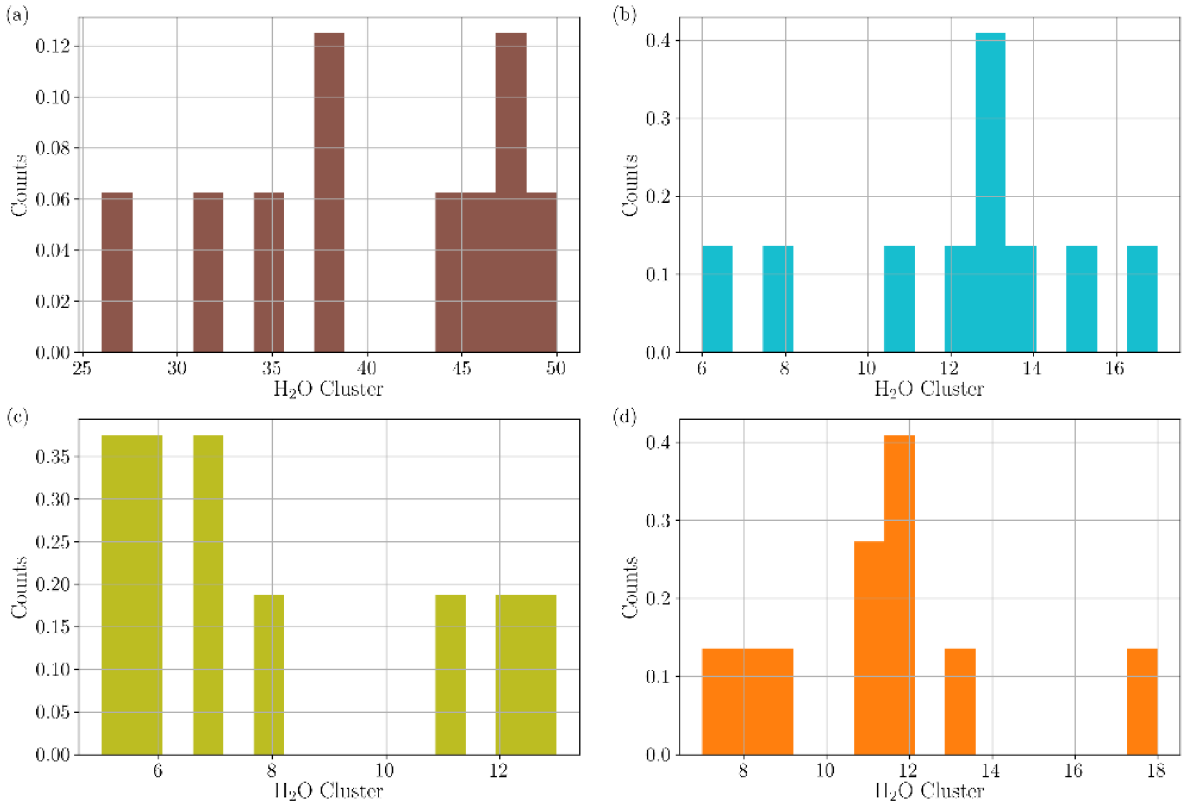

Figure D.10.: Distribution of cluster sizes in a) C_{60}, b) CBP, c) TCTA, and d) NPB.

E. Appendix: Chapter 7 Efficient OLED

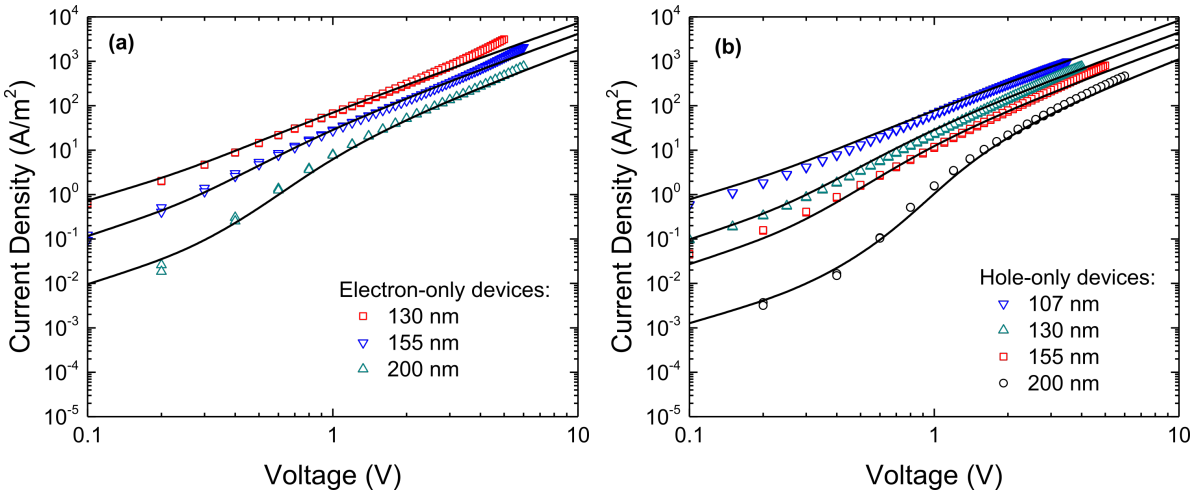

Figure E.1.: Current density-voltage characteristics of CzDBA electron- (a) and hole-only (b) devices for a varying thickness of the CzDBA layer. Symbols are experimental data and solid lines are fits with a numerical drift-diffusion model. (a) For all layer thicknesses, an electron mobility of 5×10^{-5} cm^{2}V^{-1}s^{-1} was used in the simulations, in combination with an electron-trap density of 1.4×10^{16} cm^{-3}. (b) For all layer thicknesses, a hole mobility of 3×10^{-5} cm^{2}V^{-1}s^{-1} was used, with a hole-trap density of 1.7×10^{16} cm^{-3}. For all electron- and hole-only devices, the injection barrier was set to 0 eV (Ohmic contact). The excellent agreement between simulation and experiment demonstrates that the hole and electron contacts are truly Ohmic. The current at low voltage has a stronger layer-thickness dependence than at high voltage, where the current scales inversely with layer thickness to the third power ($J \propto L^{-3}$; SCLC). The stronger thickness dependence is in agreement with trapping and cannot be explained with an injection barrier, which should result in a smaller thickness dependence than a space-charge-limited current (SCLC).

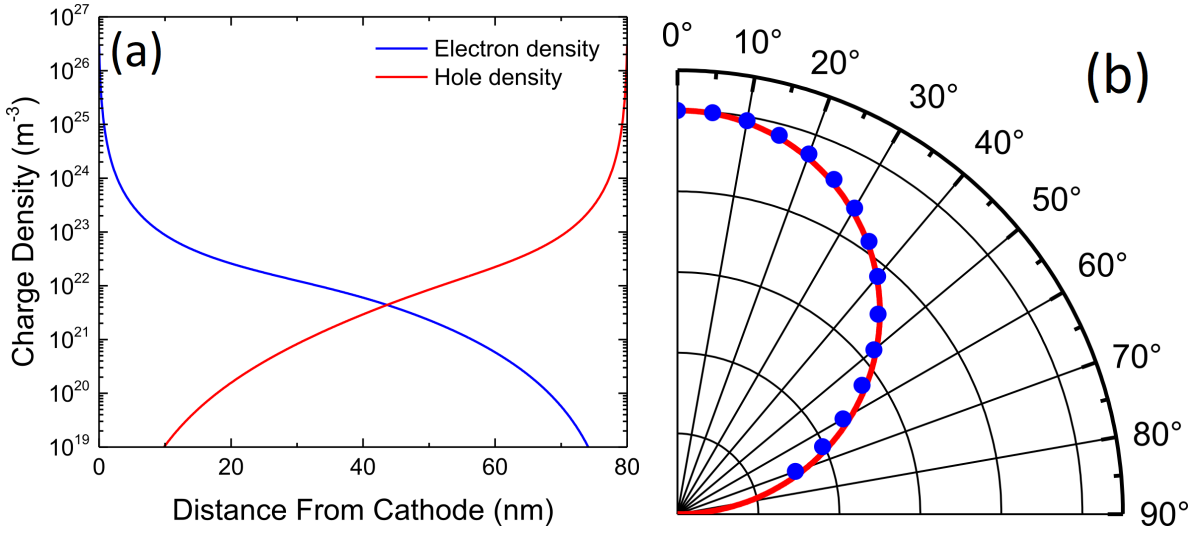

Figure E.2.: (a) Normalized electron- and hole-density distribution simulated for an 80 nm CzDBA OLED at 2.4 V, corresponding to a luminance close to $1,000$ cdm^{-2}. Due to the Ohmic electron and hole contacts, a high density of electrons and holes is present at the cathode and anode, respectively. As a result, the hole density near the cathode diminishes, since holes recombine bimolecularly with the excess of electrons. Similarly, the electron density near the anode reduces due to the high density of holes. Therefore, these Ohmic contacts cause an electron and hole blocking effect, without the need for incorporating blocking layers, explaining the high efficiency of the OLED. (b) Angular dependence of the light intensity emitted by the single-layer CzDBA OLED (symbols). The red line represents the calculated light-emission distribution for a Lambertian source, in which the light intensity proportional to the cosine of the angle with respect to the surface normal.

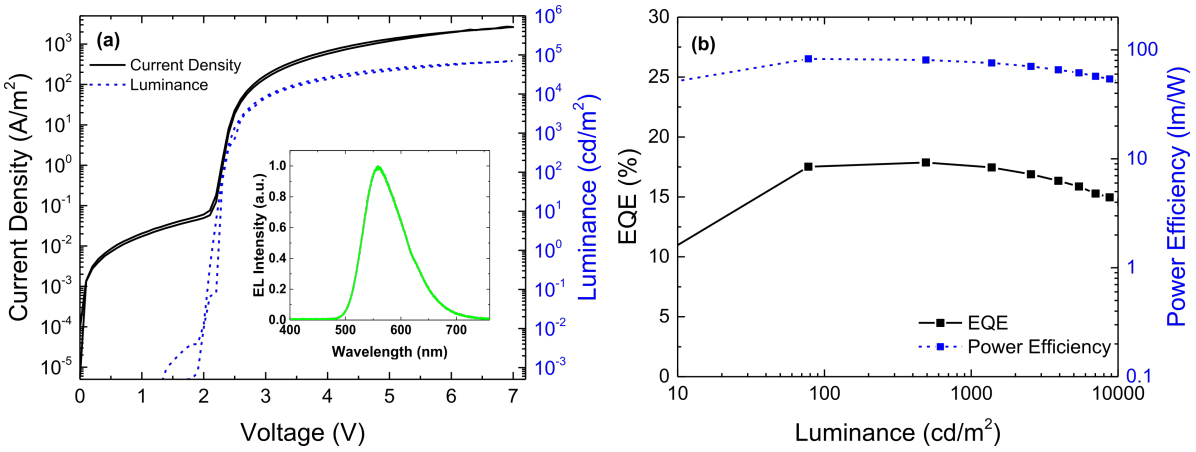

Figure E.3.: (a) Current density-voltage and luminance-voltage characteristics of a CzDBA OLED with a 20 nm CBP (4,4′-bis(N-carbazolyl)-1,1′-biphenyl) electron-blocking/hole-transport layer inserted between the MoO_3/C_{60} anode and the CzDBA emitter. (b) Corresponding EQE as a function of luminance. The maximum EQE is about $\sim 18\%$ and maximum power efficiency is about 83 $\mathrm{lmW^{-1}}$. It is observed that the performance is not significantly altered with respect to the single-layer OLED without electron-blocking layer, showing that excitons and electrons do not reach the C_{60} interlayer where the charges and excitons would be quenched. This confirms that the Ohmic hole contact obviates the need for a conventional blocking layer, as would be expected from the simulations in Figure E.2 (a).

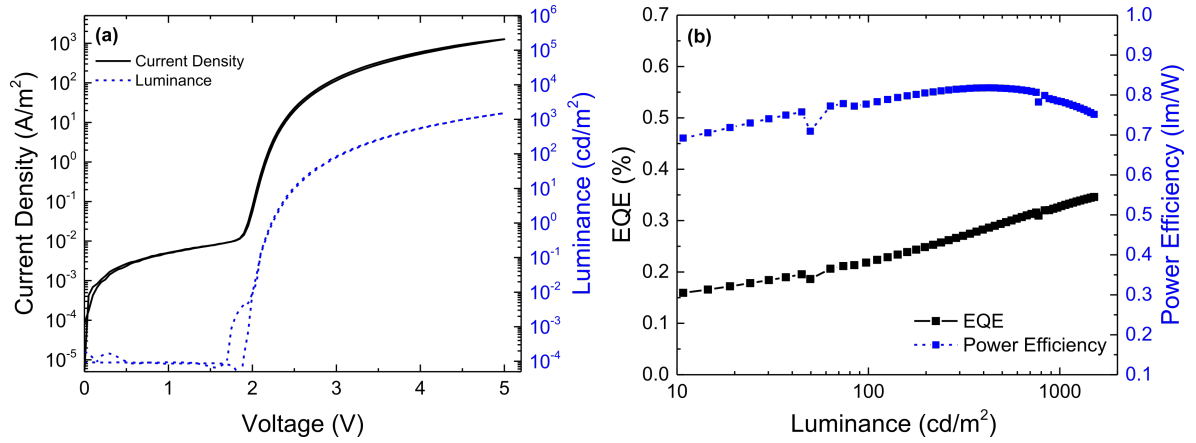

Figure E.4.: (a) Current density-voltage and luminance-voltage characteristics of a CzDBA single-layer OLED with a conventional LiF (1 nm) electron-injection layer instead of a TPBi interlayer. (b) Corresponding EQE and power efficiency as a function of luminance. The EQE is reduced substantially due to the non-Ohmic electron injection of the LiF/Al electrode into CzDBA, remaining below 0.4%.

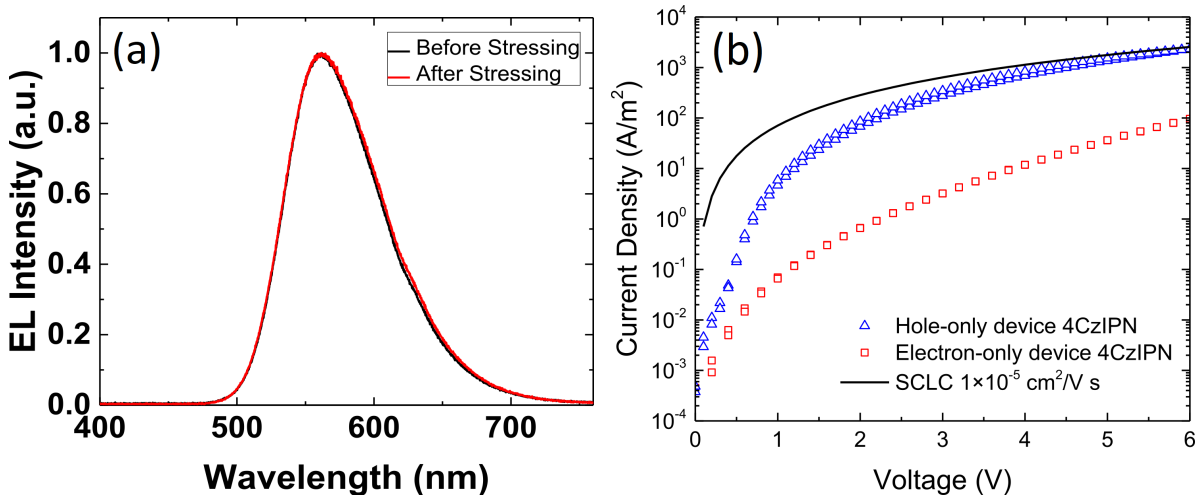

Figure E.5.: (a) Electroluminescence spectrum of a CzDBA single-layer OLED before and after stressing at 5000 cdm^{-2} for 470 hours (beyond LT_{50}). No apparent changes were observed. (b) Current density-voltage characteristics of 4CzIPN electron- and hole-only devices with a 4CzIPN layer thickness of 75 nm. For reference, a space-charge-limited current (SCLC) for a constant field independent mobility of 1×10^{-5} cm^{2}V^{-1}s^{-1} is plotted as a solid line. The charge transport is rather unbalanced, with hole transport being up to two orders of magnitude higher at low and moderate voltages. As an indication for the magnitude of charge transport, the hole mobility approximately approaches 1×10^{-5} cm^{2}V^{-1}s^{-1} at high fields. As a result, charge transport in neat layers of 4CzIPN is unbalanced and inferior to charge transport in CzDBA.

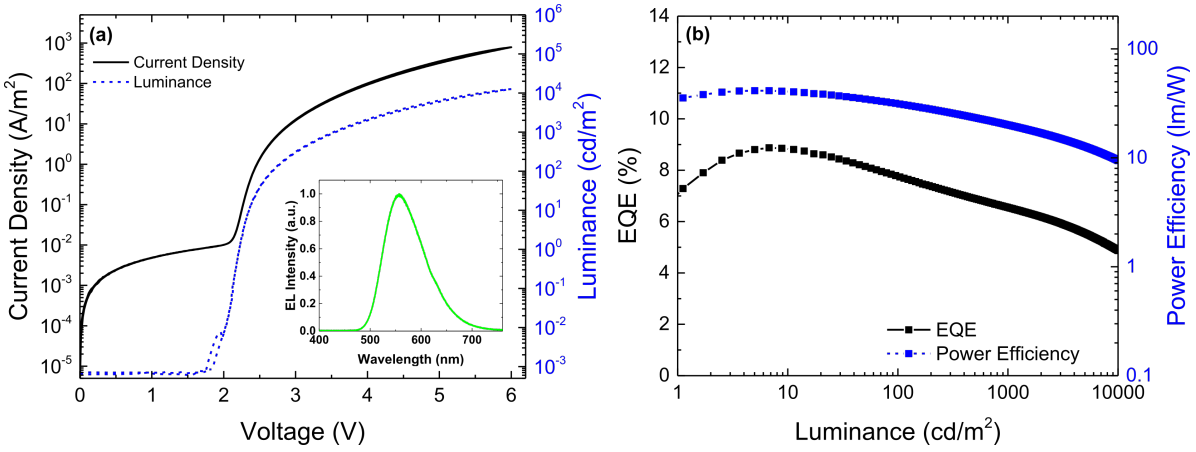

Figure E.6.: (a) Current density-voltage and luminance-voltage characteristics of a 4CzIPN single-layer OLED in a ITO/PEDOT:PSS/MoO_3(6 nm)/C_{60}(3 nm)/4CzIPN(80 nm)/TPBi(4 nm)/Al(100 nm) structure. The inset shows the electroluminescence (EL) spectrum. (b) Corresponding EQE and power efficiency as a function of luminance. The maximum EQE is 8.8% and the maximum power efficiency reaches 41 lmW^{-1}. These are reasonably good values considering the unbalanced electron and hole transport (Figure E.5)(b) and the low photoluminescence quantum yield of 35% [223]. The decent EQE and power efficiency are a result of the used Ohmic contacts. In addition, low driving voltages are observed, with a turn-on voltage at 1 cdm^{-2} of 2.21 V, reaching 100 cdm^{-2} at 2.67 V, and 1,000 cdm^{-2} at 3.52 V, showing that decent performance can be obtained in spite of the suboptimal charge-transport and emitter properties.

F. List of Publications

F.1. Publications covered in this thesis

1. **Naresh B Kotadiya**, Paul WM Blom, and Gert-Jan AH Wetzelaer. Efficient and stable single-layer organic light-emitting diodes based on thermally activated delayed fluorescence. *Nature Photonics*, 13(11):765–769, 2019.

2. **Naresh B Kotadiya**, Anirban Mondal, Paul WM Blom, Denis Andrienko, and Gert-Jan AH Wetzelaer. A window to trap-free charge transport in organic semiconducting thin films. *Nature materials*, 18(11):1182–1186, 2019.

3. **Naresh B Kotadiya**, Paul WM Blom, and GAH Wetzelaer. Trap-free space-charge-limited hole transport in a fullerene derivative. *Physical Review Applied*, 11(2):024069, 2019.

4. **Naresh B Kotadiya***,Anirban Mondal*, Shiyun Xiong, Paul WM Blom, Denis Andrienko, and Gert-Jan AH Wetzelaer. Rigorous characterization and predictive modeling of hole transport in amorphous organic semiconductors. *Advanced Electronic Materials*, 4(12):1800366, 2018. *Equal Contributions.

5. **Naresh B Kotadiya**, Hao Lu, Anirban Mondal, Yutaka Ie, Denis Andrienko, Paul WM Blom, and Gert-Jan AH Wetzelaer. Universal strategy for ohmic hole injection into organic semiconductors with high ionization energies. *Nature materials*, 17(4):329, 2018.

F.2. Other Publications

1. Pascal Friederich, Artem Fediai, Jing Li, Anirban Mondal, **Naresh Kotadiya**, Gabriele D'Avino, Franz Symalla, Gert-Jan Wetzelaer, Denis Andrienko, David Beljonne, et al. The influence of impurities on the charge carrier mobility of small molecule organic semiconductors. *arXiv preprint arXiv:1908.11854*, 2019.

2. Davood Abbaszadeh, Alexander Kunz, **Naresh B Kotadiya**, Anirban Mondal, Denis Andrienko, Jasper J Michels, Gert-Jan AH Wetzelaer, and Paul WM Blom. Electron trapping in conjugated polymers. *Chemistry of Materials*, 31(17):6380–6386, 2019.

3. Antonio Gaetano Ricciardulli, Sheng Yang, **Naresh B Kotadiya**, Gert-Jan AH Wetzelaer, Xinliang Feng, and Paul WM Blom. Improved hole injection into perovskite light-emitting diodes using a black phosphorus interlayer. *Advanced Electronic Materials*, 5(2):1800687, 2019.

4. Thorsten Schultz, Patrick Amsalem, **Naresh B Kotadiya**, Thomas Lenz, Paul WM Blom, and Norbert Koch. Importance of substrate work function homogeneity for reliable ionization energy determination by photoelectron spectroscopy. *physica status solidi (b)*, 256(2):1800299, 2019.

5. Yutaka Ie, Koki Morikawa, Wojciech Zajaczkowski, Wojciech Pisula, **Naresh B Kotadiya**, Gert-Jan AH Wetzelaer, Paul WM Blom, and Yoshio Aso. Enhanced photovoltaic performance of amorphous donor–acceptor copolymers based on fluorine-substituted benzodioxocyclohexene-annelated thiophene. *Advanced Energy Materials*, 8(13):1702506, 2018.

6. Thorsten Schultz, Thomas Lenz, **Naresh Kotadiya**, Georg Heimel, Gunnar Glasser, Rüdiger Berger, Paul WM Blom, Patrick Amsalem, Dago M de Leeuw, and Norbert Koch. Reliable work function determination of multicomponent surfaces and interfaces: the role of electrostatic potentials in ultraviolet photoelectron spectroscopy. *Advanced Materials Interfaces*, 4(19):1700324, 2017.

7. Roland Rohloff, **Naresh B Kotadiya**, NI Crăciun, Paul WM Blom, and GAH Wetzelaer. Electron and hole transport in the organic small molecule α-npd. *Applied Physics Letters*, 110(7):073301, 2017.

8. Yutaka Ie, Koki Morikawa, Makoto Karakawa, **Naresh B Kotadiya**, Gert-Jan AH Wetzelaer, Paul WM Blom, and Yoshio Aso. Synthesis, properties, and photovoltaic characteristics of p-type donor copolymers having fluorine-substituted benzodioxocyclohexene-annelated thiophene. *Journal of Materials Chemistry A*, 5(37):19773–19780, 2017.

9. Sebastian Stolz, Martin Petzoldt, **Naresh Kotadiya**, Tobias Rödlmeier, Ralph Eckstein, Jan Freudenberg, Uwe HF Bunz, Uli Lemmer, Eric Mankel, Manuel Hamburger, et al. One-step additive crosslinking of conjugated polyelectrolyte interlayers: improved lifetime and performance of solution-processed oleds. *Journal of Materials Chemistry C*, 4(47):11150–11156, 2016.

10. **Naresh B Kotadiya**, Anjana J Kothari, Devendra Tiwari, and Tapas K Chaudhuri. Photoconducting nanocrystalline lead sulphide thin films obtained by chemical bath deposition. *Applied Physics A*, 108(4):819–824, 2012.

F.3. Conference Presentations

1. **Naresh B Kotadiya**, Paul WM Blom, and Gert-Jan AH Wetzelaer. Efficient and stable single-layer organic light-emitting diodes based on thermally activated delayed fluorescence. *15^{th} European Conference on Molecular Electronics Linköping, Sweden*, ECME 2019. ***Oral Presentation*** .

2. **Naresh B Kotadiya**, Hao Lu, Anirban Mondal, Yutaka Ie, Denis Andrienko, Paul WM Blom, and Gert-Jan AH Wetzelaer. Universal strategy for ohmic hole

injection into organic semiconductors with high ionization energies. *MRS fall meeting, Boston Massachusetts, USA*, December 2018. ***Poster Presentation***.

3. **Naresh B Kotadiya**, Roland Rohloff, Paul WM Blom, and GAH Wetzelaer. Charge Transport in Thermally-Evaporated Organic Small Molecule. *Poster Presentation 14th European Conference on Molecular Electronics, Dresden, Germany*, ECME 2017. ***Poster Presentation***.

References

[1] Denjung Wang, Vincent Noël, and Benoît Piro. Electrolytic gated organic field-effect transistors for application in biosensors—a review. *Electronics*, 5(1):9, 2016.

[2] Guglielmo Lanzani. Materials for bioelectronics: organic electronics meets biology. *Nature materials*, 13(8):775, 2014.

[3] Jonathan Rivnay, Sahika Inal, Alberto Salleo, Róisín M Owens, Magnus Berggren, and George G Malliaras. Organic electrochemical transistors. *Nature Reviews Materials*, 3(2):17086, 2018.

[4] Joseph T Smith, Benjamin A Katchman, Dixie E Kullman, Uwadiae Obahiagbon, Yong-Kyun Lee, Barry P O'Brien, Gregory B Raupp, Karen S Anderson, and Jennifer Blain Christen. Application of flexible oled display technology to point-of-care medical diagnostic testing. *Journal of Display Technology*, 12(3):273–280, 2016.

[5] Sung-Min Lee, Jeong Hyun Kwon, Seonil Kwon, and Kyung Cheol Choi. A review of flexible oleds toward highly durable unusual displays. *IEEE Transactions on Electron Devices*, 64(5):1922–1931, 2017.

[6] Ching W Tang and Steven A VanSlyke. Organic electroluminescent diodes. *Applied physics letters*, 51(12):913–915, 1987.

[7] Haiwei Chen, Guanjun Tan, and Shin-Tson Wu. Ambient contrast ratio of lcds and oled displays. *Optics Express*, 25(26):33643–33656, 2017.

[8] Eric A Margulies, Pierre-Luc T Boudreault, Vadim I Adamovich, Bert D Alleyne, Michael S Weaver, and Julie J Brown. 65-1: Invited paper: Narrow spectrum deep red emitters for oled lighting and display. In *SID Symposium Digest of Technical Papers*, volume 50, pages 911–913. Wiley Online Library, 2019.

[9] Kody Klimes, Zhi-Qiang Zhu, and Jian Li. Efficient blue phosphorescent oleds with improved stability and color purity through judicious triplet exciton management. *Advanced Functional Materials*, page 1903068, 2019.

[10] Thanh-Tuân Bui, Fabrice Goubard, Malika Ibrahim-Ouali, Didier Gigmes, and Frédéric Dumur. Recent advances on organic blue thermally activated delayed fluorescence (tadf) emitters for organic light-emitting diodes (oleds). *Beilstein journal of organic chemistry*, 14(1):282–308, 2018.

[11] Hisahiro Sasabe and Junji Kido. Multifunctional materials in high-performance oleds: challenges for solid-state lighting. *Chemistry of Materials*, 23(3):621–630, 2010.

[12] Sebastian Reineke, Michael Thomschke, Björn Lüssem, and Karl Leo. White organic light-emitting diodes: Status and perspective. *Reviews of Modern Physics*, 85(3):1245, 2013.

[13] Takatoshi Tsujimura. *OLED display fundamentals and applications*. John Wiley & Sons, 2017.

[14] Stephane Berny, Nicolas Blouin, Andreas Distler, Hans-Joachim Egelhaaf, Michal Krompiec, Andreas Lohr, Owen R Lozman, Graham E Morse, Lana Nanson, Agnieszka Pron, et al. Solar trees: first large-scale demonstration of fully solution coated, semitransparent, flexible organic photovoltaic modules. *Advanced Science*, 3(5):1500342, 2016.

[15] Guiying Xu, Liang Shen, Chaohua Cui, Shanpeng Wen, Rongming Xue, Weijie Chen, Haiyang Chen, Jingwen Zhang, Hongkun Li, Yaowen Li, et al. High-performance colorful semitransparent polymer solar cells with ultrathin hybrid-metal electrodes and fine-tuned dielectric mirrors. *Advanced Functional Materials*, 27(15):1605908, 2017.

[16] Yaowen Li, Guiying Xu, Chaohua Cui, and Yongfang Li. Flexible and semitransparent organic solar cells. *Advanced Energy Materials*, 8(7):1701791, 2018.

[17] Qian Zhang, Bin Kan, Feng Liu, Guankui Long, Xiangjian Wan, Xiaoqing Chen, Yi Zuo, Wang Ni, Huijing Zhang, Miaomiao Li, et al. Small-molecule solar cells with efficiency over 9%. *Nature Photonics*, 9(1):35, 2015.

[18] Xiaozhou Che, Yongxi Li, Yue Qu, and Stephen R Forrest. High fabrication yield organic tandem photovoltaics combining vacuum-and solution-processed subcells with 15% efficiency. *Nature Energy*, 3(5):422, 2018.

[19] Mark Nikolka, Iyad Nasrallah, Bradley Rose, Mahesh Kumar Ravva, Katharina Broch, Aditya Sadhanala, David Harkin, Jerome Charmet, Michael Hurhangee, Adam Brown, et al. High operational and environmental stability of high-mobility conjugated polymer field-effect transistors through the use of molecular additives. *Nature materials*, 16(3):356, 2017.

[20] Xiaojia Jia, Canek Fuentes-Hernandez, Cheng-Yin Wang, Youngrak Park, and Bernard Kippelen. Stable organic thin-film transistors. *Science advances*, 4(1):eaao1705, 2018.

[21] Marc A Baldo, DF O'brien, Y You, A Shoustikov, S Sibley, ME Thompson, and Stephen R Forrest. Highly efficient phosphorescent emission from organic electroluminescent devices. *Nature*, 395(6698):151, 1998.

[22] Chihaya Adachi, Marc A Baldo, Mark E Thompson, and Stephen R Forrest. Nearly 100% internal phosphorescence efficiency in an organic light-emitting device. *Journal of Applied Physics*, 90(10):5048–5051, 2001.

[23] Hiroki Uoyama, Kenichi Goushi, Katsuyuki Shizu, Hiroko Nomura, and Chihaya Adachi. Highly efficient organic light-emitting diodes from delayed fluorescence. *Nature*, 492(7428):234, 2012.

[24] Qisheng Zhang, Bo Li, Shuping Huang, Hiroko Nomura, Hiroyuki Tanaka, and Chihaya Adachi. Efficient blue organic light-emitting diodes employing thermally activated delayed fluorescence. *Nature Photonics*, 8(4):326, 2014.

[25] Rico Meerheim, BjÖrn Lussem, and Karl Leo. Efficiency and stability of pin type organic light emitting diodes for display and lighting applications. *Proceedings of the IEEE*, 97(9):1606–1626, 2009.

[26] Wolfgang Brütting. Introduction to the physics of organic semiconductors. *Physics of organic semiconductors*, pages 1–14, 2005.

[27] Klaus Müllen and Ullrich Scherf. *Organic light emitting devices: synthesis, properties and applications*. John Wiley & Sons, 2006.

[28] Veaceslav Coropceanu, Jérôme Cornil, Demetrio A da Silva Filho, Yoann Olivier, Robert Silbey, and Jean-Luc Brédas. Charge transport in organic semiconductors. *Chemical reviews*, 107(4):926–952, 2007.

[29] Anna Köhler and Heinz Bässler. *Electronic processes in organic semiconductors: An introduction*. John Wiley & Sons, 2015.

[30] photonicswiki. Band gap control in organic semiconductors. http://photonicswiki.org.

[31] Slawomir Braun, William R Salaneck, and Mats Fahlman. Energy-level alignment at organic/metal and organic/organic interfaces. *Advanced materials*, 21(14-15):1450–1472, 2009.

[32] Martijn Kuik, Gert-Jan AH Wetzelaer, Herman T Nicolai, N Irina Craciun, Dago M De Leeuw, and Paul WM Blom. 25th anniversary article: Charge transport and recombination in polymer light-emitting diodes. *Advanced Materials*, 26(4):512–531, 2014.

[33] Heinz Bässler. Charge transport in disordered organic photoconductors a monte carlo simulation study. *physica status solidi (b)*, 175(1):15–56, 1993.

[34] Allen Miller and Elihu Abrahams. Impurity conduction at low concentrations. *Physical Review*, 120(3):745, 1960.

[35] VI Arkhipov, EV Emelianova, and H Bässler. Equilibrium carrier mobility in disordered hopping systems. *Philosophical Magazine B*, 81(9):985–996, 2001.

[36] SD Baranovskii. Theoretical description of charge transport in disordered organic semiconductors. *physica status solidi (b)*, 251(3):487–525, 2014.

[37] VI Arkhipov, II Fishchuk, A Kadashchuk, and H Bässler. Charge transport in disordered organic semiconductors. *Photophysics of Molecular Materials: From single molecules to single crystals*, pages 261–366, 2005.

[38] Nir Tessler, Yevgeni Preezant, Noam Rappaport, and Yohai Roichman. Charge transport in disordered organic materials and its relevance to thin-film devices: a tutorial review. *Advanced Materials*, 21(27):2741–2761, 2009.

[39] C Tanase, EJ Meijer, PWM Blom, and DM De Leeuw. Unification of the hole transport in polymeric field-effect transistors and light-emitting diodes. *Physical review letters*, 91(21):216601, 2003.

[40] WF Pasveer, Jeroen Cottaar, C Tanase, Reinder Coehoorn, PA Bobbert, PWM Blom, DM De Leeuw, and MAJ Michels. Unified description of charge-carrier mobilities in disordered semiconducting polymers. *Physical review letters*, 94(20):206601, 2005.

[41] Ilias Katsouras, A Najafi, K Asadi, AJ Kronemeijer, AJ Oostra, LJA Koster, Dago M de Leeuw, and Paul WM Blom. Charge transport in poly (p-phenylene vinylene) at low temperature and high electric field. *Organic Electronics*, 14(6):1591–1596, 2013.

[42] Siebe LM van Mensfoort, SIE Vulto, Rene AJ Janssen, and Reinder Coehoorn. Hole transport in polyfluorene-based sandwich-type devices: Quantitative analysis of the role of energetic disorder. *Physical Review B*, 78(8):085208, 2008.

[43] James C Blakesley, Helen S Clubb, and Neil C Greenham. Temperature-dependent electron and hole transport in disordered semiconducting polymers: Analysis of energetic disorder. *Physical Review B*, 81(4):045210, 2010.

[44] Gert-Jan AH Wetzelaer, Martijn Kuik, Yoann Olivier, Vincent Lemaur, Jérôme Cornil, Simone Fabiano, Maria Antonietta Loi, and Paul WM Blom. Asymmetric electron and hole transport in a high-mobility n-type conjugated polymer. *Physical Review B*, 86(16):165203, 2012.

[45] Peter Mark and Wolfgang Helfrich. Space-charge-limited currents in organic crystals. *Journal of Applied Physics*, 33(1):205–215, 1962.

[46] MM Mandoc, B de Boer, G Paasch, and PWM Blom. Trap-limited electron transport in disordered semiconducting polymers. *Physical Review B*, 75(19):193202, 2007.

[47] Paul WM Blom, MJM De Jong, and JJM Vleggaar. Electron and hole transport in poly (p-phenylene vinylene) devices. *Applied Physics Letters*, 68(23):3308–3310, 1996.

[48] HT Nicolai, MM Mandoc, and PWM Blom. Electron traps in semiconducting polymers: Exponential versus gaussian trap distribution. *Physical Review B*, 83(19):195204, 2011.

[49] Martijn Kuik, Joke Vandenbergh, Ludwig Goris, Eline J Begemann, Laurence Lutsen, Dirk JM Vanderzande, Jean V Manca, and Paul WM Blom. Optical detection of deep electron traps in poly (p-phenylene vinylene) light-emitting diodes. *Applied Physics Letters*, 99(18):240, 2011.

[50] Herman T Nicolai, M Kuik, GAH Wetzelaer, B De Boer, C Campbell, C Risko, JL Brédas, and PWM Blom. Unification of trap-limited electron transport in semiconducting polymers. *Nature materials*, 11(10):882, 2012.

[51] Simon M Sze and Kwok K Ng. *Physics of semiconductor devices*. John wiley & sons, 2006.

[52] VI Arkhipov, EV Emelianova, YH Tak, and H Bässler. Charge injection into light-emitting diodes: Theory and experiment. *Journal of Applied Physics*, 84(2):848–856, 1998.

[53] JG Simmons. Richardson-schottky effect in solids. *Physical Review Letters*, 15(25):967, 1965.

[54] Heinz Bässler. Injection, transport and recombination of charge carriers in organic light-emitting diodes. *Polymers for Advanced Technologies*, 9(7):402–418, 1998.

[55] J Campbell Scott and George G Malliaras. Charge injection and recombination at the metal–organic interface. *Chemical physics letters*, 299(2):115–119, 1999.

[56] J Appenzeller, M Radosavljević, J Knoch, and Ph Avouris. Tunneling versus thermionic emission in one-dimensional semiconductors. *Physical review letters*, 92(4):048301, 2004.

[57] Fu-Chien Chiu. A review on conduction mechanisms in dielectric films. *Advances in Materials Science and Engineering*, 2014, 2014.

[58] iapporganicelectronics. Doping of organic semiconductors. https://www.iapp.de/organische-elektronik.de/en/?Basics_Doping, 2019.

[59] Björn Lüssem, Moritz Riede, and Karl Leo. Doping of organic semiconductors. *physica status solidi (a)*, 210(1):9–43, 2013.

[60] S Olthof, W Tress, R Meerheim, B Lüssem, and K Leo. Photoelectron spectroscopy study of systematically varied doping concentrations in an organic semiconductor layer using a molecular p-dopant. *Journal of Applied Physics*, 106(10):103711, 2009.

[61] M Pfeiffer, K Leo, X Zhou, JS Huang, M Hofmann, A Werner, and J Blochwitz-Nimoth. Doped organic semiconductors: Physics and application in light emitting diodes. *Organic Electronics*, 4(2-3):89–103, 2003.

[62] Paul WM Blom and MCJM Vissenberg. Charge transport in poly (p-phenylene vinylene) light-emitting diodes. *Materials Science and Engineering: R: Reports*, 27(3-4):53–94, 2000.

[63] GAH Wetzelaer and Paul WM Blom. Ohmic current in organic metal-insulator-metal diodes revisited. *Physical Review B*, 89(24):241201, 2014.

[64] NI Craciun, JJ Brondijk, and PWM Blom. Diffusion-enhanced hole transport in thin polymer light-emitting diodes. *Physical Review B*, 77(3):035206, 2008.

[65] NF Mott and RW Gurney. Electronic processes in ionic crystals oxford. book, 1945.

[66] Exciton engineering. http://web.mit.edu/stranogroup/index.php/research/29-exciton-engineering.html, October 2013.

[67] Ian D. Johnson and Michael W. Davidson. Olympus microscopy resource center. https://www.olympus-lifescience.com/en/microscope-resource/primer/java/jablonski/jabintro/, October 2019.

[68] Stephen R Forrest. Exciton formation statistics under electrical injection in organic semiconductor thin films. *Journal of luminescence*, 110(4):378–383, 2004.

[69] Hartmut Yersin. *Highly efficient OLEDs with phosphorescent materials*. Wiley Online Library, 2008.

[70] Xinyi Cai and Shi-Jian Su. Marching toward highly efficient, pure-blue, and stable thermally activated delayed fluorescent organic light-emitting diodes. *Advanced Functional Materials*, 28(43):1802558, 2018.

[71] Tianyu Huang, Wei Jiang, and Lian Duan. Recent progress in solution processable tadf materials for organic light-emitting diodes. *Journal of Materials Chemistry C*, 6(21):5577–5596, 2018.

[72] Paul WM Blom and Marc JM De Jong. Electrical characterization of polymer light-emitting diodes. *IEEE Journal of selected topics in quantum electronics*, 4(1):105–112, 1998.

[73] Norbert Koch. Organic electronic devices and their functional interfaces. *ChemPhysChem*, 8(10):1438–1455, 2007.

[74] M Kuik, LJA Koster, AG Dijkstra, GAH Wetzelaer, and PWM Blom. Non-radiative recombination losses in polymer light-emitting diodes. *Organic Electronics*, 13(6):969–974, 2012.

[75] D Abbaszadeh, GAH Wetzelaer, Herman T Nicolai, and Paul WM Blom. Exciton quenching at pedot: Pss anode in polymer blue-light-emitting diodes. *Journal of Applied Physics*, 116(22):224508, 2014.

[76] DE Markov and PWM Blom. Exciton quenching in poly (phenylene vinylene) polymer light-emitting diodes. *Applied Physics Letters*, 87(23):233511, 2005.

[77] Alexander L Burin and Mark A Ratner. Exciton migration and cathode quenching in organic light emitting diodes. *The Journal of Physical Chemistry A*, 104(20):4704–4710, 2000.

[78] Martin Pfeiffer, Stephen R Forrest, Karl Leo, and Mark E Thompson. Electrophosphorescent p–i–n organic light-emitting devices for very-high-efficiency flat-panel displays. *Advanced Materials*, 14(22):1633–1636, 2002.

[79] K Walzer, B Maennig, M Pfeiffer, and K Leo. Highly efficient organic devices based on electrically doped transport layers. *Chemical reviews*, 107(4):1233–1271, 2007.

[80] Gufeng He, Martin Pfeiffer, Karl Leo, Michael Hofmann, Jan Birnstock, Robert Pudzich, and Josef Salbeck. High-efficiency and low-voltage p-i-n electrophosphorescent organic light-emitting diodes with double-emission layers. *Applied Physics Letters*, 85(17):3911–3913, 2004.

[81] A Jolt Oostra, Paul WM Blom, and Jasper J Michels. Prevention of short circuits in solution-processed oled devices. *Organic Electronics*, 15(6):1166–1172, 2014.

[82] GAH Wetzelaer, M Kuik, HT Nicolai, and PWM Blom. Trap-assisted and langevin-type recombination in organic light-emitting diodes. *Physical Review B*, 83(16):165204, 2011.

[83] GAH Wetzelaer, LJA Koster, and PWM Blom. Validity of the einstein relation in disordered organic semiconductors. *Physical review letters*, 107(6):066605, 2011.

[84] Youtian Tao, Chuluo Yang, and Jingui Qin. Organic host materials for phosphorescent organic light-emitting diodes. *Chemical Society Reviews*, 40(5):2943–2970, 2011.

[85] Michael Y Wong and Eli Zysman-Colman. Purely organic thermally activated delayed fluorescence materials for organic light-emitting diodes. *Advanced Materials*, 29(22):1605444, 2017.

[86] Norbert Koch and Antje Vollmer. Electrode-molecular semiconductor contacts: Work-function-dependent hole injection barriers versus fermi-level pinning. *Applied physics letters*, 89(16):162107, 2006.

[87] MG Helander, ZB Wang, J Qiu, MT Greiner, DP Puzzo, ZW Liu, and ZH Lu. Chlorinated indium tin oxide electrodes with high work function for organic device compatibility. *Science*, 332(6032):944–947, 2011.

[88] Henry Méndez, Georg Heimel, Stefanie Winkler, Johannes Frisch, Andreas Opitz, Katrein Sauer, Berthold Wegner, Martin Oehzelt, Christian Röthel, Steffen Duhm, et al. Charge-transfer crystallites as molecular electrical dopants. *Nature communications*, 6:8560, 2015.

[89] Cindy G Tang, Mervin CY Ang, Kim-Kian Choo, Venu Keerthi, Jun-Kai Tan, Mazlan Nur Syafiqah, Thomas Kugler, Jeremy H Burroughes, Rui-Qi Png, Lay-Lay Chua, et al. Doped polymer semiconductors with ultrahigh and ultralow work functions for ohmic contacts. *Nature*, 539(7630):536, 2016.

[90] M Kröger, S Hamwi, J Meyer, T Riedl, W Kowalsky, and Antoine Kahn. Role of the deep-lying electronic states of moo 3 in the enhancement of hole-injection in organic thin films. *Applied physics letters*, 95(12):251, 2009.

[91] Michael Kröger, Sami Hamwi, Jens Meyer, Thomas Riedl, Wolfgang Kowalsky, and Antoine Kahn. P-type doping of organic wide band gap materials by transition metal oxides: A case-study on molybdenum trioxide. *Organic Electronics*, 10(5):932–938, 2009.

[92] Jens Meyer, Sami Hamwi, Michael Kröger, Wolfgang Kowalsky, Thomas Riedl, and Antoine Kahn. Transition metal oxides for organic electronics: energetics, device physics and applications. *Advanced Materials*, 24(40):5408–5427, 2012.

[93] PS Davids, IH Campbell, and DL Smith. Device model for single carrier organic diodes. *Journal of Applied Physics*, 82(12):6319–6325, 1997.

[94] Rebecca A Belisle, Pratham Jain, Rohit Prasanna, Tomas Leijtens, and Michael D McGehee. Minimal effect of the hole-transport material ionization potential on the open-circuit voltage of perovskite solar cells. *ACS Energy Letters*, 1(3):556–560, 2016.

[95] Robin T White, Emmanuel S Thibau, and Zheng-Hong Lu. Interface structure of moo 3 on organic semiconductors. *Scientific reports*, 6:21109, 2016.

[96] Chen Li, Lian Duan, Haoyuan Li, and Yong Qiu. Universal trap effect in carrier transport of disordered organic semiconductors: Transition from shallow trapping to deep trapping. *The Journal of Physical Chemistry C*, 118(20):10651–10660, 2014.

[97] Mark T Greiner, Michael G Helander, Wing-Man Tang, Zhi-Bin Wang, Jacky Qiu, and Zheng-Hong Lu. Universal energy-level alignment of molecules on metal oxides. *Nature materials*, 11(1):76, 2012.

[98] SC Tse, KC Kwok, and SK So. Electron transport in naphthylamine-based organic compounds. *Applied physics letters*, 89(26):262102, 2006.

[99] Udo Bach, Kenny De Cloedt, Hubert Spreitzer, and Michael Grätzel. Characterization of hole transport in a new class of spiro-linked oligotriphenylamine compounds. *Advanced Materials*, 12(14):1060–1063, 2000.

[100] Seunguk Noh, CK Suman, Yongtaek Hong, and Changhee Lee. Carrier conduction mechanism for phosphorescent material doped organic semiconductor. *Journal of Applied Physics*, 105(3):033709, 2009.

[101] Noriyuki Matsusue, Yuichiro Suzuki, and Hiroyoshi Naito. Charge carrier transport in neat thin films of phosphorescent iridium complexes. *Japanese journal of applied physics*, 44(6R):3691, 2005.

[102] Yuki Seino, Susumu Inomata, Hisahiro Sasabe, Yong-Jin Pu, and Junji Kido. High-performance green oleds using thermally activated delayed fluorescence with a power efficiency of over 100 lm w- 1. *Advanced Materials*, 28(13):2638–2643, 2016.

[103] Naresh B Kotadiya, Hao Lu, Anirban Mondal, Yutaka Ie, Denis Andrienko, Paul WM Blom, and Gert-Jan AH Wetzelaer. Universal strategy for ohmic hole injection into organic semiconductors with high ionization energies. *Nature materials*, 17(4):329, 2018.

[104] James C Blakesley and Neil C Greenham. Charge transfer at polymer-electrode interfaces: The effect of energetic disorder and thermal injection on band bending and open-circuit voltage. *Journal of Applied Physics*, 106(3):034507, 2009.

[105] Martin Oehzelt, Norbert Koch, and Georg Heimel. Organic semiconductor density of states controls the energy level alignment at electrode interfaces. *Nature communications*, 5:4174, 2014.

[106] Martin Oehzelt, Kouki Akaike, Norbert Koch, and Georg Heimel. Energy-level alignment at organic heterointerfaces. *Science Advances*, 1(10):e1501127, 2015.

[107] MA Baldo and SR Forrest. Interface-limited injection in amorphous organic semiconductors. *Physical Review B*, 64(8):085201, 2001.

[108] BN Limketkai and MA Baldo. Charge injection into cathode-doped amorphous organic semiconductors. *Physical Review B*, 71(8):085207, 2005.

[109] Wen-Yi Hung, Tung-Huei Ke, Yu-Ting Lin, Chung-Chih Wu, Tsung-Hsi Hung, Teng-Chih Chao, Ken-Tsung Wong, and Chih-I Wu. Employing ambipolar oligofluorene as the charge-generation layer in time-of-flight mobility measurements of organic thin films. *Applied physics letters*, 88(6):064102, 2006.

[110] Yasuhiko Shirota and Hiroshi Kageyama. Charge carrier transporting molecular materials and their applications in devices. *Chemical reviews*, 107(4):953–1010, 2007.

[111] Laura Calió, Samrana Kazim, Michael Grätzel, and Shahzada Ahmad. Hole-transport materials for perovskite solar cells. *Angewandte Chemie International Edition*, 55(47):14522–14545, 2016.

[112] Uli Würfel, Dieter Neher, Annika Spies, and Steve Albrecht. Impact of charge transport on current–voltage characteristics and power-conversion efficiency of organic solar cells. *Nature communications*, 6:6951, 2015.

[113] Dieter Neher, Juliane Kniepert, Arik Elimelech, and L Jan Anton Koster. A new figure of merit for organic solar cells with transport-limited photocurrents. *Scientific reports*, 6:24861, 2016.

[114] James C Blakesley, Fernando A Castro, William Kylberg, George FA Dibb, Caroline Arantes, Rogério Valaski, Marco Cremona, Jong Soo Kim, and Ji-Seon Kim. Towards reliable charge-mobility benchmark measurements for organic semiconductors. *Organic Electronics*, 15(6):1263–1272, 2014.

[115] Sergei D Baranovskii. Mott lecture: Description of charge transport in disordered organic semiconductors: Analytical theories and computer simulations. *physica status solidi (a)*, 215(12):1700676, 2018.

[116] A Massé, R Coehoorn, and PA Bobbert. Universal size-dependent conductance fluctuations in disordered organic semiconductors. *Physical review letters*, 113(11):116604, 2014.

[117] RoGo Kepler. Charge carrier production and mobility in anthracene crystals. *Physical Review*, 119(4):1226, 1960.

[118] PWM Blom and MCJM Vissenberg. Dispersive hole transport in poly (p-phenylene vinylene). *Physical review letters*, 80(17):3819, 1998.

[119] Alexander Lukyanov and Denis Andrienko. Extracting nondispersive charge carrier mobilities of organic semiconductors from simulations of small systems. *Physical Review B*, 82(19):193202, 2010.

[120] Pascal Kordt, Thomas Speck, and Denis Andrienko. Finite-size scaling of charge carrier mobility in disordered organic semiconductors. *Physical Review B*, 94(1):014208, 2016.

[121] PM Borsenberger, L Th Pautmeier, and H Bässler. Nondispersive-to-dispersive charge-transport transition in disordered molecular solids. *Physical Review B*, 46(19):12145, 1992.

[122] Cyrus YH Chan, Ka Kin Tsung, Wing Hong Choi, and Shu Kong So. Achieving time-of-flight mobilities for amorphous organic semiconductors in a thin film transistor configuration. *Organic Electronics*, 14(5):1351–1358, 2013.

[123] Nevill Francis Mott and Ronald Wilfrid Gurney. *Electronic processes in ionic crystals*. Clarendon Press, 1940.

[124] GAH Wetzelaer. Analytical description of the current-voltage relationship in organic-semiconductor diodes. *AIP Advances*, 8(3):035320, 2018.

[125] Reinder Coehoorn and Peter A Bobbert. Effects of gaussian disorder on charge carrier transport and recombination in organic semiconductors. *physica status solidi (a)*, 209(12):2354–2377, 2012.

[126] Pascal Kordt, Ole Stenzel, Björn Baumeier, Volker Schmidt, and Denis Andrienko. Parametrization of extended gaussian disorder models from microscopic charge transport simulations. *Journal of chemical theory and computation*, 10(6):2508–2513, 2014.

[127] Andrea Massé, Pascal Friederich, Franz Symalla, Feilong Liu, Robert Nitsche, Reinder Coehoorn, Wolfgang Wenzel, and Peter A Bobbert. Ab initio charge-carrier mobility model for amorphous molecular semiconductors. *Physical Review B*, 93(19):195209, 2016.

[128] Lambert JA Koster, ECP Smits, VD Mihailetchi, and PWM Blom. Device model for the operation of polymer/fullerene bulk heterojunction solar cells. *Physical Review B*, 72(8):085205, 2005.

[129] John E Anthony, Antonio Facchetti, Martin Heeney, Seth R Marder, and Xiaowei Zhan. n-type organic semiconductors in organic electronics. *Advanced Materials*, 22(34):3876–3892, 2010.

[130] Jian Liu, Li Qiu, Giuseppe Portale, Marten Koopmans, Gert Ten Brink, Jan C Hummelen, and L Jan Anton Koster. N-type organic thermoelectrics: Improved power factor by tailoring host–dopant miscibility. *Advanced Materials*, 29(36):1701641, 2017.

[131] Guang Yang, Hong Tao, Pingli Qin, Weijun Ke, and Guojia Fang. Recent progress in electron transport layers for efficient perovskite solar cells. *Journal of Materials Chemistry A*, 4(11):3970–3990, 2016.

[132] Gang Yu, Jun Gao, Jan C Hummelen, Fred Wudl, and Alan J Heeger. Polymer photovoltaic cells: enhanced efficiencies via a network of internal donor-acceptor heterojunctions. *Science*, 270(5243):1789–1791, 1995.

[133] Martijn Lenes, Gert-Jan AH Wetzelaer, Floris B Kooistra, Sjoerd C Veenstra, Jan C Hummelen, and Paul WM Blom. Fullerene bisadducts for enhanced open-circuit voltages and efficiencies in polymer solar cells. *Advanced Materials*, 20(11):2116–2119, 2008.

[134] Youjun He, Hsiang-Yu Chen, Jianhui Hou, and Yongfang Li. Indene- c60 bisadduct: a new acceptor for high-performance polymer solar cells. *Journal of the American Chemical Society*, 132(4):1377–1382, 2010.

[135] Hanying Li, Benjamin CK Tee, Judy J Cha, Yi Cui, Jong Won Chung, Sang Yoon Lee, and Zhenan Bao. High-mobility field-effect transistors from large-area solution-grown aligned c60 single crystals. *Journal of the American Chemical Society*, 134(5):2760–2765, 2012.

[136] Quinn Burlingame, Caleb Coburn, Xiaozhou Che, Anurag Panda, Yue Qu, and Stephen R Forrest. Centimetre-scale electron diffusion in photoactive organic heterostructures. *Nature*, 554(7690):77, 2018.

[137] Christophe Jehoulet, Allen J Bard, and Fred Wudl. Electrochemical reduction and oxidation of c60 films. *Journal of the American Chemical Society*, 113(14):5456–5457, 1991.

[138] Lay-Lay Chua, Jana Zaumseil, Jui-Fen Chang, Eric C-W Ou, Peter K-H Ho, Henning Sirringhaus, and Richard H Friend. General observation of n-type field-effect behaviour in organic semiconductors. *Nature*, 434(7030):194, 2005.

[139] E Frankevich, Y Maruyama, and H Ogata. Mobility of charge carriers in vapor-phase grown c60 single crystal. *Chemical physics letters*, 214(1):39–44, 1993.

[140] R Könenkamp, G Priebe, and B Pietzak. Carrier mobilities and influence of oxygen in c 60 films. *Physical Review B*, 60(16):11804, 1999.

[141] J Mort, M Machonkin, R Ziolo, and I Chen. Electronic carrier transport and photogeneration in buckminsterfullerene films. *Applied physics letters*, 61(15):1829–1831, 1992.

[142] Dipankar Sarkar and NJ Halas. Dember effect in c60 thin films. *Solid state communications*, 90(4):261–265, 1994.

[143] Thomas D Anthopoulos, Cristina Tanase, Sepas Setayesh, Eduard J Meijer, Jan C Hummelen, Paul WM Blom, and Dago M de Leeuw. Ambipolar organic field-effect transistors based on a solution-processed methanofullerene. *Advanced Materials*, 16(23-24):2174–2179, 2004.

[144] Ardalan Armin, Safa Shoaee, Qianqian Lin, Paul L Burn, and Paul Meredith. On the unipolarity of charge transport in methanofullerene diodes. *npj Flexible Electronics*, 1(1):13, 2017.

[145] P De Bruyn, AHP Van Rest, GAH Wetzelaer, Dago M de Leeuw, and Paul WM Blom. Diffusion-limited current in organic metal-insulator-metal diodes. *Physical review letters*, 111(18):186801, 2013.

[146] Naresh B Kotadiya, Paul WM Blom, and GAH Wetzelaer. Trap-free space-charge-limited hole transport in a fullerene derivative. *Physical Review Applied*, 11(2):024069, 2019.

[147] Valentin D Mihailetchi, Jeroen KJ van Duren, Paul WM Blom, Jan C Hummelen, René AJ Janssen, Jan M Kroon, Minze T Rispens, Wil Jan H Verhees, and Martijn M Wienk. Electron transport in a methanofullerene. *Advanced Functional Materials*, 13(1):43–46, 2003.

[148] Stephen Logan, Jenny E Donaghey, Weimin Zhang, Iain McCulloch, and Alasdair J Campbell. Compatibility of amorphous triarylamine copolymers with solution-processed hole injecting metal oxide bottom contacts. *Journal of Materials Chemistry C*, 3(17):4530–4536, 2015.

[149] Bernd Ebenhoch, Stuart AJ Thomson, Kristijonas Genevičius, Gytis Juška, and Ifor DW Samuel. Charge carrier mobility of the organic photovoltaic materials ptb7 and pc71bm and its influence on device performance. *Organic Electronics*, 22:62–68, 2015.

[150] DB Shinde, Jagadish K Salunke, Nuno R Candeias, Francesca Tinti, Massimo Gazzano, PP Wadgaonkar, Arri Priimagi, Nadia Camaioni, and Paola Vivo. Crystallisation-enhanced bulk hole mobility in phenothiazine-based organic semiconductors. *Scientific reports*, 7:46268, 2017.

[151] Robert Steyrleuthner, Sebastian Bange, and Dieter Neher. Reliable electron-only devices and electron transport in n-type polymers. *Journal of Applied Physics*, 105(6):064509, 2009.

[152] Murat Mesta, Marco Carvelli, Rein J De Vries, Harm Van Eersel, Jeroen JM Van Der Holst, Matthias Schober, Mauro Furno, Björn Lüssem, Karl Leo, Peter Loebl, et al. Molecular-scale simulation of electroluminescence in a multilayer white organic light-emitting diode. *Nature materials*, 12(7):652, 2013.

[153] Benjamin D Naab, Scott Himmelberger, Ying Diao, Koen Vandewal, Peng Wei, Björn Lussem, Alberto Salleo, and Zhenan Bao. High mobility n-type transistors based on solution-sheared doped 6, 13-bis (triisopropylsilylethynyl) pentacene thin films. *Advanced Materials*, 25(33):4663–4667, 2013.

[154] L Bozano, SA Carter, JC Scott, GG Malliaras, and PJ Brock. Temperature- and field-dependent electron and hole mobilities in polymer light-emitting diodes. *Applied Physics Letters*, 74(8):1132–1134, 1999.

[155] MM Mandoc, B De Boer, and PWM Blom. Electron-only diodes of poly (dialkoxy-p-phenylene vinylene) using hole-blocking bottom electrodes. *Physical Review B*, 73(15):155205, 2006.

[156] BK Crone, IH Campbell, PS Davids, and DL Smith. Charge injection and transport in single-layer organic light-emitting diodes. *Applied Physics Letters*, 73(21):3162–3164, 1998.

[157] D Abbaszadeh, Alexander Kunz, GAH Wetzelaer, Jasper J Michels, NI Crăciun, Kaloian Koynov, Ingo Lieberwirth, and Paul WM Blom. Elimination of charge carrier trapping in diluted semiconductors. *Nature materials*, 15(6):628, 2016.

[158] Yuan Zhang, Bert de Boer, and Paul WM Blom. Trap-free electron transport in poly (p-phenylene vinylene) by deactivation of traps with n-type doping. *Physical Review B*, 81(8):085201, 2010.

[159] H Morishita, WJ Baker, DP Waters, R Baarda, JM Lupton, and C Boehme. Mechanisms of spin-dependent dark conductivity in films of a soluble fullerene derivative under bipolar injection. *Physical Review B*, 89(12):125311, 2014.

[160] Abay Gadisa, Kristofer Tvingstedt, Koen Vandewal, Fengling Zhang, Jean V Manca, and Olle Inganäs. Bipolar charge transport in fullerene molecules in a bilayer and blend of polyfluorene copolymer and fullerene. *Advanced Materials*, 22(9):1008–1011, 2010.

[161] D Poplavskyy, J Nelson, and DDC Bradley. Ohmic hole injection in poly (9, 9-dioctylfluorene) polymer light-emitting diodes. *Applied physics letters*, 83(4):707–709, 2003.

[162] DR Haynes, A Tokmakoff, and SM George. Temperature-dependent absolute fluorescence quantum yield of c60 multilayers. *Chemical physics letters*, 214(1):50–56, 1993.

[163] Ming L Tang, Anna D Reichardt, Peng Wei, and Zhenan Bao. Correlating carrier type with frontier molecular orbital energy levels in organic thin film transistors of functionalized acene derivatives. *Journal of the American Chemical Society*, 131(14):5264–5273, 2009.

[164] HT Nicolai, GAH Wetzelaer, M Kuik, AJ Kronemeijer, B De Boer, and PWM Blom. Space-charge-limited hole current in poly (9, 9-dioctylfluorene) diodes. *Applied Physics Letters*, 96(17):172107, 2010.

[165] Roland Rohloff, Naresh B Kotadiya, NI Crăciun, Paul WM Blom, and GAH Wetzelaer. Electron and hole transport in the organic small molecule α-npd. *Applied Physics Letters*, 110(7):073301, 2017.

[166] Nevill Francis Mott and RW Gurney. Electronic processes in ionic crystals. *Clarendon Press*, 1948.

[167] Naresh B Kotadiya, Anirban Mondal, Shiyun Xiong, Paul WM Blom, Denis Andrienko, and Gert-Jan AH Wetzelaer. Rigorous characterization and predictive

modeling of hole transport in amorphous organic semiconductors. *Advanced Electronic Materials*, 4(12):1800366, 2018.

[168] Akchheta Karki, Gert-Jan AH Wetzelaer, Gollapalli Narayana Manjunatha Reddy, Vojtech Nádaždy, Martin Seifrid, Franz Schauer, Guillermo C Bazan, Bradley F Chmelka, Paul WM Blom, and Thuc-Quyen Nguyen. Unifying energetic disorder from charge transport and band bending in organic semiconductors. *Advanced Functional Materials*, 29(20):1901109, 2019.

[169] MCJM Vissenberg and PWM Blom. Transient hole transport in poly (-p-phenylene vinylene) leds. *Synthetic metals*, 102(1-3):1053–1054, 1999.

[170] Solmaz Torabi, Fatemeh Jahani, Ineke Van Severen, Catherine Kanimozhi, Satish Patil, Remco WA Havenith, Ryan C Chiechi, Laurence Lutsen, Dirk JM Vanderzande, Thomas J Cleij, et al. Strategy for enhancing the dielectric constant of organic semiconductors without sacrificing charge carrier mobility and solubility. *Advanced Functional Materials*, 25(1):150–157, 2015.

[171] Andrea Seemann, Tobias Sauermann, Christoph Lungenschmied, Oskar Armbruster, Siegfried Bauer, H-J Egelhaaf, and Jens Hauch. Reversible and irreversible degradation of organic solar cell performance by oxygen. *Solar Energy*, 85(6):1238–1249, 2011.

[172] Pabitra K Nayak, Ron Rosenberg, Lee Barnea-Nehoshtan, and David Cahen. O2 and organic semiconductors: Electronic effects. *Organic Electronics*, 14(3):966–972, 2013.

[173] Jing-Mei Zhuo, Li-Hong Zhao, Rui-Qi Png, Loke-Yuen Wong, Perq-Jon Chia, Jie-Cong Tang, Sankaran Sivaramakrishnan, Mi Zhou, Eric C-W Ou, Soo-Jin Chua, et al. Direct spectroscopic evidence for a photodoping mechanism in polythiophene and poly (bithiophene-alt-thienothiophene) organic semiconductor thin films involving oxygen and sorbed moisture. *Advanced materials*, 21(46):4747–4752, 2009.

[174] Guangzheng Zuo, Mathieu Linares, Tanvi Upreti, and Martijn Kemerink. General rule for the energy of water-induced traps in organic semiconductors. *Nature materials*, 18(6):588, 2019.

[175] Ralph H Page, Robert J Larkin, YR Shen, and Yuan-Tseh Lee. High-resolution photoionization spectrum of water molecules in a supersonic beam. *The Journal of chemical physics*, 88(4):2249–2263, 1988.

[176] Russell G Tonkyn, Jerry W Winniczek, and Michael G White. Rotationally resolved photoionization of o2+ near threshold. *Chemical physics letters*, 164(2-3):137–142, 1989.

[177] NB Kotadiya, A Mondal, PWM Blom, D Andrienko, and GAH Wetzelaer. Supplementary information: A window to trap-free charge transport in organic semiconducting thin films. *Nature materials*, 2019.

[178] DM De Leeuw, MMJ Simenon, AR Brown, and REF Einerhand. Stability of n-type doped conducting polymers and consequences for polymeric microelectronic devices. *Synthetic Metals*, 87(1):53–59, 1997.

[179] Jeremy H Burroughes, Donal DC Bradley, AR Brown, RN Marks, K Mackay, Richard H Friend, PL Burns, and AB Holmes. Light-emitting diodes based on conjugated polymers. *nature*, 347(6293):539, 1990.

[180] Junji Kido, Masato Kimura, and Katsutoshi Nagai. Multilayer white light-emitting organic electroluminescent device. *Science*, 267(5202):1332–1334, 1995.

[181] Yuchao Liu, Chensen Li, Zhongjie Ren, Shouke Yan, and Martin R Bryce. All-organic thermally activated delayed fluorescence materials for organic light-emitting diodes. *Nature Reviews Materials*, 3(4):18020, 2018.

[182] Lin-Song Cui, Shi-Bin Ruan, Fatima Bencheikh, Ryo Nagata, Lei Zhang, Ko Inada, Hajime Nakanotani, Liang-Sheng Liao, and Chihaya Adachi. Long-lived efficient delayed fluorescence organic light-emitting diodes using n-type hosts. *Nature communications*, 8(1):2250, 2017.

[183] Qisheng Zhang, Daniel Tsang, Hirokazu Kuwabara, Yasuhiro Hatae, Bo Li, Takehiro Takahashi, Sae Youn Lee, Takuma Yasuda, and Chihaya Adachi. Nearly 100% internal quantum efficiency in undoped electroluminescent devices employing pure organic emitters. *Advanced Materials*, 27(12):2096–2100, 2015.

[184] Tien-Lin Wu, Min-Jie Huang, Chih-Chun Lin, Pei-Yun Huang, Tsu-Yu Chou, Ren-Wu Chen-Cheng, Hao-Wu Lin, Rai-Shung Liu, and Chien-Hong Cheng. Diboron compound-based organic light-emitting diodes with high efficiency and reduced efficiency roll-off. *Nature Photonics*, 12(4):235, 2018.

[185] Mi Zhou, Rui-Qi Png, Siong-Hee Khong, Sankaran Sivaramakrishnan, Li-Hong Zhao, Lay-Lay Chua, Richard H Friend, and Peter KH Ho. Effective work functions for the evaporated metal/organic semiconductor contacts from in-situ diode flatband potential measurements. *Applied Physics Letters*, 101(1):013501, 2012.

[186] Kwan Chi Kao. Electrical transport in solids with particular reference to organic semiconductors. *International series in the science of the Solid State*, 1981.

[187] NC Giebink, BW D'andrade, MS Weaver, PB Mackenzie, JJ Brown, ME Thompson, and SR Forrest. Intrinsic luminance loss in phosphorescent small-molecule organic light emitting devices due to bimolecular annihilation reactions. *Journal of Applied Physics*, 103(4):044509, 2008.

[188] Yifan Zhang, Jaesang Lee, and Stephen R Forrest. Tenfold increase in the lifetime of blue phosphorescent organic light-emitting diodes. *Nature communications*, 5:5008, 2014.

[189] Jae-Min Kim, Chang-Heon Lee, and Jang-Joo Kim. Mobility balance in the light-emitting layer governs the polaron accumulation and operational stability of organic light-emitting diodes. *Applied Physics Letters*, 111(20):203301, 2017.

[190] Quan Niu, Roland Rohloff, Gert-Jan AH Wetzelaer, Paul WM Blom, and N Irina Crăciun. Hole trap formation in polymer light-emitting diodes under current stress. *Nature materials*, 17(6):557, 2018.

[191] Rico Meerheim, Mauro Furno, Simone Hofmann, Björn Lüssem, and Karl Leo. Quantification of energy loss mechanisms in organic light-emitting diodes. *Applied Physics Letters*, 97(25):275, 2010.

[192] Rico Meerheim, Karsten Walzer, Gufeng He, Martin Pfeiffer, and Karl Leo. Highly efficient organic light emitting diodes (oled) for diplays and lighting. In *Organic Optoelectronics and Photonics II*, volume 6192, page 61920P. International Society for Optics and Photonics, 2006.

[193] Hisahiro Sasabe, Hiromi Nakanishi, Yuichiro Watanabe, Shogo Yano, Masakatsu Hirasawa, Yong-Jin Pu, and Junji Kido. Extremely low operating voltage green phosphorescent organic light-emitting devices. *Advanced Functional Materials*, 23(44):5550–5555, 2013.

[194] Dongdong Zhang, Juan Qiao, Deqiang Zhang, and Lian Duan. Ultrahigh-efficiency green pholeds with a voltage under 3 v and a power efficiency of nearly 110 lm w-1 at luminance of 10 000 cd m- 2. *Advanced Materials*, 29(40):1702847, 2017.

[195] Hisahiro Sasabe, Ryo Sato, Katsuaki Suzuki, Yuichiro Watanabe, Chihaya Adachi, Hironori Kaji, and Junji Kido. Ultrahigh power efficiency thermally activated delayed fluorescent oleds by the strategic use of electron-transport materials. *Advanced Optical Materials*, 6(17):1800376, 2018.

[196] GCM Silvestre, MT Johnson, A Giraldo, and JM Shannon. Light degradation and voltage drift in polymer light-emitting diodes. *Applied Physics Letters*, 78(11):1619–1621, 2001.

[197] Michel Schaer, Frank Nüesch, Detlef Berner, William Leo, and Libero Zuppiroli. Water vapor and oxygen degradation mechanisms in organic light emitting diodes. *Advanced Functional Materials*, 11(2):116–121, 2001.

[198] Peter van de Weijer, Kangbo Lu, Richard R Janssen, Suzanne HPM de Winter, and Hylke B Akkerman. Mechanism of the operational effect of black spot growth in oleds. *Organic Electronics*, 37:155–162, 2016.

[199] Radhika Phatak, TY Tsui, and H Aziz. Dependence of dark spot growth on cathode/organic interfacial adhesion in organic light emitting devices. *Journal of Applied Physics*, 111(5):054512, 2012.

[200] P De Bruyn, DJD Moet, and PWM Blom. All-solution processed polymer light-emitting diodes with air stable metal-oxide electrodes. *Organic Electronics*, 13(6):1023–1030, 2012.

[201] Shi Tang, Andreas Sandström, Petter Lundberg, Thomas Lanz, Christian Larsen, Stephan van Reenen, Martijn Kemerink, and Ludvig Edman. Design rules for light-emitting electrochemical cells delivering bright luminance at 27.5 percent external quantum efficiency. *Nature communications*, 8(1):1190, 2017.

[202] Mallesham Godumala, Suna Choi, Min Ju Cho, and Dong Hoon Choi. Recent breakthroughs in thermally activated delayed fluorescence organic light emitting diodes containing non-doped emitting layers. *Journal of Materials Chemistry C*, 7(8):2172–2198, 2019.

[203] Stephen R Forrest, Donal DC Bradley, and Mark E Thompson. Measuring the efficiency of organic light-emitting devices. *Advanced Materials*, 15(13):1043–1048, 2003.

[204] Victor Rühle, Alexander Lukyanov, Falk May, Manuel Schrader, Thorsten Vehoff, James Kirkpatrick, Björn Baumeier, and Denis Andrienko. Microscopic simulations of charge transport in disordered organic semiconductors. *Journal of chemical theory and computation*, 7(10):3335–3345, 2011.

[205] Carl Poelking and Denis Andrienko. Long-range embedding of molecular ions and excitations in a polarizable molecular environment. *Journal of chemical theory and computation*, 12(9):4516–4523, 2016.

[206] JJM Van Der Holst, MA Uijttewaal, B Ramachandhran, Reinder Coehoorn, PA Bobbert, GA De Wijs, and RA De Groot. Modeling and analysis of the three-dimensional current density in sandwich-type single-carrier devices of disordered organic semiconductors. *Physical Review B*, 79(8):085203, 2009.

[207] Ilja Lange, James C Blakesley, Johannes Frisch, Antje Vollmer, Norbert Koch, and Dieter Neher. Band bending in conjugated polymer layers. *Physical review letters*, 106(21):216402, 2011.

[208] Carl Tengstedt, Wojciech Osikowicz, William R Salaneck, Ian D Parker, Che-H Hsu, and Mats Fahlman. Fermi-level pinning at conjugated polymer interfaces. *Applied Physics Letters*, 88(5):053502, 2006.

[209] DJD Moet, M Lenes, JD Kotlarski, SC Veenstra, J Sweelssen, MM Koetse, B De Boer, and PWM Blom. Impact of molecular weight on charge carrier dissociation in solar cells from a polyfluorene derivative. *Organic Electronics*, 10(7):1275–1281, 2009.

[210] Frédéric Laquai and Dirk Hertel. Influence of hole transport units on the efficiency of polymer light emitting diodes. *Applied physics letters*, 90(14):142109, 2007.

[211] IH Campbell, TW Hagler, DL Smith, and JP Ferraris. Direct measurement of conjugated polymer electronic excitation energies using metal/polymer/metal structures. *Physical review letters*, 76(11):1900, 1996.

[212] IN Hulea, HB Brom, AJ Houtepen, D Vanmaekelbergh, JJ Kelly, and EA Meulenkamp. Wide energy-window view on the density of states and hole mobility in poly (p-phenylene vinylene). *Physical review letters*, 93(16):166601, 2004.

[213] Umut Aygül, Heiko Peisert, Johannes Frisch, Antje Vollmer, Norbert Koch, and Thomas Chassé. Electronic properties of interfaces between pcpdtbt and prototypical electrodes studied by photoemission spectroscopy. *ChemPhysChem*, 12(12):2345–2351, 2011.

[214] AW Grice, DDC Bradley, MT Bernius, M Inbasekaran, WW Wu, and EP Woo. High brightness and efficiency blue light-emitting polymer diodes. *Applied Physics Letters*, 73(5):629–631, 1998.

[215] JE Lyon, AJ Cascio, MM Beerbom, R Schlaf, Y Zhu, and SA Jenekhe. Photoemission study of the poly (3-hexylthiophene)/au interface. *Applied physics letters*, 88(22):222109, 2006.

[216] SH Park, JG Jeong, Hyo-Jin Kim, Seung-Han Park, Mann-Ho Cho, Sang Wan Cho, Yeonjin Yi, Min Young Heo, and Hyunchul Sohn. The electronic structure of c60/znpc interface for organic photovoltaic device with blended layer architecture. *Applied Physics Letters*, 96(1):2, 2010.

[217] Hiroyuki Yoshida. Low-energy inverse photoemission study on the electron affinities of fullerene derivatives for organic photovoltaic cells. *The Journal of Physical Chemistry C*, 118(42):24377–24382, 2014.

[218] Ze-Lei Guan, Jong Bok Kim, Yueh-Lin Loo, and Antoine Kahn. Electronic structure of the poly (3-hexylthiophene): indene-c60 bisadduct bulk heterojunction. *Journal of Applied Physics*, 110(4):043719, 2011.

[219] Alicia Godoy, Linda Cattin, Jean Christian Bernède, Fernando Díaz, and Mará Angélica del Valle. Effect of perylene as electron acceptor and poly (tetrabromo-p-phenylene diselenide) as "buffer layer" on heterojunction solar cells performances. In *Macromolecular Symposia*, volume 304, pages 109–114. Wiley Online Library, 2011.

[220] Hisahiro Sasabe, Jun-ichi Takamatsu, Takao Motoyama, Soichi Watanabe, Gerhard Wagenblast, Nicolle Langer, Oliver Molt, Evelyn Fuchs, Christian Lennartz, and Junji Kido. High-efficiency blue and white organic light-emitting devices incorporating a blue iridium carbene complex. *Advanced materials*, 22(44):5003–5007, 2010.

[221] Shi-Jian Su, Takayuki Chiba, Takashi Takeda, and Junji Kido. Pyridine-containing triphenylbenzene derivatives with high electron mobility for highly efficient phosphorescent oleds. *Advanced Materials*, 20(11):2125–2130, 2008.

[222] Shipan Wang, Yuewei Zhang, Weiping Chen, Jinbei Wei, Yu Liu, and Yue Wang. Achieving high power efficiency and low roll-off oleds based on energy transfer from thermally activated delayed excitons to fluorescent dopants. *Chemical Communications*, 51(60):11972–11975, 2015.

[223] Akitsugu Niwa, Takashi Kobayashi, Takashi Nagase, Kenichi Goushi, Chihaya Adachi, and Hiroyoshi Naito. Temperature dependence of photoluminescence properties in a thermally activated delayed fluorescence emitter. *Applied Physics Letters*, 104(21):79_1, 2014.

Acknowledgements

This thesis would have not been possible without the help of so many people in many ways. I wish to express my gratitude to them for helping me during my thesis.

First of all, I would like to express my sincere gratitude to Dr. Gert-Jan A. H. Wetzelaer and Prof. Dr. Paul W. M. Blom for giving me an opportunity to work on many exciting and challenging research projects in their group at the Max Planck Institute for Polymer Research (MPIP) Mainz.

Thank you very much Prof. Blom for giving an overall direction for my work, all the stimulating discussions, encouragements, great advice, questions and comments. I appreciate your kind support for my PhD registration at the Karlsruhe Institute of Technology (KIT). I also appreciate your help and supports apart from scientific work. Thank you very much for being my promoter, I feel deeply honored to have worked under your guidance, I have learned a lot from you.

I would like to say big thanks to my direct supervisor Dr. Wetzelaer, for his immense support and guidance on a daily basis throughout this thesis. Thank you very much for all the exciting discussions, encouragements, suggestions in the experimental work, help with the theories, data analysis, constant feedbacks, writing the articles and corrections of this thesis. Your support has helped me to create many first-ever results in organic electronics, within a short span of a PhD thesis. I deeply appreciate your knowledge of the subject and your guidance, it has grown my scientific understandings and it was a memorable experience for me to work with you.

I would like to convey my deep gratitude to Prof. Uli Lemmer (KIT) for his kind support in doctoral registration and supervision of my PhD thesis at KIT. Your lectures on plastic electronics at KIT has developed my interest in organic electronics, encouraged me to do a Master thesis on OLEDs under your guidance and subsequently to do a PhD in organic electronics. Thank you very much for all your support and help since my master studies at KIT.

I would like to appreciate all collaborators and co-authors, for their great efforts and contributions in my research. I am grateful to Dr. Anirban Mondal and Dr. Denis Andrienko for fruitful discussions and wonderful molecular simulations on charge injection, charge transport and charge trapping in organic small molecules. Your work has added great values to my dissertation. I am grateful to Prof. Yutaka Ie (Osaka University, Japan) for his distinctive support by synthesizing TADF emitters, electron transport materials and teaching me the chemistry and purification of organic small molecules. Your materials helped me throughout this thesis. It was a great pleasure to work with you side by side in the labs. I appreciate Dr. Hao Lu for his great support in UPS

measurements and discussions. I am grateful to Roland Rohloff for his valuable support in getting familiar with the device fabrication, analysis and modelling at the beginning of my PhD. I appreciate Christoph Deckers for his contribution in the purification of organic small molecules during his internship with me at MPIP.

I would like to acknowledge Dr. Thomas Lenz, for his great scientific support, advice and making me familiar with MPIP during microcontact printing project with him. I am thankful to, Dr. Ellen Backus for sum-frequency generation measurements. I am grateful to Prof. Dago M de Leeuw, Dr. Thorsten Schultz, Dr. Patrick Amsalem and Dr. Rüdiger Berger for our successful completion of microcontact printing project. I am grateful to Dr. Antonio Ricciardulli for helping me with the solar simulator, our fruitful discussions and collaborations. I am grateful to Ke Zhang, for our fruitful discussions, improving my knowledge of transistors and collaborations. I also appreciate Dr. Tomasz Marszalek and Prof. Wojciech Pisula for discussions and ongoing collaborations. I would like to thank, Bas van der Zee for helping me with impedance measurements and ongoing collaborations. I would like to thank, Esther del Pino Rosendo and Dr. Charusheela Ramanan for fruitful discussions and ongoing collaborations. I am grateful to Dr. Kamal Asadi for helping me with kelvin probe and capacitive measurements, fruitful discussions and ongoing collaborations.

I would like to convey my special gratitude to Kai Philipps for the German translation of abstract and summary of this dissertation, for helping me with chemical analysis and ChemDraw. I am thankful to Dr. Rüdiger for helping me with AFMs. I am grateful to Alexander Kunz for helping me with measurements, scientific advice and tremendous help in moving my furniture in Mainz. I am thankful to Dr. Dongcheng Chen for fruitful discussions on OLEDs and his advice. I am grateful to Dr. Paschalis Gkoupidenis for his scientific and career-related advice. I would like to say thanks to Dr. Jasper J. Michels, Dr. Christian Kasparek, Ann-Kathrin Schönbein, and Dr. Changguo Xue for their help and scientific advice. I appreciate Dr. Xuelin Yao and other members of Dr. Akimitsu Narita group at MPIP for helping me with sublimation set up. I also appreciate all members of molecular electronics group (AK Blom) for their advice and supports during my PhD. I appreciate Xavier Montane, Simon Benneckendorf, Michal Borkowski, Wojtek Zajaczkowski, Hanna and all my officemates for their help, cheerful moments and happy discussions beyond science.

I would like to say many thanks to Mr. Frank Keller, Mr. Hans-Jürgen Guttmann, Mr. Christian Bauer, Ms. Verona Maus, Ms. Michelle Beuchel and Mr. Hanspeter Raich, Mr. Gunnar Glasser, Mr. Uwe Rietzler, Ms Helma Burg for their great technical supports and help in my work. I am grateful to Ms. Petra Pausch for her kind support in dealing with administrative works and general matters. I appreciate supports from entire electronic workshop team Mr. Alfons Becker, Mr. Alex Steinmetz, Mr. Benjamin Zwietasch, Mr. Marc Rohmann and Mr. Gerald Weinmann. I also appreciate Glassblower Mr. Rene Schmuck for his help. I would like to say special thanks to Mr. Hans-Josef Beauvisage, for your kind helps, during my countless lengthy day and night

work schedules at MPIP. I am grateful to Dr.Jurana Hetterich for helping me with PhD registration and documentations at KIT. I appreciate Mr. Larry Lowe for his help in filling forms at MPIP. I also acknowledge all the people at MPIP, who have helped me in various forms.

I would like to thank all members of the defense committee for their valuable time in examining my work. I would like to acknowledge, funding from the European Union Horizon 2020 research project grant no. 646176 (EXTMOS) for my work.

I would like to acknowledge everyone who has provided me previous opportunities to work in their labs and helped me in developing robust technical skills. Without those previous experiences, I could have not imagined achieving so many impressive results during my PhD. I am grateful to Prof. Dago M de Leeuw, for hiring me at MPIP in the first place to work on microcontact printing project, for his advice and encouragements. I would like to appreciate Dr. Madhav Singh at Helmholtz Research Center Karlsruhe, for an opportunity to work on Li-Ion batteries and developing my skills to work on totally new topics. I am grateful to Prof. Uli würfel, Dr. Sarah Röttinger, Dr. Markus Kohlstädt and your whole group at Fraunhofer Institute for Solar Energy, Freiburg. For enhancing my skills in device fabrication and characterization, learnings form your lab was extremely helpful. I am grateful to Dr. Norman Machau for Master thesis and subsequent research job at InnovationLab (IL), Heidelberg. I am humbled with your warm supports even after my master thesis. I am grateful to Dr. Sebastian Stolz my daily supervisor at IL, for teaching me fabrication of OLEDs right from the scratch and teaching many other experimental techniques. I also thank Dr. Ralph Eckstein, Stefan Nester, Dr. Michael Scherer, Dr. Jan Preinfalk, Dr. Gerardo Hernández-Sosa and all other members of the InnovationLab for their kind help during my research there. I am grateful to Prof. Timo Mappes and Dr. Tobias Wienhold, for an internship opportunity at Helmholtz Research Center Karlsruhe and developing my skills in microfabrication. I am grateful to Prof. Tapas K. Chaudhuri and Dr. Anjana J. Kothari for their enormous support in my Master thesis on the growth and characterization of compound semiconductors in India, it was my very first research experience and our first publication. I also appreciate your warm supports even still today. I am grateful Prof. B. S. Chakrabarty and Prof. P.B. Joshi for their supports during my Master studies in india and afterworlds. I would also like to appreciate all my professors, teachers and guides form India and Germany who have taught, supported and guided me at different stages of my education.

Finally, I am forever indebted to my parents, brother whole family and in-laws for their constant encouragement, invaluable support and prayers for my success. Hima my better half, it was your sacrifice, tremendous care, love and prayers, that allowed me to work days and nights tirelessly and achieve nearly impossible targets in a short time. Thank you for being a part of my life. I acknowledge all my friends and relatives who believed in my dreams, provided me moral supports and stood by me in hard times. I deeply appreciate Ketan Bavalia for his warm hospitality and open-hearted

support in all tough times. I am grateful to Rajnikant Bhayani, Hardik vamja, Sandip Dhanani, Nikunj Visaveliya, Kubandarin Kolanji, Sandeep Ummethala, Dhrubajyoti Bhattacharjya, Timo Mattusch, Paul Schlett, Gaurang Khot, Sanket Panchal, Sumit Singh, Chaitanya Dingare, Hitesh Patel, Purvesh Soni, Manish Sanghani, Mustahsin Adib, Parth Thanki, Ghanshyam Kachadiya, Hitesh Chauhan, Alpesh Tarapara, Vairag Godhani, Kirit Siddhapara, Anand Patel, Malkesh Patel, Paresh Dhameliya, Ashutosh Kumar, Subarna Babu Sapkota, Hardik Dobariya and all other.... friends, for helping me in multiple ways during my PhD.

I have tried my best to acknowledge everyone for their help. My sincere apologies, if I have missed anyone.